Issue 1 2020 | Volume 16

The Journal on Advanced Studies in Theoretical and Experimental Physics, including Related Themes from Mathematics

PROGRESS IN PHYSICS

"All scientists shall have the right to present their scientific research results, in whole or in part, at relevant scientific conferences, and to publish the same in printed scientific journals, electronic archives, and any other media." — Declaration of Academic Freedom, Article 8

ISSN 1555-5534

The Journal on Advanced Studies in Theoretical and Experimental Physics, including Related Themes from Mathematics

PROGRESS IN PHYSICS

A quarterly issue scientific journal, registered with the Library of Congress (DC, USA). This journal is peer reviewed and included in the abstracting and indexing coverage of: Mathematical Reviews and MathSciNet (AMS, USA), DOAJ of Lund University (Sweden), Scientific Commons of the University of St. Gallen (Switzerland), Open-J-Gate (India), Referativnyi Zhurnal VINITI (Russia), etc.

Electronic version of this journal:
http://www.ptep-online.com

ISSN: 1555-5534 (print)
ISSN: 1555-5615 (online)

Standard Address Number: 297-5092
Printed in the United States of America

April 2020 **Vol. 16, Issue 1**

CONTENTS

Information for Authors

Progress in Physics has been created for rapid publications on advanced studies in theoretical and experimental physics, including related themes from mathematics and astronomy. All submitted papers should be professional, in good English, containing a brief review of a problem and obtained results.

All submissions should be designed in LaTeX format using *Progress in Physics* template. This template can be downloaded from *Progress in Physics* home page http://www.ptep-online.com

Preliminary, authors may submit papers in PDF format. If the paper is accepted, authors can manage LaTeXtyping. Do not send MS Word documents, please: we do not use this software, so unable to read this file format. Incorrectly formatted papers (i.e. not LaTeXwith the template) will not be accepted for publication. Those authors who are unable to prepare their submissions in LaTeXformat can apply to a third-party payable service for LaTeX typing. Our personnel work voluntarily. Authors must assist by conforming to this policy, to make the publication process as easy and fast as possible.

Abstract and the necessary information about author(s) should be included into the papers. To submit a paper, mail the file(s) to the Editor-in-Chief.

All submitted papers should be as brief as possible. Short articles are preferable. Large papers can also be considered. Letters related to the publications in the journal or to the events among the science community can be applied to the section *Letters to Progress in Physics*.

All that has been accepted for the online issue of *Progress in Physics* is printed in the paper version of the journal. To order printed issues, contact the Editors.

Authors retain their rights to use their papers published in *Progress in Physics* as a whole or any part of it in any other publications and in any way they see fit. This copyright agreement shall remain valid even if the authors transfer copyright of their published papers to another party.

Electronic copies of all papers published in *Progress in Physics* are available for free download, copying, and re-distribution, according to the copyright agreement printed on the titlepage of each issue of the journal. This copyright agreement follows the *Budapest Open Initiative* and the *Creative Commons Attribution-Noncommercial-No Derivative Works 2.5 License* declaring that electronic copies of such books and journals should always be accessed for reading, download, and copying for any person, and free of charge.

Consideration and review process does not require any payment from the side of the submitters. Nevertheless the authors of accepted papers are requested to pay the page charges. *Progress in Physics* is a non-profit/academic journal: money collected from the authors cover the cost of printing and distribution of the annual volumes of the journal along the major academic/university libraries of the world. (Look for the current author fee in the online version of *Progress in Physics*.)

The Interpretation of the Hubble-Effect and of Human Vision Based on the Differentiated Structure of Space

Gerhard Dorda

Institute of Physics, University of Armed Forces Muenchen, Werner-Heisenberg-Weg 39, 85577 Neubiberg, Germany.
E-mail: physik@unibw.de

Based on the differentiated structure of space, observed by the Quantum-Hall-Effect, a comprehensive equation is presented for the description of the Hubble-Effect. This Hubble-Effect equation reflects the experimental observation showing a casual connection to the Hubble time T_U and thus to the cosmic length L_U and the cosmic mass M_U. The obtained results are substantiated by the cosmic background radiation and by the agreement of the derived data with the experimental data of the Milky Way. It is shown that the differentiated structure of space, used for the description of the Hubble-Effect, also refers to the process of human vision, dominating the observation.

1 Introduction

After the discovery of the Quantum-Hall-Effect (QHE) and the associated exceptional side effects [1], it proved to be necessary to re-evaluate many physical and biological phenomena, e.g. the interpretation of the Hubble-Effect (HE) and, of the basis of it, even the process of human vision, referring to the *differentiated structure of space*. The differentiated structure of the three-dimensional space was first observed at the analysis of the experimental data of the QHE, which was discovered in 1980 by K. von Klitzing based on MOS-field-effect transistors.

The QHE is the first experimental observation of *quantization in the macroscopic scale* in solid-state physics. Only gradually, the fundamental importance of this discovery and of all with this discovery connected spectacular experimental observations became apparent for the entire range of physics. In the first instance, it was the observation of the QHE on GaAs–$Al_xGa_{(1-x)}As$ heterostructures [2], presented by D. C. Tsui et al, which showed that this effect is generally valid for the whole solid-state physics. More detailed investigations of the experimental data revealed that the QHE is not only independent from atomic mass, but also from the strength of the electric current used, i.e. from frequency, i.e. from time, and also from the form of the sample with the considered QHE structure, i.e. from space [3].

Really, the state of QHE shows a spectacular simultaneity of $R_{xx} = h/ie^2 = 2.58128 \times 10^4/i\,\Omega$ *and* $R_{xx} = 0\,\Omega$ (i is the quantization number), measured between different contacts *at any place* of the QHE structure. This effect of the spatial independence of the observed simultaneity in resistivity is the background of the disclosed two-dimensionality of electromagnetism at the causal situation. Besides that, it should be emphasized that the simultaneity of the quantized resistivity shows that the three-dimensional state of electromagnetism can be clearly separated spatially in two independent conditions: On one side in a 2-D state, given by the simultaneity, and on the other side in a 1-D state, realized capacitively by the interaction of the electron charges. The experimental observation of the possibility to split up electromagnetism in a 2-D and a 1-D state will be described by the "differentiated structure of the space" [3]. Analyzing all these novel experimental insights allowed to deliver convincing physical answers, for example Lee Smolin's book *The Trouble with Physics* posed fundamental and unsolved questions [4], in particular also about the category of time [3].

The description of space and time, i.e. frequency, based on the QHE, leads to the notion that also open questions in astronomy and cosmology could be answered with the help of the observations of the QHE. This, for example, includes the question about cosmic expansion, which, on the basis of the interpretation of the Hubble-Effect (HE), generated a vivid discussion, leading to the unfolding of several cosmic models, but without final solutions [5, 6]. Therefore, in this work, it is attempted to explore the experimental data of the HE on the basis of the so-called differentiated structure of space [3].

2 The analysis of the Hubble-Effect (HE) with respect to the differentiated structure of space

The cosmic expansion model is based on the experimentally observed Hubble-law, given by [5]

$$v_{\mathrm{HE,y}} = \frac{R_{\mathrm{HE,y}}}{T_U} \,. \tag{1}$$

Here in (1), $v_{\mathrm{HE,y}}$ is the velocity of a given galaxy, $R_{\mathrm{HE,y}}$ has the significance of a distance referred to a given galaxy and T_U is interpreted as the Hubble time, defining the so-called age of the cosmos (an assumption which requires the expansion of the cosmos). The index HE signifies the relation of the Hubble-Effect (HE) to the associated redshift of the observed radiation and the index y refers this redshift to the observed galaxy [5, 6].

The figures of the experimental HE in [5] and [6] show the so-called escape velocity $v_{\mathrm{HE,y}}$ in relation to the velocity of light c, meaning that (1) can be rewritten by use of c. As a result, we receive a form which defines the HE in relation

to the so-called length of the cosmos, obtained by $L_U = T_U\, c$, and we may write

$$\frac{R_{HE,y}}{L_U} = \frac{v_{HE,y}}{c} \,. \tag{2}$$

The value of the redshift is usually specified by the number z_y, which means

$$z_y = \frac{v_{HE,y}}{c} \,. \tag{3}$$

Since the HE merely reflects the observation of light, i.e. photon energies, the number z_y may, in accordance with (1) and (2) and due to the c-standardization, be considered to be related to the limit of the light frequency f_C or to the limit of the light wavelength λ_C. As shown in Section 4, this is of fundamental importance for the interpretation of the HE.

The concept of an escape velocity $v_{HE,y}$, as stated in (1), must originate from the existence of a given position, e.g. from the place of observation, or in a general sense from any localized place in the cosmos, in order to have the possibility to speak of place in sense of the classic conception of velocity, a model, which so far has been crucial for the interpretation of the HE. The concept of a place requires the existence of localization related to atomic mass, i.e. to protons and neutrons, constituting a gravitationally induced localization which only can become real through an atomic solid-state structure.

Starting from these findings it can be shown that based on the experimental data of the QHE, which is independent of atomic mass, a novel form of velocity can be defined. This velocity is also given by the relation of length and frequency, but this specific form of velocity is merely deduced from the dualistic character of the electron, i.e. without any contribution of proton-neutron-mass related gravity. This specific i.e. structural space-time condition, which is identifiable in the QHE, reveals that the electron-related velocity is given by the relation of the category of length, reflected by the electron mass m_e, and the category of frequency, realized by two-dimensional electromagnetism, i.e. by the electron charge e. This length-frequency, i.e. length-time relation is, in spatial terms, always mutually perpendicular to each other, which is the background for the notion of three-dimensionality of space and also the background for the *freedom* of choice concerning the value of light velocity. As shown in [3, pp. 33–34,45,49–50], it therefore follows the possibility of differentiation between the one-dimensionality, i.e. 1-D, and the two-dimensionality, i.e. 2-D. These fundamental circumstances were characterized in summary as a differentiated three-dimensional spatial structure.

It is evident that this electron related form of velocity is given at light effects, i.e. given by λf (λ = wavelength, f = frequency). Thus, it can be assumed that this form of velocity is also displayed in the observation of the HE-galaxies, playing an essential key role in the here presented reinterpretation of the HE. Hence, unexpected statements about the HE-galaxies may be obtained when the Hubble-law, i.e. (1), and the model of the differentiated structure of space are applied to Kepler's third law.

3 The application of the Hubble-Effect to Kepler's third law

To begin with, it seems necessary to appropriately transform Kepler's third law. In doing so, we assume that due to the cosmological principle [6], Kepler's third law has general validity in the entire universe.

Kepler's third law is given by [3],

$$\left(\frac{T_{G,y}}{2\pi}\right)^2 = t_{G,y}^2 = \frac{R_{G,y}^3}{G\, M_{G,y}} \,, \tag{4}$$

whereby G in (4) is the gravitational constant, given by

$$G = c^2\, \frac{L}{M} \,. \tag{5}$$

Eq. (4), in conformity with the MKSA- or MKS-system of units, represents a universal linkage of the category of length with the category of time, modified by the category of mass. $T_{G,y}$ in (4) is the so-called orbital period of the given solid-state celestial body (SSCB), which planets, suns and stars are to be counted as part of. $t_{G,y}$ in (4) is the so-called effective time, referred to the surface of the SSCB, $R_{G,y}$ is the distance to the center of the SSCB and $M_{G,y}$ its mass. The index G signifies the connection to the SSCBs. In (5), L bears the meaning of the Planck length, $L = 4.051 \times 10^{-35}$ m, and M represents the Planck mass, $M = 5.456 \times 10^{-8}$ kg [7]. By transforming (4), we receive the following form, being valid for all SSCBs

$$\frac{v_{G,y}^2}{c^2} = \frac{L}{R_{G,y,1-D}}\, \frac{M_{G,y}}{M} \,, \tag{6}$$

whereby

$$v_{G,y} = \frac{R_{G,y,2-D}}{t_{G,y}} \,. \tag{7}$$

In (6), the left-hand side represents the electromagnetic effect, i.e. an effect reflecting spatial two-dimensionality, and the right-hand side reflects a distance related, i.e. a one-dimensionality related gravitational effect.

Here, in (6) and (7), the findings from the Quantum-Hall-Effect (QHE) about the possibility of the differentiated space is used, according to which the three-dimensional space, in case of it being structured, can be considered partitioned, and that [3]:

1. in a one-dimensional space, described by the 1-D state, covered by $R_{G,y,1-D}$, and
2. in a two-dimensional space, described by the 2-D state, ascertainable by $R_{G,y,2-D}^2$.

Attention should be paid to the fact that the one-dimensional gravitational distance $R_{G,y,1-D}$ of the SSCBs, as given in (6), could be described by the number $a_{G,y}$, which due to the reference to one-dimensionality was termed gravitational number. In [3, see p. 14], it is given by

$$R_{G,y,1-D} = a_{G,y}\,\lambda_{G,y}\ . \tag{8}$$

Here, $\lambda_{G,y}$ is a one-dimensional reference length, defined by

$$\lambda_{G,y} = M_{G,y}\frac{L}{M}\ . \tag{9}$$

It is easily recognizable that in accordance with (4) – (8), this reference length $\lambda_{G,y}$ signifies the connection between the category length and the atomic mass related gravitation.

When discussing (6), it is of importance to consider that the Planck relation L/M in (5) and (9) possess, due to the cosmological principle, validity for the entire being in the cosmos. Therefore, as an extension of L/M, we may write

$$\frac{L}{M} = \frac{\lambda_{G,y}}{M_{G,y}} = \frac{L_U}{M_U}\ , \tag{10}$$

which is a consequence of the general validity of Kepler's third law. Here in (10), $\lambda_{G,y}$ stands for the reference length of the SSCB and $M_{G,y}$ for its related mass. Furthermore, L_U and M_U are the limit length L_U and the limit mass M_U of the cosmos, introduced by means of (1) and (2), i.e. by means of the HE.

The masses $M_{G,y}$ in (4), (6), and (9) are effective as homogeneity parameters. As will be shown, the state of homogeneity can be related to two different structures in the cosmos, which, in the three-dimensional cosmic space, are identifiable by their dot-like centered unity. These two forms are:

1. Celestial bodies which consist of solid state, i.e. SSCBs, and which can, by means of Kepler's third law, be very well described as spherical structures, given by interwoven gravitational-electromagnetic structures ([3], page 44). All planets, suns and stars are to be counted as part of this. With regard to (4), the boundary condition for the homogeneity of the SSCB is the equality $R_{G,y,1-D} = \sqrt{R^2_{G,y,2-D}}$, which enables dynamics, i.e. the category of time, to be revealed in Section 4.
2. Celestial bodies whose existence only is observable with the aid of optical methods, i.e. with the aid of eyesight and technically with the aid of optical absorption methods. This includes galaxies, theoretically ascertained by (1) and (2) of the HE. These cosmic structures are not given by a coherent, gravitational-electromagnetic interwoven state, but they are to be considered a free, i.e. dynamic cluster of different SSCBs, which, as part of above all electromagnetic interactions, form by the so-called "black hole" a homogeneous, i.e. dot-like centered unity. Due to the free cluster of SSCBs, which show only insignificant gravitational interaction, the possibility of creating the category of time by means of galaxies does not exist. Hence, we are able to clarify the boundary condition for the homogeneity of the HE-galaxies only in Section 5.

To clearly show the difference between the SSCBs and the galaxies, (6) must be adapted to (1) and (2). Based on (6) and (10), we may write

$$\left(\frac{v_{HE,y}}{c}\right)^2 = \frac{L_U}{R_{HE,y,1-D}}\frac{M_{HE,y}}{M_U}\ , \tag{11}$$

whereby $v_{HE,y}$ is given by

$$v_{HE,y} = \frac{R_{HE,y,2-D}}{T_U}\ . \tag{12}$$

$M_{HE,y}$ signifies the mass related to the given galaxy. The distances $R_{HE,y,1-D}$ and $R_{HE,y,2-D}$ in (11) and (12) are, according to the cosmological principle, to be interpreted as characteristic distances, i.e. lengths, of the given galaxy.

In conformity with (6) and (11), the fundamental difference between the SSCBs and the HE-galaxies should become above all apparent by means of the different definitions of $v_{G,y}$, (7), and of $v_{HE,y}$, (12). Thus, this difference is discussed in the following sections.

4 The difference between solid-state celestial bodies (SSCBs) and HE-galaxies

When comparing the velocities $v_{G,y}$ and $v_{HE,y}$, we proceed that both $R_{G,y,2-D}$, the distance of the given solid-state celestial body (SSCB), and $R_{HE,y,2-D}$, the distance of the given galaxy, are to be considered their distinctive characteristic. In doing so, the cosmological principle is to be heeded, stating that in the cosmos there is no center and consequently no defined position [6]. Moreover, the fundamental difference between the time statements $t_{G,y}$ and T_U, given in (4) and (1), has to be taken into account since it points out that, as (4) and (6) show, the time $t_{G,y}$ is one of the characteristic parameters of any given SSCB, whereas the time T_U, being valid for all HE-galaxies, is solely a cosmic constant. From Kepler's third law, (4) and (6), it results that the time $t_{G,y}$ is given by

$$t_{G,y} = \sqrt{a_{G,y}}\,\frac{R_{G,y,2-D}}{c}\ , \tag{13}$$

whereby $a_{G,y}$ is the SSCB related gravitational number, defined in (8). Thus, considering (6), (7), and (13), the solid-state celestial body is characterized not only by the mass $M_{G,y}$ and the radius $R_{G,y}$, but also by the SSCB related category of time $t_{G,y}$.

In contrast to $v_{G,y}$, the velocity $v_{HE,y}$ can experimentally only be experienced by optical means, in fact with aid of the

light i.e. photon energies, emitted by the given galaxy. This energy spreads from the galaxy with the velocity of light and is registered by the eye or by appropriate appliances (telescopes) via absorption. Since the respective galaxies distinguish from each other by the emitted light i.e. photon energy, it is physically permitted, in compliance with the observed value of the so-called redshift z_y, to ascribe an appropriate frequency f_y to the observed galaxy, which reflects the energy hf_y. That means, the in (2) presented relation $v_{HE,y}/c$ can be replaced by an appropriate frequency or wavelength relation, and we may write

$$z_y = \frac{hf_y}{hf_C} = \frac{hc/\lambda_y}{hc/\lambda_C} = \frac{\lambda_C}{\lambda_y} . \tag{14}$$

It then again follows that the HE can be described by means of an equation of light

$$\lambda_y f_y = \lambda_C f_C = c , \tag{15}$$

which inter alia reflects the fact that the frequency, in localized form known as the category of time, is an expression of pure electromagnetism [3].

Here in (14) and (15), f_y is the given galaxy related frequency or λ_y wavelength, whereas f_C is the Compton frequency and λ_C the Compton wavelength. In (14), z_y is, unlike in the classic Doppler-effect model, not valued as a difference from wavelengths, but as a direct information about the observed galaxy state, given by f_y or λ_y, respectively. Thus, (14) and (15) determine the state of the HE-galaxies. Hence, instead of interpreting $v_{HE,y}$ mechanically as an escape velocity of the galaxies, it proves to be physically acceptable, with regard to (14) and (15), to replace the concept of the classical velocity with the frequency or wavelength relation given by (14) and to describe the redshift as a light wave radiation, which reflects the heat radiation laws, i.e. Wien's displacement law. That means, it is postulated that any HE-galaxy emits radiation in the form of photon energy as a result of its homogeneity.

5 The equation of the Hubble-Effect

Starting the analysis of this novel description of the HE, above all it must be emphasized that the existence of the parameter of the HE galaxies, given by T_U, attests the validity of Kepler's third law for the whole cosmos, i.e. the form of the gravitational constant (5), and also the extension of L/M, presented in (10). Thus it is – from a physical point of view – legitimate to use the (4), (5), and (10) as basic equations for the further analysis of (11), at which we take the form $R_{HE,y,1-D}$ in place of $\lambda_{G,y}$ of (9). Furthermore, it appears absolute necessary for the description of the HE to apply the model of the differentiated structure of the space to (11). This requirement indicates to formulate (11) in a particular form, reflecting this spatial differentiation. It can be achieved by a completion of (11) by the factor z_y^2, hence formulating

$$\left(\frac{v_{HE,y}}{c}\right)^2 = \frac{L_U z_y^2}{R_{HE,y,1-D}} \frac{M_{HE,y}}{M_U} . \tag{16}$$

Really, it should be considered, the experimental HE data shows that the factor z_y is causally related to the distance $R_{HE,y,2-D}$, as it was on the basis of (2) and (3) expressed by (12). Thus, to be in accordance with the required differentiation of the HE-state from the usual three-dimensionality into the one-dimensionality and the two-dimensionality, we have to conclude that the factor z_y^2 must be related to the 1-D related distance $R_{HE,y,1-D}$, to ensure the causality at the whole HE-state. Evidently, these requirements are realized by means of (16).

Taking into consideration all the presented experimental data and the related conclusions, given in Sections 2 – 4, we are able to present the solution of the whole HE state, and that in form of a comprehensive, generally valid equation, given by

$$\begin{aligned} R_{HE,y,1-D} &= z_y R_{HE,y,2-D} = z_y^2 L_U \\ &= z_y^x M_{HE,y} = z_y^{x+2} M_U , \end{aligned} \tag{17}$$

at which z_y^x is given by

$$z_y^x = \frac{L}{M} = \frac{R_{HE,y,1-D}}{M_{HE,y}} = \frac{L_U}{M_U} = 7.426 \times 10^{-28}\,\mathrm{m\,kg^{-1}} . \tag{18}$$

Equation (17) shows that with respect to (2) it is possible to formulate the relations

$$R_{HE,y,2-D} = z_y L_U , \tag{19}$$

as well as

$$R_{HE,y,1-D} = z_y R_{HE,y,2-D} \tag{20}$$

and

$$M_{HE,y} = z_y^2 M_U . \tag{21}$$

Furthermore, on the basis of (16), it becomes evident that the difference between the SSCBs and the state of HE-galaxies is simply describable by the factor z_y , which is, according to (6), for the SSCBs without exception given by $z_y = 1$.

The numerical value of (18) results from the experimentally explored gravitational constant [4] $G = 6.6738 \times 10^{-11}$ $\mathrm{m^3 kg^{-1} s^{-2}}$, using (5). It demonstrates the value z_y^x to be a natural constant. Besides, it should also be emphasized that (18) is therefore significant for our model, as it discloses the functional background of the homogeneity of the HE galaxies.

The validity of (17) and (18), and thus of (19) – (21), can be verified using both the knowledge of the cosmic background radiation and the known experimental data of the Milky Way, since according to our model the Milky Way galaxy is assessed to be a homogeneous galaxy.

6 The analysis of the cosmic background radiation with respect to the Milky Way galaxy radiation

At first, when analyzing (17) and (18), which describe the state of all HE galaxies, it must be pointed out that in the spatially differentiated state, as it is the case for the optical observation of the HE galaxies, only the electron related electromagnetic variability is ascertained, so that a specific proton-neutron one-dimensional mass-effect cannot be observed at this effect by experiment. Thus to solve this problem, the observation of the cosmic background radiation is considered. It shows that this radiation, represented by the temperature $T_{\text{cosm}} = 2.73\,^{\circ}\text{K}$, is the result of the interaction of hydrogen atoms, extended over the whole cosmos, see [5] and [12].

Thus when we value the cosmic background radiation as a heat radiation effect, given by the displacement law of Wien, obtaining $z_{\text{T}} = \lambda_{\text{C}}/\lambda_{\text{cosm}} = T_{\text{cosm}}\,\lambda_{\text{C}}/(3.40\times10^{-3})$ [3, part III] and assess this value with respect to the heat radiation factor of the Milky Way, given by $z_{\text{MW}} = \lambda_{\text{C}}/\lambda_{\text{MW}}$, evidently this z_{T} value has to be modified by the relation $m_{\text{p}}/m_{\text{e}}$, corresponding to the temperature relation $T_{\text{MW}}/T_{\text{cosm}}$. Here m_{p} is the mass of the proton, m_{e} the mass of the electron and T_{MW} has reference to z_{MW}. In other words, the factor of modification $m_{\text{p}}/m_{\text{e}}$ represents the energetic difference between the cosmic background radiation, being a result of the interaction of hydrogen atoms, and the radiation of the localized, i.e. spatially differentiated electromagnetism of the HE galaxies.

Using the HE-related (9) and (10), as well as the (17) and (20), and assuming that the heat radiation factor of the Milky Way is identical with the cosmic background radiation factor z_{T}, then we obtain the following relationship

$$R_{\text{HE,MW,2–D}} = \frac{3.4\times10^{-3}}{T_{\text{cosm}}\,\lambda_{\text{C}}}\,\frac{m_{\text{e}}}{m_{\text{p}}}\,\frac{L_{\text{U}}}{M_{\text{U}}}\,M_{\text{HE,MW}} = 2.08\times10^{-22}\,M_{\text{HE,MW}}\,. \tag{22}$$

Here, in place of the Milky Way radiation factor z_{MW}, the assumed identity of z_{MW} to z_{T} was used, resulting in

$$z_{\text{MW}} = z_{\text{T}} = \frac{T_{\text{cosm}}\,\lambda_{\text{C}}}{3.4\times10^{-3}}\,\frac{m_{\text{p}}}{m_{\text{e}}} = 3.58\times10^{-6}\,. \tag{23}$$

At (23), T_{cosm} was replaced with the background radiation value $T_{\text{cosm}} = 2.73\,^{\circ}\text{K}$, and the causal relation $\lambda_{\max}\,T = 3.40\times10^{-3}$, i.e. Wien's displacement law, was used for $\lambda\,T$. When we use the Hubble time $T_{\text{U}} = 4.32\times10^{17}\,\text{s}$, reflecting a Hubble constant of $H_{\text{o}} = 71.4\,\text{km}\,\text{s}^{-1}\text{Mpc}^{-1}$, lastly obtained from the Hubble telescope, we obtain a cosmic length $L_{\text{U}} = c\,T_{\text{U}} = 1.30\times10^{26}\,\text{m}$, and by means of (10) a cosmic mass $M_{\text{U}} = 1.74\times10^{53}\,\text{kg}$.

Finally, by means of (19) – (23), for the Milky Way we obtain the values

$$\begin{aligned} R_{\text{HE,MW,2–D}} &= z_{\text{MW}}\,L_{\text{U}} = 15.05\,\text{kpc} = 4.63\times10^{20}\,\text{m}\,,\\ M_{\text{HE,MW}} &= z_{\text{MW}}^{2}\,M_{\text{U}} = 1.12\times10^{12}\ \text{solar masses}\\ &= 2.23\times10^{42}\,\text{kg}\,. \end{aligned} \tag{24}$$

Considering these results with respect to the experimentally observed data of the Milky Way, given in [6] by the approximate values of the radius $R_{\text{HE,MW,2–D}} = 15\,\text{kpc} = 4.6\times10^{20}\,\text{m}$ and of the mass $M_{\text{HE,MW}} = 10^{12}$ solar masses $= 2\times10^{42}\,\text{kg}$, we assess for the radius a factor of inaccuracy of only 3 %, and for the mass $M_{\text{HE,MW}}$ of only 12%. This finding, especially the agreement of the order of magnitude of both $R_{\text{HE,MW,2–D}}$ and $M_{\text{HE,MW}}$, is very important, as it convincingly demonstrates that (17) and (18) can be assessed as a novel, physically justified description of the Hubble-effect.

The Sections 2–6 have shown that the novel HE model is based on the QHE-observation about the differentiated structure of the 3-dimensional space. The application of the differentiated space structure on the gravitational constant G , (5), shows that c^2 is related to electromagnetism, in the case of the HE-galaxy to the 2-D state, represented by the $R_{\text{HE,y,2–D}}$ distance, whereas L/M refers to the gravity of the HE-galaxies, i.e. to the 1-D state, represented by the $R_{\text{HE,y,1–D}}$ distance, which is in this situation in a causal connection to the mass $M_{\text{HE,y}}$. The HE-circumstance, described by (16) – (18) and thus by (20), shows that the connection between the distances $R_{\text{HE,y,2–D}}$ and $R_{\text{HE,y,1–D}}$ is given by the factor z_{y}.

These results are confirmed by the agreement of the calculated data with the experimental data of the Milky Way and support also the conception, formulated by (10), that the relation $R_{\text{HE,y,(1–D)}}/M_{\text{HE,y}}$ of *any* HE galaxy is always identical with the L/M-relation.

7 The description of human vision on the basis of the differentiated structure of space

A particular confirmation of the value z_{MW} is obtained by considering the general limitation of vision. Seen in this connection, it should be pointed out that not only that of human eyes, but also the vision of all animals breaks off at the wavelength $\lambda_{\text{y}} = 6.8\times10^{2}\,\text{nm}$ [13]. This particular observation manifests the rightness of the identity between the limiting value of the wavelength of visible light and the specific wavelength of the radiation of the Milky Way $\lambda_{\text{MW}} = 6.79\times10^{2}\,\text{nm}$.

A further very interesting observation about the process of seeing is obtainable, when we become aware of the connection between human vision and the differentiated structure of space. As disclosed extensively in *The Feynman Lectures on Physics* [13], human vision is the result of processing of two signals, independently given on the one side by the rod cells, and on the other side by the uvula cells. In this textbook, it is shown that the rod cells yield signals at the twilight, i.e. signals without any colored light absorption, whereas the uvulas show signals solely by means of colorful light.

This biological differentiation reflects in an absolute manner the physical model of spatial differentiation between gravitation and electromagnetism, suggesting that the rod-signals represent the 1-D related gravitational interaction, whereas the uvula-signals the 2-D related electromagnetic interaction.

Thus it is physically acceptable to suggest the biological structure of human eyes to be the consequence of the effect of the discussed existence of the differentiated structure of space, given outside of masses. Consequently we can state that this interesting biological differentiation between rods and uvulas reflects the spatial differentiation between the 1-D state and the 2-D state, showing that the differentiated structure of space is the particular mediator of these effects.

Considering these circumstances, it becomes evident that due to the existence of the differentiated structure of space, the human eyes become the main processing not only of the perceptibility of solids and thus of the observation in general, but also, simply by the absorption of particular quanta of light, of the perceptibility of stars and galaxies, and attain therefore, together with the help of telescopes, the possibility to discover the HE and the related equations (16), (17) and (18).

8 Concluding findings

In the cosmos, there are two forms of homogeneous structures: Solid-state celestial bodies (SSCBs) and HE-galaxies (HE). Homogeneous solid-state celestial bodies consist of electromagnetic-gravitational interwoven structures, which can be described by Kepler's third law. This law shows that the SSCBs can not only be characterized by mass and radius, but also by the category time, whose lapse is dependent on the strength of gravity of the given SSCB [3].

In contrast, the existence of HE-galaxies is solely observable by means of optical signals, i.e. by eyes and/or by technical methods, using telescopes. Here, signals undisturbed by atmospheric absorption are required, which correspond to the state of a differentiated three-dimensional space. Incidentally, in this connection it should be emphasized that the Pythagorean theorem, considered in conjunction with the three-body problem, entirely corresponds to this differentiated three-dimensional space model. Therefore, it should be pointed out that the application of the differentiated structure of space to the optical signals of galaxies leads, with analyzing the HE, to (16) – (18). In addition, it was demonstrated that the validity of (17) and (18) can be established by the cosmic background radiation, and what is more, by the excellent agreement of the deduced data of mass and radius of the Milky Way with the corresponding values.

The presented new model of the Hubble-effect, which is based on the black-body radiation, shows – according to the *experimental*, generally valid disclosures of the Quantum-Hall-Effect (QHE) – that the so-called HE-velocity $v_{\mathrm{HE,y}}$ is a pure electron effect. Therefore it has been stated that, according to the differentiated structure of space, the frequency, i.e. the category time, should not be considered an absolute basic magnitude, but an electromagnetic 2-D state, which becomes localized, i.e. observable only in connection with the existence of masses. Therefore, as generally known – and also being in agreement with the differentiated space model – time can be observed only in a causal relation to the 1-D length state [4]. This conclusion follows from (4) and (8) and has been manifested by experimental data of the lapse of time, in particular described in [3] by (26).

Finally, the importance of the differentiated structure of space in nature has been further made evident by the analysis of human vision, showing that the difference of the function of the uvula cells and the rod cells reflects the separateness of the 2-D and 1-D spatial state of seeing, an effect, being in accordance with the description of the Hubble-Effect. This observation is of extraordinary importance, as the process of seeing is the main background of the human observation of all being. As will be shown in a next paper, this important conclusion can be additionally substantiated by the physical description of the process of hearing [14, 15].

Acknowledgements

The author is indebted to *Prof. Walter Hansch*, University of Armed Forces, Muenchen, for the support of this subject and for his critical comments to several statements of this paper. He would also like to thank *Torsten Sulima* for the scientific-technical assistance, *Alexander Hirler* for the extensive completion of the paper for printable publication and *Franz Wittmann*, Technical University, Muenchen, for his cooperation to select the proper journal for publication. Finally, the author expresses many thanks to *Klara Kirschner* for the translation of the text into English.

Received on December 5, 2019

References

1. von Klitzing K., Dorda G. and Pepper M. New method for high-accuracy determination of fine-structure constant based on quantized Hall resistance. *Phys. Rev. Lett.*, 1980, v. 45, 494–497.
2. Tsui D. C., Störmer H. L. and Gossard A. C. *Phys. Rev. Lett.*, 1982, v. 48, 1559–1561.
3. Dorda G. Die Struktur von Raum und Zeit und die Interpretation der Wärme. Cuvillier Verlag, Göttingen, ISBN 978-3-7369-9388-4, eISBN 978-3-7369-8388-5, 2016.
4. Smolin L. The Trouble with Physics. Houghton Mifflin Company, New York, 2006. In German: Die Zukunft der Physik. Deutsche Verlags-Anstalt, München, 2009, pp. 344–346.
5. Silk J. A short history of the universe. *Scientific American Library*, W. H. Freeman and Company, New York, 1994. In German: Die Geschichte des Kosmos. Spektrum, Berlin, 1996, pp. 34–42.
6. Bernhard H., Lindner K. and Schukowski M. Wissensspeicher Astronomie. Volk und Wissen Verlag, Berlin, ISBN 3-06-081705-7, 1995.
7. Kostro L. De Broglie waves and natural units. In: van der Merwe A. and Garuccio A., eds. Waves and particles in light and matter. Plenum Press, New York, 1994, 345.
8. Gerthsen C. and Vogel H. Physik. Springer-Verlag, Berlin, 1993, pp. 570–571.
9. Hausamann D. and Further J. Einstein und die Satellitennavigation, In: Einsteins Relativitätstheorien, Deutsches Museum. Deutsches Museum-Verlag, München, 2005, pp. 24–34.
10. Pound R. V. and Rebka G. A. *Phys. Rev. Lett.*, 1960, v. 4, 337–341.

11. Bublath J. Geheimnisse unseres Universums – Zeitreisen, Quantenwelten, Weltformel. Droemer Verlag, München, 1999, ch. 10, pp. 114–115.

12. Fritzsch H. Vom Urknall zum Zerfall. In: Serie Piper SP518, R.Piper & Co. Verlag, München, 1987, pp. 255–256, 283.

13. Feynman R. P., Leighton R. B. and Sands M. The Feynman Lectures on Physics, Vol. 1. California Institute of Technology, 1963, ch. 35–36. In German: Vorlesungen über Physik, Band 1. Oldenbourg Verlag, München, 1987, pp. 477–505.

14. Fletcher H. and Munson W. A. Loudness, its definition, measurement and calculation. *J. Acoust. Soc. Am.*, 1933, v. 5, 82.

15. Dorda G. Die Interpretation des Schalls auf der Basis der differenzierten Struktur des drei-dimensionalen Raumes. University of the Armed Forces, Muenchen, Germany, to be published.

Predictability Is Fundamental

Felix Tselnik
E-mail: tselnik@bgu.ac.il

1 General concept of trajectory

In his relationship with Nature, the person might be active if he wants to get to some state of the world, and then he is looking for a means to reach this state. Although the content of the state is completely in his mind, he needs the prediction for his action to reach the desired. Typically, this is difficult in real life, and people act according to more or less uncertain hopes, past experience, beliefs etc. However, sometimes predictions might exist to recommend actions with the universally guarantied results – always and everywhere. Though infrequent, such predictions are therefore recommended to be looked for first of all, and our so valued technologies are based solely on these.

The related scheme of the world states must be able to formulate predictions in its own internal terms. If some state in the scheme is associated with the desired, so being the final for the person's purpose, the initial state, from which the action should start, must be defined in the internal terms of the scheme as well. Since the final state is not reached as yet, it should be set in the future with respect to the initial. If being in the initial state the person is guaranteed to reach the final, no prediction is needed. As the first order development, we might include in the scheme some intermediate state such that transitions from the initial state to this intermediate and from the intermediate to the final are both sure. Then the problem is reduced to finding this intermediate state. Only one such state might be there, because the existence of even one more would provide uncertainty as to which one to choose, so making the prediction incomplete.

Giving the number 0 to the initial state and 1 to the final, let us give $\frac{1}{2}$, say, to this intermediate (no metric is implied – just the order). In the same way we define next $\frac{1}{4}$ and $\frac{3}{4}$ states and so on. This procedure involves only rational numbers, so some infinite sequences of the states might not converge to a state with the rational number to become the initial for the further part of the sequence. Therefore all sequences, i.e., all real numbers are required for guaranteed predictions (Dedekind). In so doing, only order is important, and a state might correspond either to the rational or irrational number as well. Again, no state not belonging to this sequence can exist in the prediction of the steady transition from 0 to 1, otherwise the prediction becomes incomplete. In the Lagrange's version of mechanics, its basic least action principle reflects just this singleness.

Such state sequences are called trajectories, and we are ready now to approach the Newton's scheme, starting with the very condition of the universal predictability. It should be stressed that the scheme is only the necessary language for making universal predictions; it is supported by, though not coming from, our senses that connect us with Nature also in great many other respects.

2 Principles of the Newtonian mechanics

In this essay, I don't consider the post-Newton development of his ideas; even the contribution of Maxwell and Einstein will not be discussed here. My purpose is to understand whether or not the very scheme of mechanics elaborated by Newton is the only possible one. Upon working over many decades in experimental physics, I couldn't refrain from asking myself as to what if there is some other and more efficacious way to address Nature. To this end, I'm going to scrutinize the Newton's scheme in every respect.

Following the method of Descartes of representing geometrical figures with numbers and related equations, Newton has formulated his three 'Laws of Mechanics' in order to apply the similar procedure to physics, i.e., to describe also motion by means of Cartesian coordinates.

The first Newton's law introduces rectilinear and uniform trajectories as free from an external influence ("force"). However, this law is just a vicious circle. As Einstein mentioned in his "The Meaning of Relativity": "The weakness of the principle of inertia lies in this, that it involves an argument in a circle: a mass moves without acceleration if it is sufficiently far from other bodies; we know that it is sufficiently far from other bodies only by the fact that it moves without acceleration."

Aiming at numbering arbitrary motions, we have first of all to match abstract geometric images with real operations. Indeed, what does it mean "rectilinear" in Nature? How rectilinear a trajectory should be for the scheme still being suitable? How to make it sure that a line is straight? Suffices it to be described by linear equations in a reference frame formed as the Cartesian structure? But then, we have to recognize first that our reference frame itself is comprised of straight axes. The commonly accepted agreement suggests using some standard rigid rods. How rigid? Sometimes rigid might appear soft. This depends on the inter-atomic distances, but the concept of distance is still to be introduced using standard rods. (Circle!) We are to transport the rod as along the reference frame axes for marking them evenly, so also over the whole space with parallel shifts and rotations, being sure that it remains rigid. In so doing, we believe that

no actions destroy these operations. The marks on the axes define Cartesian coordinates, which will further be used to define a scalar – squared "length" as the sum of the squared coordinate differences. Only then can we construct the full Cartesian structure using equal length rods to obtain the necessary symmetries of reference frames. (One more circle!) Also collimated light rays might be used, whenever diffraction (still depending on wavelength!) could be neglected, either solely to define linearity, or together with rods for parallelism and other symmetries. Being applied to measurements of motions, we inquire the relevance of these devices, since in fact this procedure has nothing to do with the motion in question. It might well happen that in the study of motion our artificial rods either add something of their own or hide something, so being suitable within only some limited scope of motions. We cannot refer here to great many successful technical applications as well as to the broad experimental support, since all these are carried out within the introduced in advance basic conceptions, so being relevant only within some narrow areas of the implied research.

Even more difficult questions spring up upon considering the time intervals measurement and its universal applicability to real motion. How do we know that the duration of one hour now is equal to that in the future (see, e.g., H.Weyl, "Space-Time-Matter")? How uniform free motion is to be for the scheme to remain suitable? Beginning with Zeno, Aristotle etc., philosophers were burdened by the mystery of time, and Newton himself attempted, in vain, to develop the concept of "genuine" time, that runs uniformly and is free from any influence, our astronomic time being only an approximation of. The summary of his meditations might be found in his "Mathematical Principles of Natural Philosophy": "I do not define time, space, place, and motion, as being well-known to all."

Not belonging to these "all", I want to examine the very necessity of the conventional definitions. Intrinsic to our mind (i.e., being a priory, as in Kant's works) ideas of "space" and "time" suggest only some freedom of motion. However in the Newtonian scheme, the space is already supplied with the three-dimensional Euclidean geometry, that is, it is a somehow defined set of elements – positions – that form the non-compact metric space with all the related properties. The time is not merely "past-now-future" but also a one-dimensional metric space with the countable base of open sets (neighborhoods), and its metrics is monotonous. Why all these?

Imagine a body placed into empty space. How can we tell between its being at rest and moving? The question is quite senseless provided nothing else is there. A reference frame is this "else" in the Newtonian mechanics. Only then can we define the trajectory of this body using readings on the reference frame axes. Still, this frame is only an auxiliary means in the problem. But why do we need to know this trajectory? This becomes meaningful only if some other bodies may come into contact with this one, and it is this contact that is in question of any real problem in mechanics and generally – in physics.

The purpose actually consists in predictions of the contacts, implying the further action to influence the reaching of this contact. Then, why do we need an intermediary like an external reference frame, rather than to directly consider only the motion of the bodies of interest in our problem? If the event of contact in question does occur, the coordinates of the bodies coincide at some time moment. Hence, the trajectories must (in the Newtonian mechanics) be written in numbers as time-functions of the coordinates taken from the reference frame. Only if times for different trajectories are appropriately coordinated, the predictions of contacts become possible. The accepted solution is one time for all trajectories in the problem, and the synchronized clocks are needed at each position in the reference frame.

All this rather complex measurement system is feasible, provided:

(i) Synchronizing signals connect all positions of the reference frame instantly. Believing that "for any fast motion a faster one might be found", an overcoming signal must always be used, so that observation of the body that could come into contact of interest would never have been lost.

(ii) Suitable clocks are to be made somehow. In daily life rough astronomical timing: years, months, days, hours, might be inappropriate. However, the design of mechanical clocks is based on the previously established principles of mechanics that are still under examination in our essay (One more circle!).

(iii) Identity of the clocks periods is perfect.

The second Newton's law describes some external influence on the trajectory – a force. The idea consists in integrating the series of free trajectories' segments to approximate the actual trajectory as altered from the free motion by this (smooth) force. The end points of each segment contact those of its neighbors. With the reference frame readings their lengths can be used to obtain the measure for integration. The transitions between the segments normalized to the related time intervals define the proportional to the force 'acceleration' as the measure for the transitions between the segments. Leaving aside the mathematical details of these approximations and their limits to the Calculus, I want to focus on the very measurement of a force in Newtonian mechanics. Indeed, where to find the vector of the force? Traditionally, some particular kind of forces is suggested for the problem of interest like the gradient of an external potential (as, e.g., in oscillations, gravity), friction, electromagnetic field etc. There is no general concept of force in the geometrical terms of the scheme itself. Provided the force is given in advance all over space-time, the whole trajectory can be found step by step. However, this approach cannot produce a genuine prediction as yet, being dependent on the knowledge of force up to the final state where no prediction is already in-

teresting. In the Newtonian mechanics, inertia determining acceleration makes the scheme really predictable: Given the force, a sufficiently big mass of the body will send this force to the second order perturbation in the trajectory determining equation. It is just the demand of predictability that is responsible for second order terms in the equations to be sufficient: Force collected over the first order linear segment provides the next inter-segment transition, and no higher order terms are needed to determine them. So, the specification of only the initial free segment suffices to predict the final contact. This fact is not always understood, especially by mathematicians, believing in the known from experiment harmony of Nature. For instance, V. Arnold in his famous textbook "Mathematical Methods of Classical Mechanics" declared: "It is possible to fancy a world, in which for the determination of the future of a system one has to know in the initial moment also acceleration. Experiment shows that our world is not such."

However, any statement and result of experiment is formulated in terms of the already accepted theoretical models (Einstein: "In order to measure the velocity of light, the theoretical concept of velocity is necessary."). All these concepts originate in predictability. As a matter of fact, there is no harmony in our world, but the demand for predictability bounds us to develop a scheme ready for advising the person, looking obliviously around for the solution of his problem, to try first of all physics for the reaching of his wanted state.

The third Newton's law introduces the concept of interaction between bodies as a sole source of force, so providing some certainty to the second Newton's law. Then, an isolated from external influences collection of either or not interacting bodies taken as a whole must move freely according to the first Newtonian law. In particular, a solid body, considered as comprised of two parts separated with an infinitesimally thin gap, moves freely while, according to the second Newton's law, an additional force would be needed to keep each part moving free in spite of their reciprocal attraction. Hence we have to admit that the action of one part on the other is compensated by the opposite action.

3 Alternative numbering of motion

Newton considered velocities of bodies extendable in their values up to infinity, and then the using of located in advance clocks and rods became indispensible. Success in geometry tempted the using of the trajectory as the basic entity to start a theory with. On the contrary, the existence of the top-speed signal makes it possible to suggest a different numbering of motion. In so doing, we need no metric – no rods, no clocks, no material points, no reference frames. Our main concept is "contact", defined solely by its existence – "yes/no". The concept of body will be used just as a picturesque representation of contacts. It is the prediction of a contact using some auxiliary contacts – the Contact Problem (CP), that is the only issue of physics as a method to make universal predictions whenever relevant.

Attempts to define the space-time geometry with trajectories of limited velocities have been carried out in the middle of the past century [1-6]. In the interior of the light cone, trajectories were used to define neighborhoods generating the space-time topology as sets of points (events) such that any trajectory reaching a point of the neighborhood starting from outside passes also some other points of it, and there is some open interval in the order of the 1-dimensional continuum of this trajectory contained in this neighborhood (see Ref. 7 for details).

Consider two bodies A and B moving, each one along its (ordered) trajectory, toward their possible contact denoted (A,B). Let a set of auxiliary bodies be simultaneously emitted from A so that some of them reach B. Find the first of them to come into contact with B in the own B-order (One might imagine this first to put a mark on B, so that others meet B already marked.). Such a body will be taken for the top-speed signal, provided the emitted set is rich enough to cover all possible applications. A top speed must exist in the scheme for B not to be lost from observation upon its accelerations, so making predictions impossible. In so doing, we don't provide this top speed with a numerical value (no cm/sec, just topmost as defined!). Let further B emit instantly in response a similar set to reach A; it might be regarded as 'reflected' from B. This procedure being multiple repeated will be called the oscillation of the top-speed signal between A and B.

Our scheme of numbering motion consists solely in counting the numbers of these oscillations n_{AB}. Let us start this counting at some state of A. If (A,B) exists, the number of the oscillations is infinite, since were it finite some last oscillation before (A,B) will be there, in contradiction with the top-speed property of the signal, since either A or B would then reach (A,B) sooner. It is tempting to take the infinity of nAB for the prediction of the contact, but in the absence of (A,B) this number is still infinite though in the Newtonian scheme it would take infinite time; but we claim to use no measure for time, only the order.

In order to obtain the prediction, we can use an auxiliary body X with (A,X) known in advance and measure the ratio n_{AB}/n_{AC} for the triple (A,B,X), beginning at arbitrary point. (Both numbers being infinite, the ratio doesn't depend on this point.) The prediction of (A,B) follows from that of (A,B,X) provided such X can be found that this ratio is finite. Again, this is not a genuine prediction as yet, because we are counting the ratio up to the (A,B,X), and then nothing is left to predict. Hence, a scheme is to be developed to predict (A,B) already at the beginning of the oscillation numbers (ON) counting. Although we dispensed with all Newtonian intermediaries and turned to measure a motion solely by means of some auxiliary motions, we have yet to develop a scheme similar to the Newtonian to obtain genuine predictability.

For this to be possible, we ought now to consider suitable for our numbering scheme intersections of trajectories that allow for using the related concept of force. To this end, we define first the class Q of trajectories, the contacts between which are not too dense, so that with ON counting it be always possible to distinguish contacts however multiple. For instance, two trajectories, which in the Newtonian version have contacts only in all points with rational values of even one of coordinates, don't belong to Q. Hence, if trajectories from Q have two or more mutual contacts, ON counting, wherever started, might become infinite for only one of these. Only trajectories from Q are suitable for CP.

If the top-speed body signal S emitted from A at some of its point to contact B at some of its point, then no body emitted from A simultaneously with S can contact B in all points earlier than (S,B) in the B-order. So, we have now points in A and B that cannot be connected with trajectories unlike that in the Newtonian scheme. The set of all points, no pair of which can be so connected is called "spacelike hypersurface" W, and its elements will be called positions; therefore the trajectory of A, say, can contact W only at a single position. In particular, all top-speed signals connecting a point of A apart from W define some boundary in W: Only positions of W within this boundary can be connected with the part of A bounded by this point. An open in its order interval of A, crossing W at some of its points can be projected on W inside this boundary. This can be done using a series of mutually "parallel" trajectories (The notion of parallelism might be defined using a system of four ratios of ON's, and so defined parallel trajectories are not necessarily straight lines.) as follows. Take r points on A such that the finite ON's between neighboring pairs of parallel trajectories, connecting them to W, differ by only one oscillation. Increase r keeping this condition. In the limit r going to infinity we obtain a path of positions in W, which are in one-to-one correspondence with the set of r points in A trajectory to form (again being completed with irrational limits) the one-dimensional continuum. Unlike trajectories, paths might have self-intersections, though "rarefied" in accord with the trajectories they are projections of.

The whole W is an "envelope" for various combinations of possibly intersecting paths. If paths intersect, then the contact of their trajectories either exists or not. However, if paths don't intersect no contact can be there. It is only this purely topological property that is important for CP. W must have enough freedom to allow all the variety of combinations of passes. Since paths and their allowed combinations are one-dimensional, they might be topologically embedded in the 3-dimensional Euclidean space (Remember traffic interchanges. In general, a wide class of n-dimensional spaces, including our paths, might be so embedded in the Euclidean space of the dimension 2n+1, according to the Noebeling-Pontryagin theorem. Hence the geometry of space, taken in the Newtonian scheme as fallen from heaven, merely results from the union of all paths, and more dimensions for W would be redundant, because already some 3-dimensional subspace of it can include all cases for CP. Importantly, W cannot be considered as a sub-space of the 4-dimentional Lorentz space-time, otherwise its meaningless topology with non-countable neighborhoods would be only1-dimensional in both Lebesgue and Poincare senses.

A top-speed signal cannot have more than one contact with any other trajectory in our scheme. Some other trajectories might have single contacts too, and these will be useful to define a force. Let us therefore select a special class of trajectories – the measurement X-kit with the following properties:

(i) Two trajectories from X either have no contacts or have only one;

(ii) Any point of a trajectory from Q has contacts with some trajectories from X.

(iii) Any two points of a trajectory from Q can be connected by a trajectory from X. Free trajectories of the first Newton's law are such, and just these properties of them, perhaps only locally, are actually needed in our scheme too.

In the second Newton's law acceleration is determined by force. Let us now inverse this law so as to determine force via acceleration, though not of the body of interest in the CP but of a body from the specially prepared auxiliary test P-kit with the same scheme of contacts as the X-kit, however comprised of bodies with some fixed constants to be specified for the particular kind of forces. Provided such standard constants exist over the whole Q, one is able to determine the acceleration of the body A that is of interest in CP comparing its acceleration at each point to that of the test body from the P-kit here, given the related constants of both. If the bodies participating in this comparison differ from each other only by the values of their constants, the trajectory of A can be defined, and therefore it is worthwhile to represent a force as the product of a constant and an entity defined by the ON counting – field. With the definition of our two kits, the said comparison might always be achieved with the counting of ON's and their ratios. The mentioned properties of the kits are specified just to allow for this comparison, so defining situations, in which we claim to make reliable predictions.

In the chain of links approximating a trajectory with a broken line, it is sufficient to specify only the first link. Then the force defining inter-link transitions (given the required constants) provide the prediction.

It remains now to define the required constants in terms of ON. We specify first a regular P-star, comprised of trajectories of some P's from the P-kit with the common contact, in which the ON ratios are distributed regularly:

(i) Each trajectory of P has the neighbors, that is, a number of trajectories, the ratios of the ON between P and any its neighbor to that between P and any other trajectory from the star exceeds 1; it follows that the ratios of the ON between P and any pair of its neighbors equals 1.

(ii) This feature is the same for all trajectories of the star.

In 3-dimensional Q these conditions can be exact only for a star with the configuration of a Platonic solid (If a star comprises great many trajectories, this inexactness might be ignored in the definition of a measure as the numbers of trajectories in subsets of the star; this is used, e.g., in the problems of field propagation, however not referred to further on in this essay restricted to mechanics.).

Consider a Platonic solid star with the bodies from the P-kit moving from its vertices toward the center solely under their interactions (Remember the third Newton law.). It is convenient to describe the gauge procedure for the constants in Newtonian terms (translation into the ON counting will be evident). These bodies are assumed to have some masses m and charges q. The completely identical bodies can reach the center only being mutually attracted as for gravity; otherwise some charge compensation is needed. Then only two of the Platonic solids might be relevant: the cube and the icosahedron. Indeed, in both it is possible to distribute opposite charges so as to obtain a regular star for bodies from P-kit.

The cube might be arranged out of two interwoven tetrahedrons – one with $+q$, another with $-q$; hence the star is neutral as a whole. All 8 initial velocities are radial and equal, and 8 equal initial radii are also the same for all bodies of the cube. All these bodies are being equally accelerated proportionally to q^2/m toward the center along rays, whatever radial dependence of their (isotropic) interaction force. We ascribe the cube star to electromagnetic (EM) interaction, the magnetic component of which is then equal 0 on the rays, and the electric field is purely radial.

Starting ON counting from the initial radii, we find their ratios for each ray with its neighbors to be 1 for any n. Reversing argument, the value 1 of these ratios can be taken as the criterion for the cube star to be perfect. After passing the star center the bodies decelerate to reach initial velocity at the same radii as the initial ones. Here some of them can be used, with an appropriate order of the vertices, to form the descendant star from this seed, adding more similar bodies. A triple of the neighboring seed star bodies completely determines all other members of the descending star with ON ratios counting. In the progress of this descending step by step in all directions, the charge and mass are transported over the whole network in Q, so determining the same pair of standard constants everywhere. Importantly, both m and q must be the same in the cube: Varying any of them in a part of cube, even keeping the value q^2/m unchanged, destroys the star symmetry. Hence, the network transports both standards unchanged.

In a more general case of CP, e.g., with an arbitrary external EM field, the source of which is not known in advance, unlike that in the Newtonian approach, the acceleration of charged bodies is proportional to the q/m rather than to q^2/m. However, the value of q/m is also determined by the cube star gauge, since both q and m are preserved upon the descent transportation. So, predictions based on ON counting are available in CP even beyond the Newtonian scheme.

The icosahedron regular star of oppositely charged bodies (also neutral as a whole) exists only if, in the Newtonian sense, the interaction force increases with radius. Whereas the cube is a sub-star of the full dodecahedron, the icosahedron stands alone; hence its charge and mass have nothing in common with EM q and m. With the distance increasing of its force, allowing for confinement and asymptotic freedom, the icosahedron star symmetry might be suggested to explain the Dark Cold Matter and the Dark Energy in cosmology.

4 Postscript

The origin of the "Laws of Nature" for any method of numbering motion as well as of the concept of motion itself results merely from the very problem statement by the person-user to find, whenever possible, a universally predictable course of action. To this end, physics suggests CP. Nature has no harmony of its own; only living creatures are looking for reliable schemes to make predictions. In particular, it is clear now why quantum mechanics had not developed its own variables instead of classical position and momentum. However modified, these variables still present information in terms required by the user.

Received on November 19, 2019

References

1. Zeeman E.C. *Topology*, 1967, v. 6, 161.
2. Tselnik F. *Sov. Math. Dokl.*, 1968, v. 9, 1151.
3. Hawking S.W., King A.R., McCarty P.J. *J. Math. Phys.*, 1976, v. 17, 174.
4. Gobel R. *Comm. Math. Phys.*, 1976, v. 46, 289.
5. Ehlers J., Pirani F.A.E. and Schild A. In: General relativity, ed. L. O'Raifeartaigh. (1972).
6. Marzke R.F., Wheeler J.A. In: Gravitation and relativity, ed. H.Y. Chiu and W.F. Hoffmann, New York, (1964).
7. Tselnik F. *Progress in Physics*, 2016, v. 12, no. 2.

The Interpretation of Sound on the Basis of the Differentiated Structure of Three-Dimensional Space

Gerhard Dorda

Institute of Physics, University of Armed Forces Muenchen, Werner-Heisenberg-Weg 39, 85577 Neubiberg, Germany.
E-mail: physik@unibw.de

It is shown that the experimental data of sound, obtained by the investigation of H. Fletcher and W. A. Munson [4], can be physically described on the basis of the differentiated structure of three-dimensional space (DSS), showing an analogy to the physical interpretation of the process of human vision. The analysis of the experimental data indicates that the process of hearing at frequencies below 800 Hz depends on the differentiated structure of the space related to air. Furthermore, it has been shown that the existence of sound at frequencies higher than 800 Hz is the result of quantization phenomena of the differentiated space-related state of the air, revealing to be an analogy to the quantum effects of the differentiated structure of space of the quantum-Hall-effect (QHE). The presented results about sound, considered with respect to the findings of the QHE, the Hubble-effect galaxies and the process of seeing, result in the fundamental statement that the human ability of the observation of being refers exclusively to the existence of the differentiated structure of three-dimensional space.

1 Introduction

The discovery of a macroscopic quantization in the field of solid state physics, called quantum-Hall-effect (QHE) or Klitzing-effect [1], which was first experimentally observed by K. von Klitzing in 1980, opened the door to a new interpretation of various physical phenomena, such as the origin of the category time or dynamics in the field of mechanics, or thermodynamics and theory of heat [2], but also to some human-related biological processes [3]. The experimental findings of the QHE provided basic indications of the possibility of the existence of a specific space state, characterized by a division of three-dimensional space into a clearly separated, independent 2-D and 1-D dimensional space, called *Differentiated Structure of Space (DSS)* [2, 3]. This separation is recognizable e.g. by the simultaneous existence of two different forms of electromagnetism, effective not only in the context of MOS transistors, but also in the observation of the Hubble-effect (HE) galaxies, a process that is even reflected in the process of human vision, among other things. As shown in [3], the fundamental investigations into the existence of HE galaxies lead to the physical realization that the vision of humans, and to some extent also of animals, depends on the given DSS-state of space. The fundamental importance of the DSS-space state for humans becomes additionally apparent when we discuss the sound process physically. The experimental data of the investigations of human hearing carried out by H. Fletcher & W. A. Munson in 1933 [4], which show the relationships found between the sound pressure, the sound intensity and the loudness level on the one hand and the sound frequency on the other hand, presented here in Fig. 1, have so far been interpreted as biologically caused effects [5–7]. In contrast, the presented work shows that all the dependencies measured by Fletcher & Munson [4] (except for the conditions at the initial and final frequencies of human sound sensitivity are almost exclusively of physical origin, since, as is shown, they are due solely to the existence of the DSS-state of the air atmosphere.

Based on the data in Fig. 1, it must first be pointed out that for the investigation of sound intensity and sound pressure at the boundary condition of approximately 20° C and a sound velocity of $v_s = 343\,\mathrm{m/s}$, the frequency of $f_0 = 800\,\mathrm{Hz}$ proves to be a suitable boundary condition, since the physical processes involved in the realization of sound, arising at frequencies $f_x < f_0$, differ considerably from the processes at frequencies $f_x > f_0$. Therefore, we divide the physical analysis of the sound process into Part I and Part II.

2 The analysis of the Part I area of sound

Sound generation and its transmission are based on the properties of air. The air molecules as components of the air, which we may evaluate as an ideal gas in the closest approximation, are mainly subject to the influence of earth gravity. Since these forces can be regarded as constant in wide areas above the earth's surface, there is the special possibility of not paying attention to the gravitational forces when analysing the origin of sound. Following this idea, we can therefore assume that in our case the kinetic energy of the air molecules and their variability can be considered as purely electromagnetic in nature, which, however, as the experimental data show, is causally related to the temperature of the environment, i.e. more precisely, the fundamental electromagnetic energy of the air molecules is indirectly proportional to the ambient temperature, observable especially in the variable value of the speed of sound. This in turn means that the air can be considered a so-called Boltzmann gas, i.e. the electromagnetic energy of the air molecules can be put into a causal

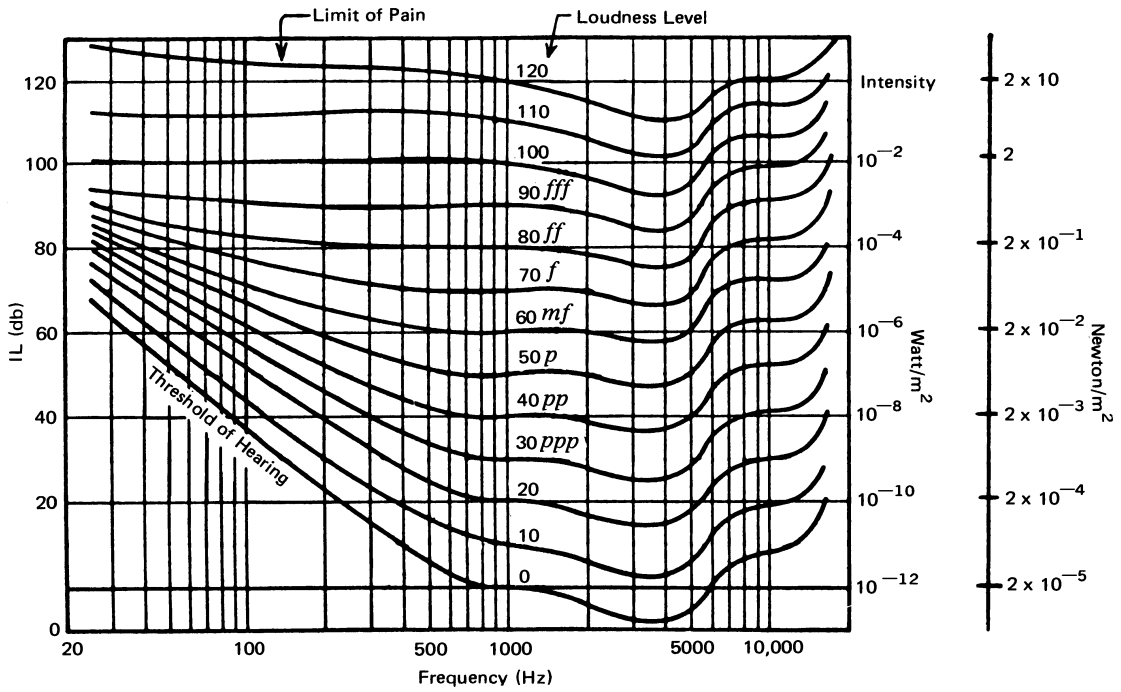

Fig. 1: Curves of equal loudness (Fletcher and Munson [4]). Reprinted from [6] by permission from *Springer Nature* (`https://rd.springer.com/chapter/10.1007/978-1-4615-9981-4_3`). This figure was first published by the *Journal of the Acoustical Society of America* and later adapted and expanded by *Springer Nature*.

relation to the Boltzmann energy kT. Based on these considerations and on the experimental data of the sound investigations of Fletcher & Munson, the following basic equation is formulated for the analysis of sound:

$$\frac{kT}{hf_x} = n_{\mathrm{B},x}\, v_{\mathrm{s}} \frac{p_x}{I_x} = n_{\mathrm{B},x} \frac{E_{p,x}}{E_{I,x}} \,. \qquad (1)$$

Here, k is the Boltzmann constant, T the temperature of the environment, h the Planck constant, f_x the given frequency, v_{s} the speed of sound, p_x the sound pressure, I_x the sound intensity, and $n_{\mathrm{B},x}$ the number of air molecules corresponding to the given frequency in order to reach the so-called hearing threshold, as shown in Fig. 1 [4]. The index x in (1) refers to the given frequency f_x for all quantities. The sound intensity energy $E_{I,x}$ occurring in (1) is given by $E_{I,x} = I_x/f_x$, and the corresponding sound pressure energy by $E_{p,x} = p_x l_x$, taking into account the sound velocity of $l_x f_x = v_{\mathrm{s}} = 343\,\mathrm{m/s}$, l_x represents the so-called sound length.

As can be seen from the definition of a so-called Boltzmann relation of sound presented in (1), this relation at the frequency f_x is given by the relation of the corresponding energies, which in turn can be determined by the indirect proportionality between the sound pressure p_x and the sound intensity I_x. In order to be in accordance with the experimental findings, the energy relation was, as shown in (1), additionally modified by the number of molecules $n_{\mathrm{B},x}$ considered at the given frequency f_x in order to be able to causally represent the variation of the energy relation. The fundamental importance and necessity of the introduction of the number $n_{\mathrm{B},x}$ will be presented in the following analysis, because this number $n_{\mathrm{B},x}$ is not only of decisive importance in the description of the course of the (human) hearing threshold at the frequencies of approximately $20\,\mathrm{Hz} < f_x < 800\,\mathrm{Hz}$, but it is the essential factor that helps to physically fathom the process of sound realization in nature.

In the following it is shown that the special form of the Boltzmann relation equation formulated in (1) can and must be used as a starting point for sound analysis.

3 The relationship between sound and the air-related DSS-condition

The experimental results of Fletcher & Munson [4] are not only fundamental for the description of human hearing, but, as is shown, are generally valid and therefore fundamental [5–7]. In the analysis to interpret the realization and propagation of sound, the following experimentally observed facts must be considered:

1) The sound intensity I_x and the sound pressure p_x are in a mutually causal relationship at any volume (indicated in phon*) and at any observed frequency. Special attention must be paid to the finding which reveals that a constant connection

*The phon is a unit of perceived loudness of pure tones, indicated in Fig. 1 as "Loudness Level".

is given between the square of the sound pressure, i.e. p_x^2, and the sound intensity I_x. This physically conditioned circumstance, which is valid for each sound intensity I_x and for each corresponding sound pressure p_x, namely at each frequency f_x [4], see Fig. 1, can be described by

$$\frac{p_x^2}{I_x} = \text{const.}\,. \tag{2}$$

This means that with an increase in sound intensity I_x (phon strength), the increase in sound pressure p_x must always be smaller than the increase in the associated sound intensity I_x

2) It should also be noted that the curves of equal loudness dependent on f_x, shown in Fig. 1 in phon, do not touch each other, i.e. the intensity distances, independent of the frequency(!), have almost the same values, i.e. the increase of the I_x-phon distances is almost always constant at a given frequency f_x. This important experimental finding indicates that the so-called loudness of the sound refers solely to the sound intensity I_x.

These two experimental findings show that the energy values characteristic of the air molecules, expressed in purely electromagnetic form using $E_{I,x} = I_x/F_x$ and $E_{p,x} = p_x l_x$, can be recorded and expressed in two different ways when sound is observed.

Here are a few remarks: The specific type of the DSS-air-state (Differentiated Space Structure state of air), seen in terms of the boundary conditions of the existence of the Hubble-effect (HE) galaxies [3], is to be sought in the theoretically possible cancellation of the gravitational effect of the Earth as a boundary condition for the emergence of the specific type of the DSS-air-state, described in the beginning of Part I.

The essential consequence of this cancellation is that the variability of the sound-related energies of the air molecules is limited to changes of electromagnetic nature alone. This means that, in contrast to the states observed in the HE galaxies, the molecules of air in the given DSS-state in this case show only purely electromagnetic variable effects, and that within the framework of our common three-dimensional understanding of space, they are separated into a so-called 2-D and a 1-D "space".

The special feature of this insight is that it clearly reveals for the first time that, "spatially" considered, air molecules as energy carriers can be observed in two different forms, i.e. "spatially" differentiated, whereas in our common, i.e. classical understanding of space, on the one hand the $E_{I,x}$-energy refers to the two-dimensionality of this energy, i.e. to the 2-D "space", which is interpreted as intensity energy, and on the other hand the $E_{p,x}$-energy refers to the one-dimensionality, i.e. to the 1-D "space", which is interpreted as pressure energy. However, the possibility of the existence of such a special state is only given if we may consider nature, evaluating in spatial categories, as differentiated, recorded as DSS-state. This specific spatial state was first discussed in 2017 in [2, pp. 33–34, 45, and 49–50], based on the analysis of the experimental findings of the quantum-Hall-effect published in 1980 by K. von Klitzing et al. [1], and its unusual existence was again proven by the analysis of HE galaxies [3]. Seen in this context, the analysis of the Fletcher & Munson data shown in Fig. 1 and its conclusion are of extraordinary importance, because they show that the possibility of sound formation is only given when this specific "differentiated space state", unusual to our daily understanding of space, is given in the air and thus the boundary condition for the formation of sound is real. The correctness of such an unusual model, which was presented on the basis of the specific electromagnetic DSS-state of the air, can be confirmed impressively and convincingly by a further detailed analysis of the experimental data of Fletcher & Munson.

The essential functional significance of the number of molecules $n_{\mathrm{B},x}$ given in (1) at the given intensity I_x is to guarantee the DSS-state of the air in the form of (1) and (2), which physically reflect the limit value of the hearing threshold as equations. This in turn means that, for the experimentally given values of sound intensity I_x and sound pressure p_x, we can use (1) to write the specific magnitude of the value $n_{\mathrm{B},x}$ as a function of the frequency f_x, where we have to define the frequency f_x, normalized in relation to the reference frequency f_0, as the relation $n_{f,x} = f_x/f_0$. And in order to be able to mathematically record the homogeneity of the air in the DSS-state, it is also necessary to define the relation $n_{p,x} = p_x/p_0$, i.e. to set the sound pressure p_x in relation to the standard value of the air pressure p_0 by means of the number $n_{p,x}$. Starting from the limit values $I_0 = 1 \times 10^{-12}\,\mathrm{W/m^2}$ and $p_0 = 2 \times 10^{-5}\,\mathrm{N/m^2}$ given in Fig. 1, for every frequency we then obtain the constant value $(n_{\mathrm{B},x}/n_{f,x}\,n_{p,x}) = 1.122$. The constancy of this value, which captures the homogeneity of the air condition, and above all the small size of this dimensionless value 1.122 suggests the possibility of replacing this value by the number 1, followed by the associated necessity to modify the experimentally given values I_x and p_x accordingly. In order to minimize the change of the value p_x^2/I_x, the validity of which must be maintained, it is sufficient to reduce the value from $I_0 = 1{\times}10^{-12}\,\mathrm{W/m^2}$ to $I_0 = 0.9{\times}10^{-12}\,\mathrm{W/m^2}$, while keeping the value $p_0 = 2 \times 10^{-5}\,\mathrm{N/m^2}$. The smallness of the correction of the I_0 value is fully acceptable, as it is within the given measuring accuracy.

If we now try to represent a causal connection of the values $n_{\mathrm{B},x}/n_{f,x}$ to the experimental values $n_{\mathrm{exp},x} = I_x/I_0$, which are given by the known data of [4], by means of an equation, an extraordinarily meaningful connection, valid for all frequencies $f_x < f_0$ emerges, which can be described by

$$n_{\mathrm{exp},x} = \left(\frac{n_{\mathrm{B},x}}{n_{f,x}}\right)^2 . \tag{3}$$

Using a simple calculation, it can be shown that (3) is a com-

pellingly necessary causal consequence of the hearing process (1) and (2).

Since in the framework of the DSS-model, the values of $n_{\mathrm{exp},x}$ readable in Fig. 1 can be unambiguously related to the specific energies of the 2-D space, i.e. to the sound-intensity radiations I_x, but the relation values $n_{\mathrm{B},x}/n_{f,x}$ within the framework of $(n_{\mathrm{B},x}/n_{f,x}\, n_{p,x}) = 1$ can be related to the specific energies of the 1-D space, i.e. with the sound-pressure values p_x, the simple and clear form of (3) proves that every frequency $x < 800$ Hz must be the condition of the differentiated state of space. Furthermore, (3) testifies that this DSS-state is necessary as a boundary condition in order to reach the sound limit by means of the I_x and p_x limit values, i.e. to generate and transmit sound in our environment of the earth's surface.

The number $n_{\mathrm{B},x}$ in (1) is also of great importance for non-physical reasons: As shown, it is necessary for the realization of the DSS-state and thus brings the mental development of man to fruition. The analysis of the sound indirectly shows clearly that the acoustic communication between humans is solely caused by the existence of this DSS-state of the air. In fact, an interesting analogy to the process of seeing and thus to the human perception process in general can be seen, because the process of seeing, as shown in [3] and explained by the existence of specifically suitable uvula and rod cells, is also based on the existence of the DSS-state, as it were, in the field of optics, i.e. light.

4 The analysis of the Part II region of sound and the analogies to the integral and fractional quantum-Hall-effect

On the basis of the sound interpretation model presented in Part I, it is clear that sound mediation at frequencies f_x above the limit value f_0, i.e. at $f_x > f_0$, must be fundamentally different from the process presented in Part I, because once the sound intensity value I_0 is reached, there should be no further normal possibility of reaching the DSS-state for the production of sound. In fact, however, it is observed that initially, with increasing values from f_0 to approximately $f_x =$ 1300 Hz, the hearing threshold limit value of I_0, given by approximately 1×10^{-12} W/m^2, remains quasi-constant in order to reach a new minimum in I_x of approximately $2{\times}10^{-13}$W/m^2 at $f_x = 3200$ Hz. Afterwards, starting at $f_x = 3200$ Hz, an increase in the hearing threshold limit values I_x is observed with increasing f_x values, followed – which is particularly important – by an indication of a small decrease in the I_x limit values at $f_x = 1.28 \times 10^4$ Hz. After that, a strong increase of the curves of equal loudness is measured further on with increasing frequency, and to stop at $f_x = 1.6 \times 10^4$ Hz, at all phon levels. In order to be able to interpret these experimentally observed complex I_x-f_x-dependencies, we have to assume the existence of two different processes which, as we will show, relate to the 2-D space component on the one hand and to the 1-D space component on the other.

One process concerns the interpretation of the minima of I_x at $f_x = 3.2x10^3$ Hz and at $f_x = 1.28 \times 10^4$ Hz: They can be interpreted as the consequence of an area quantization given in the two-dimensional space part, describable with the quantum number 4 and 16. With this, it is postulated here that – despite the sound limit value of $I_0 = 1{\times}10^{-12}$ W, as explained in Part I – also at higher frequencies, i.e. at $f_x = 3.2{\times}10^3$ Hz and $f_x = 1.28 \times 10^4$ Hz – which is due to this experimentally observable macroscopic 2-D quantization – an air-related DSS-state can be present, which means that in nature it is possible to also generate sound at $f_x > 8 \times 10^2$ Hz.

An analogous macroscopic quantization related to two-dimensional space, namely the quantization discovered by K. von Klitzing, was renamed in later years to *Integral quantum-Hall-effect* (IQHE), observed at the quantum numbers 2, 4, (6), 8, 12 and 16 [2, 8, 9]. In order to be able to consider the assumed two-dimensional surface quantization for sound as physically acceptable in comparison with IQHE quantization, some additional remarks are necessary: In the IQHE, the magnetic field B is in causal interaction with the electron density N_{e}, i.e. in the DSS-space model with the 2-D space state. In the so-called Fractional quantum-Hall-effect (FQHE), discovered for the first time by D. C. Tsui et al. at GaAs–$\mathrm{Al}_x\mathrm{Ga}_{(1-x)}$As heterostructures [10], the magnetic field B_x corresponds to a frequency f_x. This model of the different functioning of the magnetic field, given on the one hand by the IQHE and on the other hand by the FQHE, could actually be indirectly confirmed by targeted measurements within the QHE, as shown in [11, pp. 34–42]. This means that the magnitude of the magnetic field, which is expressed in Tesla units in the MKSA unit system, can also be expressed simply by the quantity "frequency" in the MKS unit system, which makes a possible analogy of the process between the sound effect and the QHE appear possible.

As already mentioned in [3], the QHE state is always present in the DSS-space state. As a consequence, IQHE quantization is to be interpreted as a 2-D space quantization, in contrast to FQHE quantization, which can be interpreted as a 1-D space quantization. This insight leads us to the additional conclusion that the discovery of the length-related harmony theory, which stems from Pythagoras, actually reflects a 1-D space quantization, which is today presented in every musical harmony theory as a consequence of the existence of overtones that always belong to the fundamental tones. But this important insight must be further expanded by the discovery of the existence of deep harmony tones associated with each fundamental tone, recognizable by the existence of the so-called deep combination tones, see [6, p. 38]. It is evident that the existence of these deep harmony tones can be understood as an analogy to the existence of FQHE quantization. This leads to the conclusion, which is important for our analysis, that the unexpected sound generation at frequencies $f_x > 8 \times 10^2$ Hz according to our model must be a consequence of the existence of 2-D space and 1-D space quanti-

zations associated with the given fundamental tones, a model which is fully consistent with the extensive experimental findings of both the IQHE and the FQHE. In addition, an interesting fact can be seen that the QHE, where the observation of the FQHE was initially completely unexpected, fully reflects this "unexpectedness" when listening to deep harmony tones [6]. The relatively small probability of low combination tones therefore means that a strong increase in the hearing threshold limit values I_x is to be expected with increasing frequency, which, as Fig. 1 shows, was actually observed.

The found sudden stop of sound generation at $f_x = 1.6 \times 10^4$ Hz at all phon values can only be interpreted in such a way that in humans in the cochlea there are no stereocilia for these high frequencies that would process such electromagnetic signals. This means that we can only speak of a physiological effect in this case of the general cessation of sound sensitivity at extremely high frequencies. The same reasoning can be applied to the description of the sudden occurrence of hearing ability observed at all phon levels, which occurs in humans at about 20 Hz. This means that the onset of hearing must be physiological and therefore cannot be attributed to a physical effect. Otherwise, as explained, the sound data of Fig. 1 observed by Fletcher & Munson can be attributed to physical processes, which all, without exception, indicate the existence of an air-related DSS-condition.

5 Summary and conclusion

Based on the analysis of experimental data of the quantum-Hall-effect [1], it was found that in nature, spatially speaking, a specific state can exist, called differentiated structure of three-dimensional space (DSS-state) [2, 3]. Based on this discovery not only a novel description of the category "time" as a consequence of localized, i.e. 1-D related electromagnetism could be presented [2, page 45], but also the background of the existence of the Hubble-effect galaxies as well as the process of human vision based on the DSS-state could be physically described [3]. This visual model, which associates the rod cells with the specific 1-D space state and the uvula cells with the specific 2-D space state, does not differ in any essential point from the process of human hearing based on the process of the DSS-state, as the analysis of the Fletcher & Munson data reveal, revealing also the analogy between the processes of sound generation and those of the quantum Hall effect. Thus, within the DSS-model, the air molecules are the "carriers" of both the 1-D space structures in terms of sound pressure p_x, and the 2-D space structures in terms of sound intensity I_x. The detailed analysis of the Fletcher & Munson data also clearly indicated that the limit of the hearing threshold is determined by the existence of the DSS-air-state. This experimental discovery is a fundamentally important discovery from a physical point of view because it proves that the process of hearing is conditioned by the existence of the DSS-state of the air molecules. Consequently, it can be concluded that the DSS-state as the basis of hearing, but also of seeing, as shown in [3], is the fundamental state that enables human kind to mentally recognize what is happening in nature, i.e. all being. But this also means that the DSS-state is the fundamental physical background which is the starting point for all human evaluations and interpretations of both static and dynamic, i.e. time-related processes in nature [2, 3, 11] and should therefore always be taken into consideration additionally.

Acknowledgements

The author is indebted to *Prof. Walter Hansch*, University of Armed Forces, Muenchen, for the support of this subject and for his critical comments to several statements of this paper. He would also like to thank *Torsten Sulima* for the scientific-technical assistance and *Franz Wittmann*, Technical University, Muenchen, for his co-operation to select the proper journal for publication. Finally, a special thanks to *Alexander Hirler* for the translation of the text into English as well as for the extensive completion of the paper for printable publication.

Received on February 4, 2020

References

1. von Klitzing K., Dorda G. and Pepper M. New Method for high-accuracy determination of fine-structure constant based on quantized Hall resistance. Phys. Rev. Lett., 1980, v. 45, 494–497.
2. Dorda G. Die Struktur von Raum und Zeit und die Interpretation der Wärme. Cuvillier Verlag, Goettingen, ISBN 978-3-7369-9388-4, eISBN 978-3-7369-8388-5, 2016.
3. Dorda G. The Interpretation of the Hubble-Effect and of Human Vision Based on the Differentiated Structure of Space. Prog. Phys., 2020, v. 16 (1), 3–9.
4. Fletcher H. and Munson W. A. Loudness, its definition, measurement and calculation. J. Acoust. Soc. Am., 1933, v. 5, 82.
5. Mende D. and Simon G. Physik. Gleichungen und Tabellen. Carl Hanser Verlag, Fachbuchverlag Leipzig, Muenchen, 2013.
6. Roederer J. G. Introduction to the Physics and Phsychophysics of Music. Heidelberg Science Library, Springer-Verlag, New York, 1973. In german: Physikalische und psychoakustische Grundlagen der Musik. Springer-Verlag, Berlin, Heidelberg, 1977.
7. Breuer H. and Breuer R. Atlas zur Physik. Deutscher Taschenbuch Verlag GmbH & Co., Muenchen, 1987/1988.
8. Wittmann F. Magnetotransport am zweidimensionalen Elektronensystem von Silizium-MOS-Inversionsschichten. Dissertation, University of Armed Forces, Muenchen, Institute of Physics, 1992.
9. Suen Y. W., Jo J., Santos M. B., Engel L. W., Hwang S. W. and Shayegan M. Missing integral quantum Hall effect in a wide single quantum well. Phys. Rev. B, 1991, v. 44, 5947–5950.
10. Tsui W. A., Störmer H. L. and Gossard A. C. Two-Dimensional Magnetotransport in the Extreme Quantum Limit. Phys. Rev. Lett., 1982, v. 48, 1559–1561.
11. Dorda G. Quantisierte Zeit und die Vereinheitlichung von Gravitation und Elektromagnetismus. Cuvillier Verlag, Goettingen, ISBN 978-3-86955-240-8, 2010. In particular: pp. 34–42, Fig. 2.1 and 2.2, and Eq. (2.14).

A Pedestrian Derivation of Heisenberg's Uncertainty Principle on Stochastic Phase-Space

G. G. Nyambuya

National University of Science and Technology, Faculty of Applied Sciences – Department of Applied Physics, Fundamental Theoretical and Astrophysics Group, P. O. Box 939, Ascot, Bulawayo, Republic of Zimbabwe.
E-mail: physicist.ggn@gmail.com

Without using the common methodologies of quantum mechanics – albeit, methodologies that always involve some demanding mathematical concepts, we herein demonstrate that one can derive in a very natural, logical and trivial manner, Heisenberg's quantum mechanical uncertainty principle on the new phase-space whose name we have herein coined *Stochastic Phase-Space*. This stochastic phase-space – is a mathematical space upon which we previously demonstrated [2] the naturally implied existence of the First Law of Thermodynamics from Liouville's theorem. In addition to Heisenberg's uncertainty principle, we derive an upper limiting uncertainty principle and it is seen that this upper limiting uncertainty principle describes non-ponderable tachyonic particles.

It must have been one evening after midnight when I suddenly remembered my conversation with Einstein and particularly his statement, 'It is the theory which decides what we can observe.' I was immediately convinced that the key to the gate that had been closed for so long must be sought right here. I decided to go on a nocturnal walk through Faelled Park and to think further about the matter ... Werner Karl Heisenberg (1901-1976). Adapted from [3, p. 6].

1 Introduction

The present paper is the third in a five part series where we make the endeavour to understand the meaning and origins of what drives the unidirectional forward arrow of thermodynamic entropy. In our first instalment [4, hereafter Paper I], we demonstrated that the *Second Law of Thermodynamics* (SLT) can possibly be understood if there exists a new kind of probability measure, p_r, which drives thermodynamic processes and this thermodynamic probability evolves in such a manner that, whenever this thermodynamic probability changes its value when a system moves from one state to the next, it always takes higher values than the value it previously held – i.e. $dp_r \geq 0$, at all physical and material times. In a nutshell, thermodynamic events will at the very least, progressively evolve from a probabilistically less likely state – to a probabilistically more likely state. Such an evolution sequence is what is naturally expected from probability calculus anchored on common binary logic where natural systems are expected to steadily progress into their most likely state.

In the construction of our new ideas, naturally, we expected that this thermodynamic probability p_r, would turn out to be the usual Boltzmann probability, i.e.

$$p_r = Z^{-1} \exp\left(-E_r/k_{\mathrm{B}}T\right) ,$$

where p_r is the probability that for a system at temperature T, the microstate with energy E_r, will be occupied and Z is the partition function. As will be demonstrated in the sequel paper [5, hereafter Paper IV], this probability p_r, cannot be the usual Boltzmann probability, but a new kind of probability associated not with the occupation of the given microstate, but its evolution; where by evolution, it is understood to mean – moving or progression from its present state to a new state altogether.

Further on, in the paper [2, hereafter Paper II], we demonstrated that Liouville's theorem [6] can actually be viewed as a subtle statement of the *First Law of Thermodynamics* (FLT). This we did by defining the Liouville density function, $\delta\varrho$, in-terms of some new physical quantity, $\delta\mathcal{S}_{\mathrm{TD}}$, that we called the *thermodynamic phase* (or the *thermodynamic action*), i.e. $\delta\varrho = \exp(\delta\mathcal{S}_{\mathrm{TD}}/\hbar)$, where $\hbar$ is Planck's normalized constant. Furthermore, in Paper IV, we shall identify $\delta\varrho$ as the appropriate thermodynamic probability of evolution, that is, the thermodynamic probability responsible for the SLT.

In the present paper, we shall demonstrate that when cast as a probability measure, $\delta\varrho$ naturally yields the universally celebrated quantum mechanical uncertainty principle of Heisenberg [1]. In addition to Heisenberg's lower limiting (i.e. $\delta E\,\delta t \geq \hbar/2$ and $\delta p\,\delta x \geq \hbar/2$) uncertainty principle, we derive an upper limiting uncertainty principle – i.e. $\delta E\,\delta t \leq \hbar/2$ and $\delta p\,\delta x \leq \hbar/2$. As initially pointed out in [7], this upper limiting uncertainty principle strongly appears to describe non-ponderable tachyonic particles.

Without a doubt, Heisenberg's quantum mechanical uncertainty principle is certainly one of the most famous aspects of quantum mechanics and this very aspect of the theory is universally regarded as the most distinctive feature of the theory. It is a unique characteristic feature which makes quan-

tum mechanics differ radically from all classical theories of the physical world. For example, the uncertainty principle for position and momentum $\delta p\,\delta x \leq \hbar/2$ states that one cannot simultaneously assign exact values to the position and momentum of a physical system. Rather, these quantities can only be determined with some intrinsic, inherent and characteristic uncertainties that cannot – simultaneously – become arbitrarily small.

In its popular understanding, the Heisenberg uncertainty principle is assumed to be a principle to do with the accuracy in the results of measurements of physical variables such as momentum, position, energy, *etc*. Strictly speaking, this is not true. For example Millette [8] argues that the Heisenberg uncertainty principle arises from the dependency of momentum on wave number ($\boldsymbol{p} = \hbar\boldsymbol{k}$) that exists at the quantum level, and that ultimately the uncertainty principle is purely a relationship between the effective widths of Fourier transform pairs of conjugate variables. Our ideas propagated herein do support these views and as an addition, these quantum mechanical uncertainties associated with physical variables are seen to arise from pure stochastic processes occurring on some new phase-space that we have coined the stochastic phase space.

Now, in closing this introductory section, we shall give a synopsis of the present paper – i.e. this paper is organised as follows: in §2, we derive the uncertainty relations that govern ordinary ponderable matter and thereafter in §3, we derive the uncertainty relations that govern exotic non-ponderable matter. Lastly, in §4, we give a general discussion.

2 Derivation of the uncertainly principle

As stated in the introductory section, we are going to demonstrate in this section (i.e. in §2.2) that one can derive in a very natural and logical manner, the position-momentum and energy-time quantum mechanical Heisenberg uncertainty principle on the newly proposed *Stochastic Phase-Space* (hereafter $\delta\Gamma$-space) upon which we demonstrated [2] the naturally implied existence of the FLT from Liouville's theorem. In addition to Heisenberg's uncertainty principle, we will also derive in §3, upper limiting position-momentum and energy-time uncertainty principles and these upper limiting uncertainty principles describe non-ponderable tachyonic particles.

Before we proceed, we need to explain what it is we mean by *upper limiting uncertainty principle*. If there is an upper limiting uncertainty principle, from the viewpoint of common logic, there also must be a *lower limiting uncertainty principle*. Indeed, the uncertainty principle of Heisenberg is a lower limiting uncertainty principle because it gives the lowest possible value that the product of the energy (δE) & time (δt), and momentum (δp) & position (δr) uncertainties would ever take. That is to say, the products $\delta E\,\delta t$ and $\delta p\,\delta r$, can take whatever value they can or may take for so long as this value does not exceed the minimum threshold value of $\hbar/2$, hence, in this way, it becomes pristine clear that the Heisenberg uncertainty principle ($\delta E\,\delta t \geq \hbar/2$ and $\delta p\,\delta r \geq \hbar/2$) is indeed a lower limiting uncertainty principle.

Now, if – by the sleight of hand, we are to flip the sign in the Heisenberg lower limiting uncertainty principle so that we now have $\delta E\,\delta t \leq \hbar/2$ and $\delta p\,\delta r \leq \hbar/2$, the resulting uncertainty principle is an upper limiting uncertainty principle since it now gives an upper limit in the value that the products ($\delta E\,\delta t$ and $\delta p\,\delta r$) of the uncertainties can ever take. Whence, we must hasten at this point and say we already have discussed the implications of a upper limiting uncertainty principle in our earlier works (i.e. in [7]) where we argued that if such particle exist to being with, not only will they travel at superluminal speeds – they also will have to be non-ponderable as-well; that is to say, they must be invisible and absolutely permeable. In simpler colloquial terms, such particles must be capable of passing through solid walls with no hindrance at all whatsoever.

2.1 Preliminaries

Now, before we can go on to present our derivation of Heisenberg's uncertainty principle in §2.2, we will need to set-up the stage for that event. First, in order for that, we shall give in §2.1.1, a description of the particle system that we shall consider, and, in §2.1.2, we shall describe the normalization across all spacetime for the thermodynamic probability function $\delta\varrho$ and in §2.1.3, we shall describe the normalization across a given space-and-momentum axis for the thermodynamic probability function, $\delta\varrho$. Lastly, in §2.1.4, we present some useful mathematical equations that we will need in our endeavours to derive the Heisenberg uncertainty principle.

2.1.1 Description of particle system

As initially suggested in Paper II, we envisage the existence of two mutually exclusive spacetimes and these we have termed – the *Classical Canonical Spacetime* (hereafter, CC-Spacetime), and, the *non-Canonical Spacetime* (hereafter, NC-Spacetime). The NC-Spacetime can also be called the *Stochastic Spacetime*. On the deterministic CC-Spacetime, a particle has its usual deterministic classical four position (x, y, z, c_0t) that we are used to know, while on the non-deterministic NC-Spacetime, the non-deterministic jittery quantum randomness and fuzziness associated with the usual deterministic classical canonical position ($\delta x, \delta y, \delta z, c_0\delta t$) are defined on this non-deterministic NC-Spacetime.

For example, considering only the x-axis, a particle will have x as its canonical position and δx as its associated non-canonical position as defined on the NC-Spacetime. It is δx that should give this particle the quantum fuzziness leading to the weird quantum probabilistic nature of physical systems. For the human observer – assuming zero human-induced error in measuring the position of the particle – the effective position $\hat{x}$ of the particle at any given time is $\hat{x} = x \pm \delta x$. So, in general, x^μ is the canonical four position of the particle and

δx^μ is the associated quantum randomness that leads to the mysterious, strange and bizarre fuzzy quantum probabilistic nature of natural systems.

In our description above, when we say particle, we mean a point-particle – i.e. particles of zero spatial dimension, hence zero volume. Obviously, there will be some trouble in accepting this – as point-particles, are – in physics – no more than idealization of real finite-sized particles that are smeared-out in a finite region of space. That is, a point-particle is in general an appropriate or convenient representation of any object whatever its size, shape, and structure – all these details of size, shape, and structure, *etc*, are irrelevant under the general particle model.

To further complicate this issue of the particle description of matter, we all know pretty well that the existence of point-particles is strictly forbade by Heisenberg's uncertainty principle. With this in mind, of these particles, what we envisage is them having all their charge such as their gravitational mass and electrical charge being concentrated on that very single point with this point being trapped in the finite sized spherical region of radius: $\delta r = \sqrt{(\delta x)^2 + (\delta y)^2 + (\delta z)^2}$, with the the centre of this finite spherical region fixed in space about the canonical position (x, y, z). Because of the fields that the trapped charged point-particle carries – i.e. fields with which this particle interacts with other particles; the fuzzy, random wandering and dotting back-and-forth, up-and-about of this particle inside this finite region should create the impression of a solid billiard-like ball of radius δr with oft cause the bulk of its charge (gravitational, electrical, *etc*) expected to be trapped in this spherical region. Surely, such a particle-system will be localized and it will have the property of ponderability that we experience with electrons, protons, *etc*. Let us call such a particle-system, a *Ponderable Material Particle*.

Now, for a minute, let us assume that the above described point-particle is not trapped. If that were the case, then, what is it that we are going to have for such a particle-system? Clearly, it must be an unbounded point-particle that is free to roam all of the Universe's length, breath and depth – from one end of the Universe, to the other in an instant! Such a particle-system should have its charge (gravitational, electrical, *etc*) spread-out evenly throughout the entire Universe. Not only this, while such a particle-system will have a definite fixed canonical position, the entire particle-system must be invisible as it will not have the property of ponderability (localization). Likewise, let us call such a particle-system, a *non-Ponderable Material Particle*.

Now, as shall soon become clear in our derivation of Heisenberg's uncertainty principle, two classes of particles will emerge and the first is that class whose random quantum fuzziness as described on the NC-Spacetime obeys the usual quantum mechanical uncertainty principle of Heisenberg, i.e. $\delta E\, \delta t \geq \hbar/2$ and $\delta p\, \delta r \geq \hbar/2$; and these particles travel at speeds less than, or equal to the speed of light in *vacuo*. The second class is that of particles whose quantum fuzziness as described on the NC-Spacetime obeys not the usual quantum mechanical uncertainty principle Heisenberg, but obey the converse of Heisenberg's uncertainty principle, namely $\delta E\, \delta t \leq \hbar$ and $\delta p\, \delta r \leq \hbar$ and these particles travel at speeds that are at the very least, greater than the speed of light in *vacuo*.

At this juncture, we feel very strongly that we have prepared our reader to meet the strange new proposal of invisible particles that travel at superluminal speeds, thus – assuming the reader somewhat accepts or at the very least, finds some modicum of sense in what we have had to say above – we shall quietly proceed to the main business of this paper – that of demonstrating the natural existence of Heisenberg's uncertainty principle on the proposed NC-Spacetime where the jittery, fuzzy quantum randomness has here been defined.

2.1.2 Normalization across all space

If $\delta\varrho$ is assumed to be some probability function, then it must be normalizable. Normalization is oft cause one of the most fundamental and most basic properties that a probability function must satisfy. As is the norm: normalization of this function, $\delta\varrho$, across all of the six dimensions of $\delta\Gamma$-space requires that:

$$\frac{1}{\hbar^3}\overbrace{\underbrace{\int\int\int}_{\delta p_{\min}}}^{\delta p_{\max}}\overbrace{\underbrace{\int\int\int}_{\delta r_{\min}}}^{\delta r_{\max}}(\delta\varrho_+)\, d^3x d^3p = 1, \tag{1}$$

where: $\delta\varrho_+ = \delta\varrho_x^+ \delta\varrho_y^+ \delta\varrho_z^+ \delta\varrho_0^+$. In writing $\delta\varrho$ in (1), we have appended a subscript + and this is not a mistake, it is deliberate. This + appendage has been instituted – for latter purposes – so that a distinction can be made between a thermodynamic system with a positive $\delta\mathcal{S}_{\rm TD}$ thermodynamic phase (action) and that with a negative $-\delta\mathcal{S}_{\rm TD}$ thermodynamic phase (action), i.e.: $\delta\varrho_+ = \delta\varrho_+(\delta\mathcal{S}_{\rm TD})$, while: $\delta\varrho_- = \delta\varrho_-(-\delta\mathcal{S}_{\rm TD})$. The two functions describe two different kinds of phenomenon, namely $\delta\varrho_+$ describes ponderable matter as we know it, while $\delta\varrho_-$ describes some (exotic) non-ponderable (invisible) tachyonic matter. This shall be made clear as we go, hence the need to make a distinction of $\delta\varrho_+$ and $\delta\varrho_-$.

Now, the normalization in (1) is the probability of finding the particle in the spatial $(\hat{r})$ and momentum $(\hat{p})$ region:

$$\begin{aligned} \delta r_{\min} \leq \quad & \hat{r} \quad \leq \delta r_{\max} \\ \delta p_{\min} \leq \quad & \hat{p} \quad \leq \delta p_{\max}\,, \end{aligned} \tag{2}$$

where $\hat{r}$ and $\hat{p}$ are the actual measured radial coordinate and magnitude of the momentum of the particle as measured from the spatial canonical point of origin of the particle (system) in question.

2.1.3 Normalization across a given axis

Now, given that $\delta\varrho_+ = \exp(\delta\mathcal{S}_{\rm TD}/\hbar)$, where:

$$\delta\mathcal{S}_{\rm TD} = \delta\boldsymbol{p}\cdot\delta\boldsymbol{r} - \delta E\delta t = \delta p_\mu \delta x^\mu\,, \tag{3}$$

it follows that the quantities $\delta\varrho_x^+$, $\delta\varrho_y^+$, $\delta\varrho_z^+$, $\delta\varrho_0^+$ are such that:

$$\begin{aligned}
\delta\varrho_x^+ &= \exp\left(\frac{\delta\mathcal{S}_x}{\hbar}\right) = \exp\left(\frac{\delta p_x\delta x}{\hbar}\right) \quad \ldots \quad (a)\\
\delta\varrho_y^+ &= \exp\left(\frac{\delta\mathcal{S}_y}{\hbar}\right) = \exp\left(\frac{\delta p_y\delta y}{\hbar}\right) \quad \ldots \quad (b)\\
\delta\varrho_z^+ &= \exp\left(\frac{\delta\mathcal{S}_z}{\hbar}\right) = \exp\left(\frac{\delta p_z\delta z}{\hbar}\right) \quad \ldots \quad (c)\\
\delta\varrho_0^+ &= \exp\left(-\frac{\delta\mathcal{S}_0}{\hbar}\right) = \exp\left(-\frac{\delta E\delta t}{\hbar}\right) \quad \ldots \quad (d)
\end{aligned} \tag{4}$$

where oft cause $\delta\mathcal{S}_x = \delta p_x\delta x$, $\delta\mathcal{S}_y = \delta p_y\delta y$, $\delta\mathcal{S}_z = \delta p_z\delta z$, and, $\delta\mathcal{S}_0 = \delta p_0\delta x_0 = \delta E\delta t$. Clearly, written in this manner, these functions $\delta\varrho_x^+$, $\delta\varrho_y^+$, $\delta\varrho_z^+$, $\delta\varrho_0^+$ are the thermodynamic probability evolution functions describing the particle across the δx-δp_x axis, δy-δp_y axis, δz-δp_z axis, and the δt-δE axis respectively.

The probability of finding the particle along the x-p_x, y-p_y, z-p_z and t-E axis respectively, in the region of its bounds is unity and this is expressed:

$$\frac{1}{\hbar}\int_{\delta p_{\rm min}}^{\delta p_{\rm max}}\int_{\delta r_{\rm min}}^{\delta r_{\rm max}} (\delta\varrho_x^+)\,dxdp_x = 1\,, \tag{5}$$

$$\frac{1}{\hbar}\int_{\delta p_{\rm min}}^{\delta p_{\rm max}}\int_{\delta r_{\rm min}}^{\delta r_{\rm max}} \left(\delta\varrho_y^+\right)dydp_y = 1\,, \tag{6}$$

$$\frac{1}{\hbar}\int_{\delta p_{\rm min}}^{\delta p_{\rm max}}\int_{\delta r_{\rm min}}^{\delta r_{\rm max}} \left(\delta\varrho_z^+\right)dzdp_z = 1\,, \tag{7}$$

$$\frac{1}{\hbar}\int_{\delta E_{\rm min}}^{\delta E_{\rm max}}\int_{\delta t_{\rm min}}^{\delta t_{\rm max}} \left(\delta\varrho_0^+\right)dtdE = 1\,. \tag{8}$$

Before we can deduce the Heisenberg uncertainty principle from the above equations (5)-(8), we shall lay down some necessary mathematical formulae.

2.1.4 Necessary mathematical equations

In our derivation of Heisenberg's uncertainty principle in §2.2 and §2.3, we are going to encounter the function e^{ax}/x, where x is the variable and a is some constant. Of this function, we will need to know its integral and limit as $x \mapsto 0$. It is not difficult to show that:

$$\int\left(\frac{e^{ax}}{x}\right)dx = \frac{e^{ax}}{ax} + k\,, \tag{9}$$

where k is some integration constant and:

$$\lim_{x\mapsto 0}\left(\frac{e^{ax}}{x}\right) = a\,. \tag{10}$$

Now, we are ready to derive Heisenberg's uncertainty principle (and more).

2.2 Position-momentum uncertainty

In this section, we are now going to derive a lower and upper bound uncertainty principle for momentum and position. Taking (5) and substituting $\delta\varrho_x^+ = \exp(\delta p_x\delta x/\hbar)$, we will have:

$$\frac{1}{\hbar}\int_{\delta p_{\rm min}}^{\delta p_{\rm max}}\int_{\delta r_{\rm min}}^{\delta r_{\rm max}} \exp\left(\frac{\delta p_x\delta x}{\hbar}\right)dxdp_x = 1\,. \tag{11}$$

Now, using the result of (9) to integrate (11) with respect to x, and evaluating the resulting integral, we will have:

$$\int_{\delta p_{\rm min}}^{\delta p_{\rm max}}\left(\frac{e^{\delta p_x\delta r_{\rm max}/\hbar} - e^{\delta p_x\delta r_{\rm min}/\hbar}}{\delta p_x}\right)dp_x = 1\,. \tag{12}$$

Further, we need to integrate (12) with respect to p_x. In doing so, we will encounter again an integral of the form given in (9). The result of this integration is therefore:

$$\hbar\left[\frac{e^{\delta p_x\delta r_{\rm max}/\hbar}}{\delta p_x\delta r_{\rm max}} - \frac{e^{\delta p_x\delta r_{\rm min}/\hbar}}{\delta p_x\delta r_{\rm min}}\right]_{\delta p_{\rm min}}^{\delta p_{\rm max}} = 1\,. \tag{13}$$

Evaluating this, we will have:

$$\begin{aligned}
&\overbrace{\frac{\hbar e^{\delta p_{\rm max}\delta r_{\rm max}/\hbar}}{\delta p_{\rm max}\delta r_{\rm max}}}^{\textbf{Term I}} - \overbrace{\frac{\hbar e^{\delta p_{\rm min}\delta r_{\rm max}/\hbar}}{\delta p_{\rm min}\delta r_{\rm max}}}^{\textbf{Term II}}\\
&\qquad - \underbrace{\frac{\hbar e^{\delta p_{\rm max}\delta r_{\rm min}/\hbar}}{\delta p_{\rm max}\delta r_{\rm min}}}_{\textbf{Term III}} + \underbrace{\frac{\hbar e^{\delta p_{\rm min}\delta r_{\rm min}/\hbar}}{\delta p_{\rm min}\delta r_{\rm min}}}_{\textbf{Term IV}} = 1\,.
\end{aligned} \tag{14}$$

Furthermore, for ponderable material particles, as discussed in §2.1.1, we want our particle system to be bounded (trapped) between the regions $0 \le \hat{r} \le \delta r_{\rm max}$ and $0 \le \hat{p}_x \le \delta p_{\rm max}$. This means that we must evaluate (14) in the limits $\delta r_{\rm min} \mapsto 0$ and $\delta p_{\rm min} \mapsto 0$.

Now, making use of the limit given (10), it follows that as:

$$\begin{aligned}
\delta r_{\rm min} &\mapsto 0\,,\\
\delta p_{\rm min} &\mapsto 0\,,
\end{aligned} \tag{15}$$

for the Terms I, II, III and IV in (14), we will have:

$$\begin{aligned}
\text{Term I} &= \frac{\dfrac{\delta p_{\rm max}\delta r_{\rm max}}{\hbar}}{\delta p_{\rm max}\delta r_{\rm max}}\,,\\
\text{Term II} &\mapsto 1\,,\\
\text{Term III} &\mapsto 1\,,\\
\text{Term IV} &\mapsto 1\,,
\end{aligned} \tag{16}$$

hence from (16), it follows from this that (14) will reduce to:

$$\hbar e^{\delta p_{\rm max}\delta r_{\rm max}/\hbar}/\delta p_{\rm max}\delta r_{\rm max} - 1 = 1\,,$$

where, after some re-arrangement, we will have:

$$\frac{\frac{1}{2}\hbar}{\delta p_{\max}\delta r_{\max}} = e^{-\delta p_{\max}\delta r_{\max}/\hbar}\,. \tag{17}$$

From a meticulous inspection of (17), it is clear and goes without saying that in order for this equation to hold true $\delta p_{\max}\delta r_{\max} > 0$, hence:

$$\frac{\frac{1}{2}\hbar}{\delta p_{\max}\delta r_{\max}} = e^{-\delta p_{\max}\delta r_{\max}/\hbar} < 1\,, \tag{18}$$

thus, we will have:

$$\delta p_{\max}\delta r_{\max} > \frac{1}{2}\hbar\,. \tag{19}$$

With the subscript "max" removed from $p_{\max}$ and $r_{\max}$, this (19) is without any doubt whatsoever the famous 1927 position-momentum quantum mechanical uncertainty principle of Heisenberg. One can work this out for the other three cases – i.e. for the $(\delta y, \delta p_y)$ dimension as given in (6) and the $(\delta z, \delta p_z)$ dimension as given in (7) and they would arrive at the same result.

It is important to note that the exact Heisenberg upper uncertainty principle involves a *greater than or equal to sign*, that is "≥", yet in (19), the equal sign "=" is missing. This issue shall be addressed in Paper IV where it shall be seen that this case represents only those particles that travel at the speed of light. Next, we consider the energy-time uncertainty relation.

2.3 Time-energy

Now, in §2.3.1 and §2.3.2, we are going to derive a lower and an upper bound uncertainty principle for energy and time and as we do this, we must have at the back of our mind that stable ponderable particles ought to have no upper bound in their temporal fluctuations. Yes, they can only have a lower bound in their temporal fluctuations and this lower bound must coincide with the moment of their creation. On the contrary, unstable ponderable particles ought to have a finite upper bound in their temporal fluctuation.

2.3.1 Lower bound energy-time uncertainty

We are now going to derive the energy-time uncertainty principle. The derivation is similar to the one given in §2.2 above. To that end, from (4*d*) and (8), we know that:

$$\frac{1}{\hbar}\int_{\delta E_{\min}}^{\delta E_{\max}}\int_{\delta t_{\min}}^{\delta t_{\max}} \exp\left(-\frac{\delta E\delta t}{\hbar}\right) dtdE = 1\,. \tag{20}$$

Now, using (9) to evaluate (20), we obtain the following:

$$\overbrace{\frac{\hbar e^{-\delta E_{\max}\delta t_{\max}/\hbar}}{\delta E_{\max}\delta t_{\max}}}^{\textbf{Term I}} - \overbrace{\frac{\hbar e^{-\delta E_{\min}\delta t_{\max}/\hbar}}{\delta E_{\min}\delta t_{\max}}}^{\textbf{Term II}} - \underbrace{\frac{\hbar e^{-\delta E_{\max}\delta t_{\min}/\hbar}}{\delta E_{\max}\delta t_{\min}}}_{\textbf{Term III}} + \underbrace{\frac{\hbar e^{-\delta E_{\min}\delta t_{\min}/\hbar}}{\delta E_{\min}\delta t_{\min}}}_{\textbf{Term IV}} = 1\,. \tag{21}$$

In the limit as:

$$\begin{aligned} \delta t_{\min} &\mapsto 0\,, \\ \delta E_{\min} &\mapsto 0\,, \end{aligned} \tag{22}$$

for Terms I, II, III and IV in (21), according to (10), we will have:

$$\begin{aligned} \text{Term I} &= \frac{\hbar e^{\frac{\delta E_{\max}\delta t_{\max}}{\hbar}}}{\delta E_{\max}\delta t_{\max}}\,, \\ \text{Term II} &\mapsto 1\,, \\ \text{Term III} &\mapsto 1\,, \\ \text{Term IV} &\mapsto 1\,, \end{aligned} \tag{23}$$

hence, it follows from this – that (21) will reduce to:

$$\hbar e^{\delta E_{\max}\delta t_{\max}/\hbar}/\delta E_{\max}\delta t_{\max} - 1 = 1\,,$$

where, after some algebraic re-arrangement, we can rewrite this equation as:

$$\frac{\frac{1}{2}\hbar}{\delta E_{\max}\delta t_{\max}} = e^{-\delta E_{\max}\delta t_{\max}/\hbar}\,. \tag{24}$$

Similarly, from an inspection of (24), one will clearly obtain that for this equation holds true $\delta E_{\max}\delta t_{\max} > 0$, hence:

$$\frac{\frac{1}{2}\hbar}{\delta E_{\max}\delta t_{\max}} = e^{-\delta E_{\max}\delta t_{\max}/\hbar} < 1\,, \tag{25}$$

thus:

$$\delta E_{\max}\delta t_{\max} > \frac{1}{2}\hbar\,. \tag{26}$$

Once again, this is the famous 1927 energy-time quantum mechanical uncertainty principle of Heisenberg. Just as in (19), the reason for having the *greater than sign* and not the *greater than or equal to sign* are the same as those given in the case of (19). This uncertainty relation (i.e. (26)) describes a ponderable (spatially bound) material particle that is unstable and has a lifetime τ that is such that $\tau < \delta t_{\max}$.

2.3.2 Upper bound energy-time uncertainty

Now, for the same reason given in §2.3.1, we are going to proceed further and consider the case of a ponderable material particle system that has no upper bound in its temporal fluctuations – i.e. a stable ponderable material particle system that can live forever (e.g. like an electron or a proton). Such a particle will have $\delta t_{\max}$ and $\delta E_{\max}$ being such that:

$$\begin{aligned} \delta t_{\max} &\mapsto \infty\,, \\ \delta E_{\max} &\mapsto \infty\,. \end{aligned} \tag{27}$$

According to (10) under the given conditions (i.e. (27)), for the Terms I, II, III and IV in (21), we will have:

$$\begin{aligned} \text{Term I} &\mapsto 0\,, \\ \text{Term II} &\mapsto 0\,, \\ \text{Term III} &\mapsto 0\,, \\ \text{Term IV} &= \frac{\hbar e^{-\dfrac{\delta E_{\min}\delta t_{\min}}{\hbar}}}{\delta E_{\min}\delta t_{\min}}\,, \end{aligned} \tag{28}$$

hence, it follows from this that (21) will reduce to:

$$\hbar e^{-\delta E_{\min}\delta t_{\min}/\hbar}/\delta E_{\min}\delta t_{\min} = 1\,,$$

where, after some basic algebraic re-arrangement, we can rewrite this equation as:

$$\frac{\hbar}{\delta E_{\min}\delta t_{\min}} = e^{\delta E_{\min}\delta t_{\min}/\hbar}\,. \tag{29}$$

As before, it is not difficult to see that for (29) to hold true, this requires that $\delta E_{\min}\delta t_{\min} > 0$, hence, and from this, it clearly follows that:

$$\frac{\hbar}{\delta E_{\min}\delta t_{\min}} = e^{\delta E_{\min}\delta t_{\min}/\hbar} < 1\,, \tag{30}$$

thus:

$$\delta E_{\min}\delta t_{\min} < \hbar\,. \tag{31}$$

Insofar as its interpretation is concerned, by no stitch of the imagination is this (31) related to the famous 1927 energy-time quantum mechanical uncertainty principle of Heisenberg and this is so because of the *less-than-sign* "<" appearing in it. What this equation is "telling" us is that the energy and time fluctuations are not bound above, but below. When it comes to the lifetime of the particle in question, this translates to the reality that the particle can live forever – i.e. $\tau = \infty$. Therefore, this uncertainty relation describes stable ponderable particle systems – i.e. ordinary electrons and protons, which by-and-large strongly appear to be stable particle systems.

3 Non-ponderable matter

From a symmetry and *bona fide* mathematical standpoint, if we have the physics of particles described by the thermodynamic phase $+\delta\mathcal{S}_{\text{TD}}$, there surely is nothing wrong, but everything natural and logical for one to consider the physics of particle systems described by the opposite thermodynamic phase – i.e. $-\delta\mathcal{S}_{\text{TD}}$. Such necessary and beautiful symmetry considerations is what lead the great English theoretical physicist – Paul Adrian Maurice Dirac (1902-1984) to foretell the existence of antimatter [9–11]. We here consider the said particle systems whose thermodynamic phase is $-\delta\mathcal{S}_{\text{TD}}$.

Before even going into investigating the said particle systems, natural questions will begin to flood the mind, questions such as: *Will such particles violate the FLT?* The answer is: *No, they will not*. To see this, one simply substitutes $-\delta\mathcal{S}_{\text{TD}}$ into the equations of Paper II, where-from they certainly will come to the inescapable conclusion that these particles will indeed obey the FLT. Further – a question such as: *Will these particle systems violate the SLT?* may also visit the curious and searching mind. An answer to this will be provided in Paper IV.

Furthermore – in the extreme and zenith of one's state of wonderment, they might excogitate: *Will such particles be visible and ponderable?* By visible it is understood to mean: will these particle systems emit or reflect electromagnetic radiation that we are able to sense? And by ponderable, we mean will such particle systems be able to clump-up and form touchable materials like rocks, *etc*? This is the question we are going to answer. To preempt our findings, such particle systems will be invisible and non-ponderable.

To commence our expedition, we shall start by writing down the functions $\delta\varrho_x^-$, $\delta\varrho_y^-$, $\delta\varrho_z^-$, $\delta\varrho_0^-$ and these are such that:

$$\begin{aligned} \delta\varrho_x^- &= \exp\left(-\frac{\delta\mathcal{S}_x}{\hbar}\right) = \exp\left(-\frac{\delta p_x\delta x}{\hbar}\right) \quad \dots \quad (a) \\ \delta\varrho_y^- &= \exp\left(-\frac{\delta\mathcal{S}_y}{\hbar}\right) = \exp\left(-\frac{\delta p_y\delta y}{\hbar}\right) \quad \dots \quad (b) \\ \delta\varrho_z^- &= \exp\left(-\frac{\delta\mathcal{S}_z}{\hbar}\right) = \exp\left(-\frac{\delta p_z\delta z}{\hbar}\right) \quad \dots \quad (c) \\ \delta\varrho_0^- &= \exp\left(\frac{\delta\mathcal{S}_0}{\hbar}\right) = \exp\left(\frac{\delta E\delta t}{\hbar}\right) \quad \dots \quad (d) \end{aligned} \tag{32}$$

Now, just as in the case of ponderable matter in the previous section, in order for us to derive the implied uncertainty relations from (32), we are going to consider (in §3.1, §3.2 and §3.3, respectively) the normalization of $\delta\varrho_x^-$ and $\delta\varrho_0^-$.

3.1 Lower bound position-momentum uncertainty

As before, normalization of $\delta\varrho_x^-$ requires that:

$$\frac{1}{\hbar}\int_{\delta p_{\min}}^{\delta p_{\max}}\int_{\delta r_{\min}}^{\delta r_{\max}} \exp\left(-\frac{\delta p_x\delta x}{\hbar}\right) dx dp_x = 1\,. \tag{33}$$

Just as we have already done with (11) and (20); integrating and evaluating (33), we obtain:

$$\overbrace{\frac{\hbar e^{-\delta p_{\max}\delta r_{\max}/\hbar}}{\delta p_{\max}\delta r_{\max}}}^{\textbf{Term I}} - \overbrace{\frac{\hbar e^{-\delta p_{\min}\delta r_{\max}/\hbar}}{\delta p_{\min}\delta r_{\max}}}^{\textbf{Term II}} - \underbrace{\frac{\hbar e^{-\delta p_{\max}\delta r_{\min}/\hbar}}{\delta p_{\max}\delta r_{\min}}}_{\textbf{Term III}} + \underbrace{\frac{\hbar e^{-\delta p_{\min}\delta r_{\min}/\hbar}}{\delta p_{\min}\delta r_{\min}}}_{\textbf{Term IV}} = 1. \quad (34)$$

Likewise, with (34) in place, one may try to bound the particle in space and momentum, in much the same way as it has been done in §2.2 by instituting the asymptotic conditions $\delta r_{\min} \mapsto 0$ and $\delta p_{\min} \mapsto 0$. So doing, they surely would obtain the unpleasant result:

$$\hbar e^{-\delta p_{\max}\delta r_{\max}/\hbar}/\delta p_{\max}\delta r_{\max} = 0\,.$$

This result is surely unpleasant because it means that we must have $\delta p_{\max}\delta r_{\max} = \infty$. Overall, this means that this particle system has no upper bounds in quantum of action $\delta p_{\max}\delta r_{\max}$; this surely is uncomfortable as the quantum of action must be bound either above or below. Given this uncomfortable result $\delta p_{\max}\delta r_{\max} = \infty$, a much better way to approach this particle system is to start off by setting no upper bounds in space and momentum and in the end obtain finite lower bounds in the quantum of action $\delta E\,\delta t$, that is to say, start off by setting:

$$\begin{aligned} \delta r_{\max} &\mapsto \infty\,, \\ \delta p_{\max} &\mapsto \infty\,. \end{aligned} \quad (35)$$

Instituting the above (35) limits into (34), for the Terms: (I), (II), (III) and (IV), one obtains:

$$\begin{aligned} \text{Term I} &\mapsto 0\,, \\ \text{Term II} &\mapsto 0\,, \\ \text{Term III} &\mapsto 0\,, \\ \text{Term IV} &= \frac{\hbar e^{-\frac{\delta p_{\min}\delta r_{\min}}{\hbar}}}{\delta p_{\min}\delta r_{\min}}\,, \end{aligned} \quad (36)$$

hence:

$$\frac{\hbar e^{-\frac{\delta p_{\min}\delta r_{\min}}{\hbar}}}{\delta p_{\min}\delta r_{\min}} = 1\,. \quad (37)$$

In much the same fashion as in the preceding sections, rearranging this (37), we will have:

$$\frac{\hbar}{\delta p_{\min}\delta r_{\min}} = e^{\frac{\delta p_{\min}\delta r_{\min}}{\hbar}} > 1\,, \quad (38)$$

hence:

$$\delta p_{\min}\delta r_{\min} < \hbar\,. \quad (39)$$

This means the fuzziness in the momentum and spatial location of the particle about its canonical centre is bounded above and not below.

3.2 Lower bound energy-time uncertainty

Further, for the energy-time uncertainty relation, normalization of $\delta\varrho_0^-$ requires that:

$$\frac{1}{\hbar}\int_{\delta E_{\min}}^{\delta E_{\max}}\int_{\delta t_{\min}}^{\delta t_{\max}} \exp\left(\frac{\delta E\delta t}{\hbar}\right) dt dE = 1\,. \quad (40)$$

As before, integrating and evaluating this (40), we obtain:

$$\overbrace{\frac{\hbar e^{-\delta E_{\max}\delta t_{\max}/\hbar}}{\delta E_{\max}\delta t_{\max}}}^{\textbf{Term I}} - \overbrace{\frac{\hbar e^{-\delta E_{\min}\delta t_{\max}/\hbar}}{\delta E_{\min}\delta t_{\max}}}^{\textbf{Term II}} - \underbrace{\frac{\hbar e^{-\delta E_{\max}\delta t_{\min}/\hbar}}{\delta E_{\max}\delta t_{\min}}}_{\textbf{Term III}} + \underbrace{\frac{\hbar e^{-\delta E_{\min}\delta t_{\min}/\hbar}}{\delta E_{\min}\delta t_{\min}}}_{\textbf{Term IV}} = 1\,. \quad (41)$$

In the limit as:

$$\begin{aligned} \delta t_{\max} &\mapsto \infty\,, \\ \delta E_{\max} &\mapsto \infty\,, \end{aligned} \quad (42)$$

for the Terms I, II, III and IV in (41), we will have:

$$\begin{aligned} \text{Term I} &\mapsto 0\,, \\ \text{Term II} &\mapsto 0\,, \\ \text{Term III} &\mapsto 0\,, \\ \text{Term IV} &= \frac{\hbar e^{-\frac{\delta E_{\min}\delta t_{\min}}{\hbar}}}{\delta E_{\min}\delta t_{\min}}\,, \end{aligned} \quad (43)$$

hence, it follows from this that (41) will reduce to:

$$\hbar e^{-\delta E_{\min}\delta t_{\min}/\hbar}/\delta E_{\min}\delta t_{\min} = 1\,,$$

where, after some re-arrangement, we can rewrite:

$$\frac{\hbar}{\delta E_{\min}\delta t_{\min}} = e^{\delta E_{\min}\delta t_{\min}/\hbar}\,. \quad (44)$$

As before, from a meticulous inspection of (44), it is abundantly clear that $\delta E_{\min}\delta t_{\min} > 0$, hence:

$$\frac{\hbar}{\delta E_{\min}\delta t_{\min}} = e^{\delta E_{\min}\delta t_{\min}/\hbar} < 1\,, \quad (45)$$

thus:

$$\delta E_{\min}\delta t_{\min} < \hbar\,. \quad (46)$$

Just as with (39), (46) means that the fuzziness in the energy and temporal fluctuations of the particle are bounded above and not below.

3.3 Upper bound energy-time uncertainty

Lastly, we now consider the case of a non-ponderable material particle system that has no upper bound in its temporal fluctuation – i.e. a stable non-ponderable material particle system that can live forever. Such a particle will have $\delta t_{\max}$ and $\delta E_{\max}$ such that:

$$\begin{aligned} \delta t_{\max} &\mapsto \infty\,, \\ \delta E_{\max} &\mapsto \infty\,. \end{aligned} \tag{47}$$

Under the given conditions (i.e. (47)), for the Terms I, II, III and IV in (41), we will have:

$$\begin{aligned} \text{Term I} &\mapsto 0\,, \\ \text{Term II} &\mapsto 0\,, \\ \text{Term III} &\mapsto 0\,, \\ \text{Term IV} &= \frac{\hbar e^{-\frac{\delta E_{\min}\delta t_{\min}}{\hbar}}}{\delta E_{\min}\delta t_{\min}}\,, \end{aligned} \tag{48}$$

hence, it follows from this that (21), will reduce to:

$$\hbar e^{-\delta E_{\min}\delta t_{\min}/\hbar}/\delta E_{\min}\delta t_{\min} = 1\,,$$

where, after some re-arrangement, we can rewrite:

$$\frac{\hbar}{\delta E_{\min}\delta t_{\min}} = e^{\delta E_{\min}\delta t_{\min}/\hbar}. \tag{49}$$

Likewise, for it to hold true always, (49) requires that $\delta E_{\min}$ $\delta t_{\min} < 0$, hence:

$$\frac{\hbar}{\delta E_{\min}\delta t_{\min}} = e^{\delta E_{\min}\delta t_{\min}/\hbar} < 1\,, \tag{50}$$

thus:

$$\delta E_{\min}\delta t_{\min} < \hbar\,. \tag{51}$$

Again, we here have an upper bounded uncertainty relation.

4 General discussion

Since the inception of Heisenberg's uncertainty principle in 1927, several attempts see e.g. [8,12–15, and references therein] have been made to derive this mysterious mathematical relationship from much more fundamental soils of physics than those on which Heisenberg [1] derived this relation. In his original paper, Heisenberg began by deriving the uncertainty relation for position and momentum on the basis of a supposed experiment in which an electron is observed using a γ-ray microscope and second, by consideration of the theory of the Compton effect, he proceeded to argue that the precision of the determination of position and momentum are connected by the uncertainty relation.

In 1929, using the usual definition of expectation values (inner product) of Hermitian Hilbert-space operators (observables) and the mathematical property of the *Cauchy–Bunyakovsky–Schwarz inequality*, Robertson [12] proceeded in a rigorous manner, to demonstrate a more general and fundamental origin of the quantum mechanical uncertainty principle. The present attempt is just but one such derivation – albeit – on the soils of a new kind of phase space – the Stochastic Phase Space.

However, unlike all previous attempts on the derivation of the uncertainty principle, what makes the present attempt different is that we have not only derived the lower limit uncertainty principle, but an upper bound uncertainty principle that seems to describe invisible non-ponderable particles that travel at superlumical speeds. This unique prediction seem to suggest not only the existence of darkmatter, but darkenergy as well. Dark matter is already required by physicists in order to explain the flat rotation curves of spiral galaxies, while dark energy is required to explain the supposed accelerated expansion of the Universe. This subject of invisible non-ponderable particles, dark matter and dark energy would require a separate and lengthy paper in order to cover it in a just manner.

Another important point to note about the present derivation is that the enigmatic jittery quantum randomness leading to the uncertainty principle is here an intrinsic and inherent property of all quantum mechanical systems, it (i.e. the jittery quantum randomness) is not induced by the act of measurement as is the case of Heisenberg's uncertainty principle and its latter versions or attempts at a derivation of this relation. Yes, human measure will introduce statistical errors that are statistically predictable. The stochastic quantum randomness is not predictable at all – not even by the most rigours known (or unknown, or yet to be unknown) statistical methods.

In closing, allow us to say that we have always held central to our philosophy of Physics the strong and seemingly unshakeable belief system similar to that of Albert Einstein – namely, that the fundamental laws of Nature are exact, and as such, one day it will be shown that this is the case. That is to say, in the character of Einstein's philosophy, we have held fast to his influential and deep philosophy that indeed *God does not play dice with the World*, and that *The moon exists whether or not one is looking at it or not*. Contrary to this, we must admit and say that as we continue to peer deeper into the fabric and labyrinth of physical and natural reality as it lies bare for us to marvel at, this dream or belief system now stands shattered into minuscule pieces – for it now seems clearer to us that the enigmatic jittery quantum randomness must be real.

Received on February 23, 2020

References

1. Heisenberg W. K. Ueber den anschaulichen Inhalt der Quantentheoretischen Kinematik and Mechanik. *Zeitschrift für Physik*, 1927,

v. 43 (3), 172–198. English Translation: Wheeler J. A. and Zurek W. H., eds. Quantum Theory and Measurement, Princeton University Press, Princeton, NJ, 1983, pp. 62–84.

2. Nyambuya G. G. Liouville's Theorem as a Subtle Statement of the First Law of Thermodynamics. *Progress in Physics*, 2019, v. 15 (3), 178–181.
3. Heisenberg W. K. Physics and Beyond. George Allen & Unwin, 1^{st} Edition, 1971.
4. Nyambuya G. G. A Simple Proof of the Second Law of Thermodynamics. *Progress in Physics*, 2019, v. 15 (3), 171–177.
5. Nyambuya G. G. On the Uni-Directional Thermodynamic Arrow of Evolution of Thermodynamic Systems. In Preparation.
6. Liouville J. Sur la Théorie de la Variation des Constantes Arbitraires. *Journ. de Math.*, 1838, v. 3, 342–349.
7. Nyambuya G. G. On the Plausibility of an Upper Bound Uncertainty Principle. *Prespacetime Journal*, 2014, v. 5 (10), 1018–1026.
8. Millette P. A. The Heisenberg Uncertainty Principle and the Nyquist-Shannon Sampling Theorem. *Progress in Physics*, 2013, v. 9 (3), 9–14.
9. Dirac P. A. M. The Quantum Theory of the Electron. *Proc. Roy. Soc. (London)*, 1928a, v. A117, 610–612.
10. Dirac P. A. M. The Quantum Theory of the Electron II. *Proc. Roy. Soc. (London)*, 1928b, v. A118, 351–361.
11. Dirac P. A. M. A Theory of Electrons and Protons. *Proceedings of the Royal Society of London A: Mathematical, Physical and Engineering Sciences*, 1930, v. 126 (801), 360–365.
12. Robertson H. P. The Uncertainty Principle. *Physical Review*, 1929, v. 34 (1), 163–164.
13. Davidson E. R. On Derivations of the Uncertainty Principle. *The Journal of Chemical Physics*, 1965, v. 42 (4), 1461–1462.
14. Briggs J. S. A Derivation of the Time-Energy Uncertainty Relation. *Journal of Physics: Conference Series*, 2008, 012002, 99.
15. Briggs J. S. and Rost J. M. *Foundations of Physics*, 2001, v. 31 (4), 693–712.

Magnetic Energy, Superconductivity, and Dark Matter

Hanno Essén
Department of Engineering Mechanics, Royal Institute of Technology, Osquars Backe 18, 100 44, Stockholm, Sweden.
E-mail: hanno@mech.kth.se

Magnetism due to the translational, possibly oscillatory, motion of charge, as opposed to the ordering of dipoles, is not well understood, but is well described by the Darwin Lagrangian. The Coulomb interaction is used universally in atomic, molecular and solid state physics, but its natural extension when going to higher accuracy, the magnetic Darwin-Breit interaction, is not. This interaction is a velocity dependent long range interaction and as such unfamiliar to the majority of theoreticians. The $(v/c)^2$ dependence makes it at most a perturbation in few-body systems, but does not stop it from becoming potentially important as the number of particles increase. For systems where particle velocities are correlated (or coherent) over larger distances this interaction is shown to have major consequences. Based on these findings I suggest that this interaction should be investigated as the interaction responsible for superconductivity. I also speculate that, on an interstellar scale, it is responsible for the missing dark matter. Some numerical estimates and intuitive arguments are presented in support, but no proofs. Instead it is my hope that the ideas presented will deserve further serious study.

A man hears what he wants to hear and disregards the rest.

Paul Simon in The Boxer

1 Introduction

We first introduce the Darwin Lagrangian which describes the magnetic interaction energy between moving charged particles. This is a velocity dependent long range interaction which is very small for few-body systems but which can become dominating in macroscopic systems. In particular the Lagrangian predicts that the effective mass, or equivalently inductive inertia, can grow with the square of the number of particles.

The Darwin Lagrangian makes simple predictions for particles that are assumed to have the same velocity. Here we use this constraint to study the effect of the magnetic interaction energy for collectively moving charges. The crucial fact that emerges from these studies is that the effective mass of many collectively moving particles far exceeds the sum of their rest masses. In the case of superconductivity this means that the zero-point energy of coherent oscillators decreases with the number of oscillators, and this presumably leads to the superconducting phase transition. In the case of cosmic plasma filaments it leads to the conclusion that their gravitational mass can far exceed the rest mass content of the participating particles. Could this be the missing dark matter? Some numerical estimates indicate that this is a possibility.

2 The Darwin Lagrangian

The Darwin Lagrangian [1] describes the majority of electromagnetic phenomena correctly. The exception is radiation, which is neglected. The theory behind this Lagrangian is presented in a few textbooks such as Landau and Lifshitz [2, §65] and Jackson [3, Sec. 12.6]. More extensive discussions can be found in Page and Adams [4, Sec. 96], Podolsky and Kunz [5, Sec. 27], Szasz [6, Appendix], Schwinger *et al.* [7, Eq. (33.23)], or Stefanovich [8]. Basic articles of interest are Breitenberger [9], Kennedy [10], Essén [11–13]. Various applications of the Darwin Lagrangian illustrating its usefulness can be found in Kaufman [14], Stettner [15], Boyer [16, 17], Krause *et al.* [18], Essén *et al.* [19–25].

Vector potentials are not always mentioned in connection with the Darwin Lagrangian, but it can be derived by approximating the Liénard-Wiechert potentials. Landau and Lifshitz [2, §65] make a gauge transformation to the Coulomb gauge after truncating series expansions of these. Jackson [3, Sec. 12.6] solves the vector Poisson equation obtained by neglecting the time derivative in the wave equation. Page and Adams derive it by approximating the forces [4, Sec. 96]. It can also be motivated as the best approximately relativistic action-at-a-distance Lagrangian [10, 26] and it can be shown to take retardation into account to order $(v/c)^2$.

The Darwin Lagrangian for N charged particles, of mass m_a and charge e_a, can be written

$$L_D = \sum_{a=1}^{N} \left[\frac{m_a}{2} \boldsymbol{v}_a^2 - \frac{e_a}{2} \phi_a(\boldsymbol{r}_a) + \frac{e_a}{2c} \boldsymbol{v}_a \cdot \boldsymbol{A}_a(\boldsymbol{r}_a) \right] \qquad (1)$$

where

$$\phi_a(\boldsymbol{r}_a) = \sum_{b(\neq a)}^{N} \frac{e_b}{|\boldsymbol{r}_a - \boldsymbol{r}_b|} \qquad (2)$$

and

$$\boldsymbol{A}_a(\boldsymbol{r}_a) = \sum_{b(\neq a)}^{N} \frac{e_b}{2c} \frac{[\boldsymbol{v}_b + (\boldsymbol{v}_b \cdot \hat{\boldsymbol{e}}_{ab})\hat{\boldsymbol{e}}_{ab}]}{|\boldsymbol{r}_a - \boldsymbol{r}_b|} \,. \qquad (3)$$

Here $\hat{\boldsymbol{e}}_{ab} = (\boldsymbol{r}_a - \boldsymbol{r}_b)/|\boldsymbol{r}_a - \boldsymbol{r}_b|$, and relativistic corrections to the kinetic energy are neglected. In many circumstances

one can neglect the magnetic interaction energies since the Coulomb electric interaction dominates strongly, especially in few-body systems. As will be seen below, however, when there are macroscopic numbers of correlated charged particles this is no longer permissible. It is noteworthy that macroscopic numbers of correlated charged particles is the rule rather than an exception in plasmas, conductors, and superconductors.

3 Plasma oscillations

One can use (1) to calculate how a charge density of electrons oscillates relative to a fixed background of positive charge. For collective motion of N electrons with velocity $\boldsymbol{v} = \dot{x}\hat{\boldsymbol{e}}_x$ the kinetic energy is simply $T = Nm_e\dot{x}^2/2$. If one further assumes that the particles have fixed distributions in space apart form the relative translational motion one can get (nearly) analytical results for the remaining two terms, for simple geometries in the continuum limit. If we denote the displacement of the negative charges by x the total Coulomb potential energy is well approximated by,

$$\Phi(x) = \sum_{a=1}^{N_{tot}} \frac{e_a}{2}\,\phi_a(\boldsymbol{r}_a) = \Phi(0) + \frac{1}{2}\left(\frac{d^2\Phi}{dx^2}\right)_{x=0} x^2\,, \qquad (4)$$

in the limit of small x. Here $\Phi(0)$ is a large negative constant that does not contribute to the dynamics; the positive background only provides the restoring force in the oscillation. The assumption that the electrons ($m_a = m_e$, $e_a = -e$) move collectively along the x-direction simplifies the magnetic contribution, the third term in (1). One finds

$$\begin{aligned} U_D &= \sum_{a=1}^{N} \frac{e}{2c}\,\boldsymbol{v}_a \cdot \boldsymbol{A}_a(\boldsymbol{r}_a) \\ &= \left(\frac{e^2}{2c^2}\sum_{a=1}^{N-1}\sum_{b=a+1}^{N} \frac{1+\cos^2\theta_{ab}}{|\boldsymbol{r}_a - \boldsymbol{r}_b|}\right)\dot{x}^2\,, \end{aligned} \qquad (5)$$

where $\cos\theta_{ab} = \hat{\boldsymbol{e}}_x \cdot \hat{\boldsymbol{e}}_{ab}$. For a charge density of electrons with fixed geometry this is simply a constant times $\dot{x}^2$. We thus find that the Darwin Lagrangian for the system becomes

$$L_D = N\left(\frac{1}{2}m_{\text{eff}}\dot{x}^2 - \frac{1}{2}\kappa x^2\right). \qquad (6)$$

Here m_{eff} is m_e plus a contribution from (5).

Calculations of the constants m_{eff} and κ can be done by elementary methods. The result will be a formula for the square of the oscillation frequency $\omega^2 = \kappa/m_{\text{eff}}$. This was done for a sphere of radius R in [19] with the result

$$\omega^2 = \frac{\frac{Ne^2}{R^3}}{m_e\left(1 + \frac{4}{5}\frac{r_e N}{R}\right)}\,. \qquad (7)$$

Here $r_e = e^2/(m_e c^2)$ is the classical electron radius. $\omega(R)$ is plotted in Fig. 1. In the limit of few particles, or negligible Nr_e/R, this gives the plasma oscillation frequency as

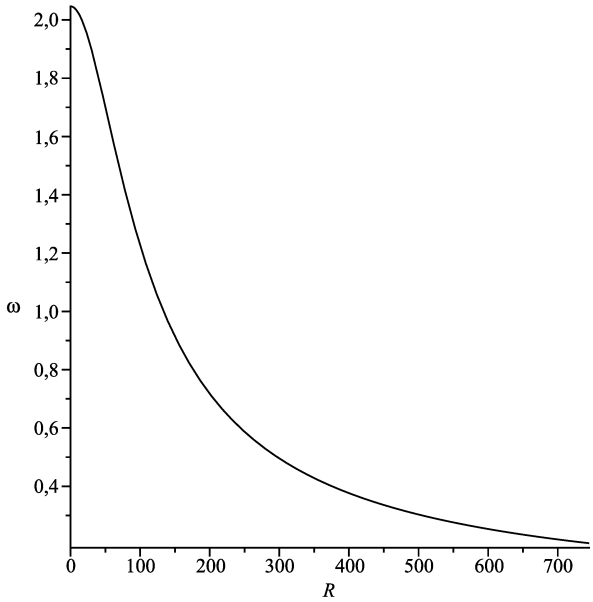

Fig. 1: The frequency ω of (7) as a function of radius R. Atomic units are used ($e = m_e = \hbar = 1$, $c = 137$) and the density is assumed to be one electron per sphere of one Bohr radius a_0. The formula plotted is $\omega(R) = \sqrt{4\pi/3\left(1 + \frac{16\pi}{15(137)^2}R^2\right)}$ and R is in atomic units (Bohr radii). The frequency is reduced by one order of magnitude at $R = 750\,a_0$.

normally given in the literature,

$$\omega_p^2 = \frac{4\pi}{3}\,\frac{e^2 n_0}{m_e} \qquad (8)$$

where $n_0 = N/V$ is the number density inside the sphere. In the opposite limit of macroscopic numbers of electrons N one obtains

$$\omega_\infty^2 = \frac{5c^2}{4R^2}\,. \qquad (9)$$

This seems to be the frequency of a longitudinal electromagnetic wave in the sphere. A similar calculation for a (two-dimensional) square of side length L gives a similar result,

$$\omega^2 = \frac{\frac{2e^2N}{L^3}K_s}{m_e\left(1 + \frac{3}{4}\frac{Nr_e}{L}C_s\right)}\,, \qquad (10)$$

where $C_s = (4/3)\left[1 - \sqrt{2} - 3\ln\left(\sqrt{2} - 1\right)\right]$ and $K_s = 16\,(2 - \sqrt{2})$ [27].

4 Superconductivity

In the early history of superconductivity it was conjectured that a transition of the electrons at the Fermi surface to a Wigner crystal [28] was responsible for the phase transition. Since no new interaction comes into play this did not seem correct, even if the Wigner crystal idea is still investigated

[29,30]. When one takes the magnetic interaction energy into account, however, the zero point energy $E_0 = \hbar\omega/2$ and oscillation frequency of the (pairs of) electrons go down considerably if they oscillate coherently with coherence length R, as indicated in Fig. 1. It is interesting to note that Vasiliev [31,32] finds that superconductivity is caused by ordering of the zero point oscillations. Frenkel [33] advanced the theory that the increased inductive inertia of correlated conduction electrons explains superconductivity, and the present author presented estimates indicating that the Darwin energy is important in superconductors [34]. In Fig. 1 it is seen that the zero point energy goes down by one order of magnitude in 750 Bohr-radii, assuming one electron per cubic Bohr-radius. In general coherence lengths in superconductors is one or two orders of magnitude larger [35], so the numbers are quite reasonable. The isotope effect agrees well with the assumption that lattice oscillations destroy the coherence.

5 Dark matter?

The decay time of currents is $\tau \sim \mathcal{L}/\mathcal{R}$ where $\mathcal{L}$ is inductance and $\mathcal{R}$ resistance. As emphasized by Kulsrud [36] these times are enormous in astrophysical plasmas. The currents producing astrophysical magnetic fields will only decay on a time scale comparable to the age of the universe. These plasmas are thus effectively superconducting. The effective mass m_{eff} of (6) is a measure of the inductance, or inductive inertia. Simple estimates show that this mass is in general much larger than the rest mass. That this is the case for conduction electrons in a metal was noted already in 1936 by Darwin [37] and several times later [23,38].

It is tempting to speculate that dark matter is in fact due to magnetic energy in interstellar plasmas. Here we make some simple estimates. The Darwin magnetic energy, the first term of (6), $U_D = Nm_{\text{eff}}\dot{x}^2/2$, will contribute $M_D = U_D/c^2$ to gravitational mass in the universe. Consider a cube of side length L. If we assume that the number of protons in this cube is N and that L also is a typical distance between them we find from (5) that

$$\frac{U_D}{c^2} = M_D \sim \frac{1}{4}\,\frac{e^2}{c^2}\,\frac{N}{L}^2\,\beta^2 \tag{11}$$

where $\beta = |\dot{x}|/c$. This magnetic mass should be compared to the total proton mass $M_p = Nm_p$. The ratio is

$$\frac{M_D}{M_p} \sim \frac{(e^2/c^2)\,(N/L)}{4m_p}\,\beta^2\,. \tag{12}$$

Putting in the numerical values gives

$$\frac{M_D}{M_p} \sim (3.83\times 10^{-19}\,\text{m})\,\frac{N}{L}\,\beta^2\,. \tag{13}$$

The number of protons is $N = n_p L^3$ where n_p is the proton number density. This gives

$$\frac{M_D}{M_p} \sim (3.83\times 10^{-19}\,\text{m})\,n_p\,L^2\beta^2\,. \tag{14}$$

To get some numbers we assume that $n_p = 4.0\,\text{m}^{-3}$ and that the ratio M_D/M_p is 10 (magnetic mass is 10 times proton mass). This gives

$$10 \sim 3.83\times 10^{-19}\times 4.0\,L^2\beta^2\,\text{m}^{-2}\,. \tag{15}$$

The side length of the cube over which velocity must be correlated is then

$$L \sim 2.5\times 10^9\,\beta^{-1}\,\text{m}\,. \tag{16}$$

assuming that the speed is $c/100$, so that $\beta = 10^{-2}$, we find that $L \sim 2.5\times 10^{11}$ m. This is somewhat more that one astronomical unit (AU $\approx 1.5\times 10^{11}$ m), a tiny distance in the interstellar perspective. So, with a density of 4 protons per cubic meter and a correlated speed of 1% of the speed of light over a distance of order of magnitude one AU one finds that the gravitational mass M_D of the magnetic energy is ten times the total proton rest mass. This suggests to me that dark matter may, in fact, reside in magnetic energy and the effective mass of the cosmic magnetic fields.

6 Conclusions

Since Darwin's 1936 paper [37] it should have been clear that investigations of conduction electrons in metals that do not take into account the magnetic interaction energy are meaningless. No amount of mathematical wizardry will make this interaction go away. It is also a natural candidate for emergent properties in larger systems, such as superconductivity, while remaining a perturbation in few body systems.

The insight that large plasmas with coherent velocities have energies that are many orders of magnitude larger than that corresponding to the rest mass of the constituent particles should be investigated as a possible candidate for dark matter. Recently Nicastro *et al.* [39] found that missing baryons are believed to reside in large-scale filaments in the warm-hot intergalactic medium. Perhaps the rest of the missing dark matter is also there in the form of magnetic energy?

Acknowledgements

The author would like to thank Dr. Arne Nordmark for help with calculations and discussions and Dr. Johan Stén for comments. Support from KTH, Department of Engineering Mechanics is acknowledged.

Received on March 3, 2020

References

1. Darwin C. G. The dynamical motions of charged particles. *Philos. Mag. (UK)*, 1920, v. 39, 537–551.
2. Landau L. D. and Lifshitz E. M. The Classical Theory of Fields, 4th edition. Pergamon, Oxford, 1975.
3. Jackson J. D. Classical Electrodynamics, 3rd edition. John Wiley, New York, 1999.
4. Page L. and Adams N. I. Electrodynamics. Van Nostrand, New York, 1940.

5. Podolsky B. and Kunz K. S. Fundamentals of Electrodynamics. Marcel Dekker, New York, 1969.
6. Szasz L. The Electronic Structure of Atoms. John Wiley, New York, 1992.
7. Schwinger J., DeRaad L. L. Jr., Milton K. A., and Tsai W.-Y. Classical Electrodynamics. Perseus Books, Reading, Massachusetts, 1998.
8. Stefanovich E. V. Relativistic Quantum Theory of Particles. II: A Non-Traditional Perspective on Space, Time, Particles, Fields, and Action-at-a-Distance. LAP Lambert, Saarbrücken, Germany, 2015.
9. Breitenberger E. Magnetic interactions between charged particles. *Am. J. Phys.*, 1968, v. 36, 505–515.
10. Kennedy F. J. Approximately relativistic interactions. *Am. J. Phys.*, 1972, v. 40, 63–74.
11. Essén H. Darwin magnetic interaction energy and its macroscopic consequences. *Phys. Rev. E*, 1996, v. 53, 5228–5239.
12. Essén H. Phase-space energy of charged particles with negligible radiation: Proof of spontaneous formation of magnetic structures and new effective forces. *Phys. Rev. E*, 1997, v. 56, 5858–5865.
13. Essén H. Magnetism of matter and phase-space energy of charged particle systems. *J. Phys. A: Math. Gen.*, 1999, v. 32, 2297–2314.
14. Kaufman A. N. and Rostler P. S. The Darwin model as a tool for electromagnetic plasma simulation. *Phys. Fluids*, 1971, v. 14, 446–448.
15. Stettner R. Conserved quantities and radiation effects for a closed system of charged particles. *Ann. Phys. (N.Y.)*, 1971, v. 67, 238–251.
16. Boyer T. H. Examples and comments related to relativity controversies. *Am. J. Phys.*, 2012, v. 80, 962–971.
17. Boyer T. H. Faraday induction and the current carriers in a circuit. *Am. J. Phys.*, 2015, v. 83, 263–442, 2015.
18. Krause T. B., Apte A., and Morrison P. J. A unified approach to the Darwin approximation. *Phys. of Plasmas*, 2007, v. 14, 102112–1–10.
19. Essén H. Magnetic dynamics of simple collective modes in a two-sphere plasma model. *Phys. of Plasmas*, 2005, v. 12, 122101–1–7.
20. Essén H. Electrodynamic model connecting superconductor response to magnetic field and to rotation. *Eur. J. Phys.*, 2005, v. 26, 279–285.
21. Essén H. From least action in electrodynamics to magnetomechanical energy – a review. *Eur. J. Phys.*, 2009, v. 30, 515–539.
22. Essén H. Classical diamagnetism, magnetic interaction energies, and repulsive forces in magnetized plasmas. *EPL*, 2011, v. 94, 47003–1–5.
23. Essén H. An exact formula for the electromagnetic momentum in terms of the charge density and the coulomb gauge vector potential. *Eur. J. Phys.*, 2018, v. 39, 025202–1–9.
24. Essén H. and Nordmark A. B. Hamiltonian of a homogeneous two-component plasma. *Phys. Rev. E*, 2004, v. 69, 036404–1–9.
25. Essén H. and Fiolhais M. C. N. Meissner effect, diamagnetism, and classical physics —- a review. *Am. J. Phys.*, 2012, v. 80, 164–169.
26. Woodcock H. W. and Havas P. Approximately relativistic Lagrangians for classical interacting point particles. *Phys. Rev. D*, 1972, v. 12, 3422–3444.
27. Essén H. and Nordmark A. B. unpublished, 2019.
28. Wigner E. On the interaction of electrons in metals. *Phys. Rev.*, 1934, v. 46, 1002–1011.
29. Pereg-Barnea T. and Franz M. Duality and the vibrational modes of a Cooper-pair Wigner crystal. *Phys. Rev. B*, 2006, v. 74, 014518.
30. Dai J. X., Tao W., Hor P., and Dai X. X. A possible mechanism of superconductivity based on Wigner crystal and BEC. *Int. J. Mod. Phys. B*, 1999, v. 13, 3499–3504.
31. Vasiliev B. V. The superconductivity as a consequence of an ordering of the electron gas zero-point oscillations. *Physica C: Superconductivity*, 2011, v. 471, 277–284.
32. Vasiliev B. V. Superconductivity and condensation of ordered zero-point oscillations. *Physica C: Superconductivity*, 2012, v. 483, 233–246.
33. Frenkel J. On a possible explanation of superconductivity. *Phys. Rev.*, 1933, v. 43, 907–912.
34. Essén H. A study of lattice and magnetic interactions of conduction electrons. *Phys. Scr.*, 1995, v. 52, 388–394.
35. Poole C. P. Jr., Prozorov R., Farach H. A., and Creswick R. J. Superconductivity, 3rd edition. Elsevier, Amsterdam, 2014.
36. Kulsrud R. M. Plasma Physics for Astrophysics. Princeton University Press, New Jersey, 2005.
37. Darwin C. G. Inertia of electrons in metals. *Proc. R. Soc. Lond. (UK)*, 1936, v. 154A, 61–66.
38. Assis A.K̇. T. and Hernandes J. A. Magnetic energy and effective inertial mass of the conduction electrons in circuit theory. *Electromagnetic Phenomena*, 2006, v. 6, 29–35.
39. Nicastro F., Kaastra J., Krongold Y., Borgani S., Branchini E., Cen R., Dadina M., Danforth C. W., Elvis M., Fiore F., Gupta A., Mathur S., Mayya D., Paerels F., Piro L., Rosa-Gonzalez D., Schaye J., Shull J. M., Torres-Zafra J., Wijers N., and Zappacosta L. Observations of the missing baryons in the warm–hot intergalactic medium. *Nature*, 2018, v. 558, 406–409.

Quantum State Tomography for Qutrits Subject to Laser Cooling

Artur Czerwinski

Institute of Physics, Faculty of Physics, Astronomy and Informatics, Nicolaus Copernicus University, Grudziadzka 5, 87-100 Torun, Poland.

E-mail: aczerwin@umk.pl

In this article we propose a dynamic quantum state tomography model for qutrits subject to laser cooling. We prove that one can reduce the number of distinct measurement setups required for state reconstruction by employing the stroboscopic approach. The results are in line with current advances in quantum tomography where there is a strong tendency to investigate the optimal criteria for state reconstruction. We believe that the stroboscopic approach can be considered an efficient tool for density matrix identification since it allows to determine the minimal number of distinct observables needed for quantum state tomography.

1 Introduction

The term *quantum tomography* is used in reference to a wide variety of methods which aim to reconstruct the accurate representation of a quantum system by performing a series of measurements. Mathematically, the complete knowledge about the state of a quantum system can be encoded in, for example, the density operator, the wavefunction or the Wigner function. In this article we discuss the problem of the density matrix reconstruction.

One of the most fundamental approaches to quantum state tomography, the so-called static tomography model, enables to reconstruct the density matrix of a quantum system provided one can measure $N^2 - 1$ distinct observables (where $N = \dim \mathcal{H}$). Any density matrix can be decomposed in the basis of $\mathrm{SU}(N)$ generators in such a way that the coefficients correspond to the mean values of the operators [1]. This approach has been excessively studied in many papers and books, such as [2, 3]. However, there is a significant disadvantage connected with this method. In a laboratory one usually is not able to define $N^2 - 1$ distinct physical quantities that could be measured.

The most important property that all tomography models should possess is practicability, which means that a theoretical model should have a potential to be implemented in an experiment in the future. Therefore, when dealing with quantum state tomography we should bear in mind the limitations related to laboratory reality. For this reason, in this article we employ the stroboscopic approach to quantum tomography, which for the first time was proposed by Andrzej Jamiolkowski in [4]. Later it was developed in other research papers such as [5] and [6]. In order to get a broad perspective one may also refer to a very well-written review paper [7]. Recently some new results concerning the stroboscopic approach has been presented in [8, 9].

The stroboscopic tomography concentrates on determining the optimal criteria for quantum tomography of open systems. The main goal of this method is to reduce the number of distinct observables required for quantum tomography by utilizing knowledge about time evolution of the system. The data for the density matrix reconstruction is provided by mean values of some hermitian operators $\{Q_1, \ldots, Q_r\}$, where naturally $Q_i = Q_i^*$. The set of observables is not informationally complete, which means that a single measurement of each operator does not provide sufficient information for quantum state reconstruction.

The underlying principle behind the stroboscopic approach claims that if one has the knowledge about the evolution of the system, each observable can be measured repeatedly at a certain number of time instants. Naturally, each individual measurement is performed over a distinct copy of the system since we do not consider the collapse of the quantum state caused by measurements. Therefore, we assume that our source can prepare a large sample of systems in the identical (but unknown) quantum state.

In the stroboscopic approach to quantum tomography the fundamental question that we are interested in concerns the minimal number of distinct observables required for quantum state reconstruction. One can recall the theorem concerning the minimal number of observables [5].

Theorem 1. *For a quantum system with dynamics given by a master equation of the form [10, 11]:*

$$\dot{\rho}(t) = \mathbb{L}[\rho(t)]\,, \tag{1}$$

one can calculate the minimal number of distinct observables for quantum tomography from the formula:

$$\eta := \max_{\lambda \in \sigma(\mathbb{L})} \{\dim \mathrm{Ker}(\mathbb{L} - \lambda \mathbb{I})\}\,, \tag{2}$$

where by $\sigma(\mathbb{L})$ one should understand the spectrum of the operator $\mathbb{L}$.

The linear operator $\mathbb{L}$ that appears in (1) shall be called the generator of evolution. The number η is usually referred to as *the index of cyclicity* of a quantum system.

The theorem 1 means that for any linear generator $\mathbb{L}$ there exists a set of observables $\{Q_1, \ldots, Q_\eta\}$ such that their ex-

pectation values determine the initial density matrix. Consequently, they also determine the complete trajectory of the state (one can compute the density matrix at any time instant).

If we denote the number of required measurements of each observable from the set $\{Q_1, ..., Q_\eta\}$ by M_i for $i = 1, \ldots, \eta$, then one can also recall the theorem on the upper limit of moments of measurement [6].

Theorem 2. *In order to provide sufficient data for the density matrix reconstruction the number of times that each observable from the set $\{Q_1, ..., Q_\eta\}$ should be measured satisfies the inequality:*

$$M_i \leq \deg \mu(\mathbb{L}), \tag{3}$$

where by $\mu(\mathbb{L})$ we denote the minimal polynomial of $\mathbb{L}$.

The theorem 2 gives the upper boundary concerning the number of measurements of each single observable. One can notice that the ability to compute the minimal polynomial of the generator $\mathbb{L}$ is crucial in order to determine the upper limit for the number of measurements. Naturally, another problem relates to the choice of the time instants. Some considerations about this issue can be found in [6].

In the next section the theorems concerning the stroboscopic tomography shall be applied to three-level quantum systems with the evolution known as laser cooling. This article brings substantial advancement to the field of quantum state tomography. In [8] the author introduced optimal criteria for quantum tomography of qubits. In the current work we proceed towards higher dimensional Hilbert space. We prove that the stroboscopic tomography can be an effective method of state reconstruction for qutrits provided one knows how the system evolves.

2 Quantum tomography schemes for three-level systems subject to laser cooling

2.1 Static approach to quantum tomography of qutrits

In case of three-level quantum systems one would naturally employ the Gell-Mann matrices in order to decompose any density matrix. We follow the original notation from [12] and therefore, the Gell-Mann matrices shall be denoted by $\{\lambda_1, \lambda_2, \ldots, \lambda_8\}$. They have the following forms:

$$\lambda_1 = \begin{bmatrix} 0 & 1 & 0 \\ 1 & 0 & 0 \\ 0 & 0 & 0 \end{bmatrix}, \quad \lambda_2 = \begin{bmatrix} 0 & -i & 0 \\ i & 0 & 0 \\ 0 & 0 & 0 \end{bmatrix}, \quad \lambda_3 = \begin{bmatrix} 1 & 0 & 0 \\ 0 & -1 & 0 \\ 0 & 0 & 0 \end{bmatrix},$$

$$\lambda_4 = \begin{bmatrix} 0 & 0 & 1 \\ 0 & 0 & 0 \\ 1 & 0 & 0 \end{bmatrix}, \quad \lambda_5 = \begin{bmatrix} 0 & 0 & -i \\ 0 & 0 & 0 \\ i & 0 & 0 \end{bmatrix}, \quad \lambda_6 = \begin{bmatrix} 0 & 0 & 0 \\ 0 & 0 & 1 \\ 0 & 1 & 0 \end{bmatrix},$$

$$\lambda_7 = \begin{bmatrix} 0 & 0 & 0 \\ 0 & 0 & -i \\ 0 & i & 0 \end{bmatrix}, \quad \lambda_8 = \frac{1}{\sqrt{3}} \begin{bmatrix} 1 & 0 & 0 \\ 0 & 1 & 0 \\ 0 & 0 & -2 \end{bmatrix}.$$

The Gell-Mann matrices are the generators of the SU(3) group. They are the generalization of the Pauli operators for three-level systems. They have some algebraic properties which are useful for quantum state tomography, i.e.:

$$\lambda_i = \lambda_i^*, \qquad \operatorname{Tr} \lambda_i = 0 \quad \text{and} \quad \operatorname{Tr} \lambda_i \lambda_j = 2\delta_{ij}. \tag{4}$$

For three-level quantum systems the initial density matrix $\rho(0) \in \mathcal{S}(\mathcal{H})$ can be decomposed in the basis of the Gell-Mann matrices [1]:

$$\rho(0) = \frac{1}{3}\mathbb{I}_3 + \frac{1}{2}\sum_{i=1}^{8} \langle \lambda_i \rangle \lambda_i, \tag{5}$$

where $\langle \lambda_i \rangle$ is the expectation value of the observable λ_i. Mathematically, it can be computed as $\langle \lambda_i \rangle = \operatorname{Tr}\{\lambda_i \rho(0)\}$.

If one would like to directly apply this decomposition in order to reconstruct the density matrix, one would have to know the mean values of eight distinct observables $\{\lambda_1, \lambda_2, \ldots, \lambda_8\}$. Such data would be necessary to complete the formula for $\rho(0)$. This approach to quantum tomography, which does not take advantage of the knowledge about evolution, shall be referred to as the static approach. This scheme appears impractical since one is not able to define eight distinct physical quantities. This observation justifies the need for more economic approach which aims to decrease the number of distinct observables.

2.2 Dynamic approach to quantum state tomography of qutrits

Laser cooling is a very widely investigated topic in modern Physics, e.g. [13, 14]. A lot of attention has been paid to different aspects of this problem. In particular, one may refer to applications of atoms subject to laser cooling in quantum information encoding [15]. In this paper we search for a link between laser cooling and quantum state tomography.

An example often studied in the area of laser spectroscopy is a quantum system subject to laser cooling with three energy levels ($\dim \mathcal{H} = 3$) [16]. The evolution of the density matrix of such a three-level system is given by a master equation of the form:

$$\begin{aligned} \frac{d\rho(t)}{dt} &= -i[H(t), \rho(t)] + \\ &+ \gamma_1 \left(E_1 \rho(t) E_1^* - \frac{1}{2}\{E_1^* E_1, \rho(t)\} \right) + \\ &+ \gamma_2 \left(E_2 \rho(t) E_2^* - \frac{1}{2}\{E_2^* E_2, \rho(t)\} \right), \end{aligned} \tag{6}$$

where $E_1 = |1\rangle\langle 2|$ and $E_2 = |3\rangle\langle 2|$. The vectors $\{|1\rangle, |2\rangle, |3\rangle\}$ denote the standard basis in $\mathcal{H}$.

This kind of dynamics appears when the excited state $|2\rangle$ decays spontaneously into two ground states $|1\rangle$ and $|3\rangle$ with corresponding decoherence rates γ_1 and γ_3.

Moreover in this analysis we take $H(t) = [0]$, where $[0]$ denotes a 3−dimensional matrix with all entries equal 0. This assumption means that we shall analyze only the Lindbladian part of the evolution equation.

In case of a three-level open quantum system with dynamics given by the master equation from (6) we can formulate and prove a theorem which provides the minimal number of distinct observables required for quantum tomography.

Theorem 3. *For a quantum system subject to laser cooling according to (6) there exists four distinct observables such that their average values (measured at selected time instants over different copies of the system) suffice to determine the initial density matrix* $\rho(0)$.

Proof. Based on the method of matrix vectorization [8, 17], the dissipative part of the generator of evolution (6) can be explicitly expressed as a matrix:

$$\mathbb{L} = \gamma_1 \left(E_1 \otimes E_1 - \frac{1}{2} \left(\mathbb{I}_9 \otimes E_1^T E_1 + E_1^T E_1 \otimes \mathbb{I}_9 \right) \right) + \\ + \gamma_2 \left(E_2 \otimes E_2 - \frac{1}{2} \left(\mathbb{I}_9 \otimes E_2^T E_2 + E_2^T E_2 \otimes \mathbb{I}_9 \right) \right) . \tag{7}$$

Taking into account the fact that the vectors $\{|1\rangle, |2\rangle, |3\rangle\}$ constitute the standard basis, the matrix form of the quantum generator $\mathbb{L}$ can be obtained:

$$\mathbb{L} = \begin{bmatrix} 0 & 0 & 0 & 0 & \gamma_1 & 0 & 0 & 0 & 0 \\ 0 & -\Gamma & 0 & 0 & 0 & 0 & 0 & 0 & 0 \\ 0 & 0 & 0 & 0 & 0 & 0 & 0 & 0 & 0 \\ 0 & 0 & 0 & -\Gamma & 0 & 0 & 0 & 0 & 0 \\ 0 & 0 & 0 & 0 & -2\Gamma & 0 & 0 & 0 & 0 \\ 0 & 0 & 0 & 0 & 0 & -\Gamma & 0 & 0 & 0 \\ 0 & 0 & 0 & 0 & 0 & 0 & 0 & 0 & 0 \\ 0 & 0 & 0 & 0 & 0 & 0 & 0 & -\Gamma & 0 \\ 0 & 0 & 0 & 0 & \gamma_2 & 0 & 0 & 0 & 0 \end{bmatrix}, \tag{8}$$

where $\Gamma = \frac{1}{2}(\gamma_1 + \gamma_2)$.

Having the matrix form of the generator of evolution $\mathbb{L}$, one can calculate its eigenvalues:

$$\sigma(\mathbb{L}) = \{0, 0, 0, 0, -2\Gamma, -\Gamma, -\Gamma, -\Gamma, -\Gamma\} . \tag{9}$$

Since in this case the operator $\mathbb{L}$ is not self-adjoint, the algebraic multiplicity of an eigenvalue does not have to be equal to its geometric multiplicity. But one can quickly determine that there are four linearly independent eigenvectors that correspond to the eigenvalue 0. Therefore, we can find the index of cyclicity for the operator in question:

$$\eta = \max_{\lambda \in \sigma(\mathbb{L})} \{\dim \mathrm{Ker}(\mathbb{L} - \lambda \mathbb{I}_9)\} = 4 , \tag{10}$$

which means that we need exactly four distinct observables to perform quantum tomography of the analyzed system. □

One can instantly notice that if the static approach was applied to three-level laser cooling, one would have to measure 8 distinct observables whereas in the dynamic approach 4 observables suffice to perform quantum tomography. If one thinks of potential applications in experiments, then our result means that one would have to prepare 4 different experimental setups instead of 8. This observation demonstrates that the stroboscopic approach has an advantage over the static approach because it is more economic when it comes to the number of distinct kinds of measurement.

The next issue that we are interested in is the minimal polynomial for the operator $\mathbb{L}$. Assuming that this polynomial has the monic form, i.e.:

$$d_3 \mathbb{L}^3 + d_2 \mathbb{L}^2 + d_1 \mathbb{L} + d_0 \mathbb{I} = 0 , \tag{11}$$

one can get :

$$d_3 = 1,\ d_2 = \frac{3}{2}(\gamma_1 + \gamma_2),\ d_1 = \frac{1}{2}(\gamma_1 + \gamma_2)^2,\ d_0 = 0 . \tag{12}$$

Thus, we see that $\deg \mu(\mathbb{L}) = 3$. This means that each observable should be measured at most at three different time instants. One can conclude that, since we need 8 independent pieces of information to reconstruct the initial density matrix, not every observable will be measured the maximum number of times. To provide a precise answer to the question concerning the algebraic structure of the observables and the choice of time instants, we shall accept additional assumptions concerning the generator of evolution.

Let us consider a special case of the generator of evolution defined in (8) such that $\gamma_1 = 1/4$ and $\gamma_2 = 3/4$. For this specific generator, we can formulate a theorem.

Theorem 4. *The initial density matrix* $\rho(0)$ *of a three-level system subject to laser cooling can be reconstructed from the mean values of four observables of the form:*

$$Q_1 = \begin{bmatrix} 1 & 0 & 0 \\ 0 & -1 & 1+i \\ 0 & 1-i & 0 \end{bmatrix}, \quad Q_2 = \begin{bmatrix} 0 & 0 & 1+i \\ 0 & 0 & 0 \\ 1-i & 0 & 0 \end{bmatrix}, \\ Q_3 = \begin{bmatrix} 0 & 1 & 0 \\ 1 & \frac{1}{\sqrt{3}} & 0 \\ 0 & 0 & -\frac{2}{\sqrt{3}} \end{bmatrix}, \quad Q_4 = \begin{bmatrix} 0 & i & 0 \\ -i & 0 & 0 \\ 0 & 0 & 0 \end{bmatrix}, \tag{13}$$

where the mean values of Q_1 *and* Q_2 *are measured at* 3 *distinct time instants and the observables* Q_3 *and* Q_4 *once at* $t = 0$.

Proof. According to the assumptions of the stroboscopic tomography, the information that one can obtain from an experiment is encoded in the mean values of some observables, which mathematically can be written as:

$$m_i(t_j) = \mathrm{Tr}\{Q_i \rho(t_j)\} , \tag{14}$$

where $\rho(t_j) = \exp(\mathbb{L}t_j)[\rho(0)]$.

One is aware that $\exp(\mathbb{L}t_j)$ can be decomposed as:

$$\exp(\mathbb{L}t) = \alpha_0(t)\mathbb{I}_9 + \alpha_1(t)\mathbb{L} + \alpha_2(t)\mathbb{L}^2\,, \tag{15}$$

where the functions $\{\alpha_0(t), \alpha_1(t), \alpha_2(t)\}$ are linearly independent. In order to determine these functions, we need to employ the minimal polynomial of $\mathbb{L}$ and then solve a system of differential equations [6, 8]. Having done the necessary computations, one gets:

$$\begin{cases} \alpha_0(t) = 1 \\ \alpha_1(t) = e^{-t} - 4e^{-\frac{1}{2}t} + 3 \\ \alpha_2(t) = 2e^{-t} - 4e^{-\frac{1}{2}t} + 2\,. \end{cases} \tag{16}$$

Since one is able to decompose $\exp(\mathbb{L}t_j)$ in the basis of three operators $\{\mathbb{I}_9, \mathbb{L}, \mathbb{L}^2\}$ due to linearity of the matrix trace we get:

$$\begin{aligned} m_i(t_j) = \alpha_0(t_j)\mathrm{Tr}\{Q_i\rho(0)\} + \alpha_1(t_j)\mathrm{Tr}\{Q_i\mathbb{L}[\rho(0)]\} + \\ + \alpha_2(t_j)\mathrm{Tr}\{Q_i\mathbb{L}^2[\rho(0)]\}\,. \end{aligned} \tag{17}$$

If by $\mathbb{L}^*$ we shall denote the dual operator to $\mathbb{L}$, then by changing the perspective from the Schrödinger picture to the Heisenberg representation we can obtain:

$$\begin{aligned} m_i(t_j) = \alpha_0(t_j)\mathrm{Tr}\{Q_i\rho(0)\} + \alpha_1(t_j)\mathrm{Tr}\{\mathbb{L}^*[Q_i]\rho(0)\} + \\ + \alpha_2(t_j)\mathrm{Tr}\{(\mathbb{L}^*)^2[Q_i]\rho(0)\}\,. \end{aligned} \tag{18}$$

This means that if the mean value of the observable Q_1 is measured at three distinct time instants, one gets a matrix equation:

$$\begin{bmatrix} m_1(t_1) \\ m_1(t_2) \\ m_1(t_3) \end{bmatrix} = \begin{bmatrix} \alpha_0(t_1) & \alpha_1(t_1) & \alpha_2(t_1) \\ \alpha_0(t_2) & \alpha_1(t_2) & \alpha_2(t_2) \\ \alpha_0(t_3) & \alpha_1(t_3) & \alpha_2(t_3) \end{bmatrix} \begin{bmatrix} \mathrm{Tr}\{Q_1\rho(0)\} \\ \mathrm{Tr}\{\mathbb{L}^*[Q_1]\rho(0)\} \\ \mathrm{Tr}\{(\mathbb{L}^*)^2[Q_1]\rho(0)\} \end{bmatrix} \tag{19}$$

Since the functions $\{\alpha_0(t), \alpha_1(t), \alpha_2(t)\}$ are linearly independent one can agree that if we select three different nonzero time instants such that $t_1 \neq t_2 \neq t_3$, then the matrix $[\alpha_k(t_j)]$ must be invertible. It implies that the measurement results $\{m_1(t_1), m_1(t_2), m_1(t_3)\}$ can be translated into a set of scalar products:

$$\left\{\mathrm{Tr}\{Q_1\rho(0)\}, \mathrm{Tr}\{\mathbb{L}^*[Q_1]\rho(0)\}, \mathrm{Tr}\{(\mathbb{L}^*)^2[Q_1]\rho(0)\}\right\}.$$

The very same measurement procedure, which must result in a matrix equation analogous to (19), can be performed for the observable Q_2. Triple measurement of Q_2 at distinct time instants yields a set of the scalar products:

$$\left\{\mathrm{Tr}\{Q_2\rho(0)\}, \mathrm{Tr}\{\mathbb{L}^*[Q_2]\rho(0)\}, \mathrm{Tr}\{(\mathbb{L}^*)^2[Q_2]\rho(0)\}\right\}.$$

Finally, a single measurement of the average value of Q_3 and Q_4 at time instant $t = 0$ provides another two scalar products: $\{\mathrm{Tr}\{Q_3\rho(0)\}, \mathrm{Tr}\{Q_4\rho(0)\}$.

One can check numerically that the operators:

$$\left\{\mathbb{I}_3, Q_1, \mathbb{L}^*[Q_1], (\mathbb{L}^*)^2[Q_1], Q_2, \mathbb{L}^*[Q_2], (\mathbb{L}^*)^2[Q_2], Q_3, Q_4\right\}$$

constitute a spanning set (they are all linearly independent), which means that they span the space $B_*(\mathcal{H})$.

The spanning criterion is the necessary and sufficient condition for the ability to reconstruct the initial density matrix of a qutrit subject to laser cooling. This condition is satisfied for the observables defined in the theorem 4, which can be observed numerically by using the software Mathematica 11.

In other words, the operators:

$$\left\{\mathbb{I}_3, Q_1, \mathbb{L}^*[Q_1], (\mathbb{L}^*)^2[Q_1], Q_2, \mathbb{L}^*[Q_2], (\mathbb{L}^*)^2[Q_2], Q_3, Q_4\right\}$$

constitute a quorum, i.e. they span the space to which $\rho(0)$ belongs. Therefore, the scalar products that one can calculate from the measurement results can be considered a complete set of information. Thus, the measurement procedure, which utilizes only 4 distinct kinds of measurement, provides 8 independent pieces of information which are sufficient for the density matrix reconstruction. □

The theorems 3 and 4 provide a complete description of the quantum tomography scheme. One knows exactly what steps should be taken in order to compute the unknown density matrix.

The results are in accord with current trends in quantum state tomography where a lot of attention is paid to the methods which aim to reduce the experimental effort, e.g. [18, 19]. If one can access the knowledge about dynamics of the system encoded in the generator of evolution, it seems more convenient to perform repeatedly the same kind of measurement (over distinct copies of the system) rather than develop a large number of different experimental setups.

3 Summary

In this paper we presented a complete quantum tomography model for qutrits subject to laser cooling. The stroboscopic approach was applied to determine the optimal criteria for density matrix reconstruction. It was demonstrated that one can reduce the number of distinct observables by 50% provided the knowledge about evolution is applied. The algebraic structure of the observables was presented along with a detailed description of the scheme. Dynamic methods of state reconstruction appear to be very practical since they allow to retrieve the initial density matrix in the most economical way, by minimizing the number of distinct measurement setups.

The article indicates a link between quantum state tomography and laser cooling. Both topics play a substantial role in the field of quantum communication. The ability to reconstruct the quantum state from measurements is crucial to determine the efficiency of quantum communication protocols. Whereas atoms subject to laser cooling are often utilized to

encode quantum information. The dynamic quantum tomography scheme presented in this article combines these two lines of research.

The current work can be extended in the future research by studying the problem of quantum state tomography for systems subject to laser cooling with more than three energy levels. This task requires advanced algebraic methods to study the spectrum of the generator of evolution as well as to determine its minimal polynomial.

Received on March 4, 2020

References

1. Kimura G. The Bloch vector for N-level systems. *Phys. Lett. A*, 2003, v. 314 (5-6), 339–349.
2. Altepeter J. B., James D. F. V., Kwiat P. G. 4 Qubit Quantum State Tomography. In: Paris M. G. A., Rehacek J. (eds.) Quantum State Estimation. Springer, Berlin, 2004, 111–145.
3. Alicki R., Lendi K. Quantum Dynamical Semigroups and Applications. Springer, Berlin, 1987.
4. Jamiolkowski A. The Minimal Number of Operators for Observability of N-level Quantum Systems. *Int. J. Theor. Phys.*, 1983, v. 22 (4), 369–376.
5. Jamiolkowski A. On complete and incomplete sets of observables, the principle of maximum entropy - revisited. *Rep. Math. Phys.*, 2000, v. 46 (3), 469–482.
6. Jamiolkowski A. On a Stroboscopic Approach to Quantum Tomography of Qudits Governed by Gaussian Semigroups. *Open Syst. Inf. Dyn.*, 2004, v. 11 (1), 63–70.
7. Jamiolkowski A. Fusion Frames and Dynamics of Open Quantum Systems. In: Lyagushyn S. (ed.) Quantum Optics and Laser Experiments. InTech, Rijeka, 2012, 67–84.
8. Czerwinski A. Applications of the Stroboscopic Tomography to Selected 2-Level Decoherence Models. *Int. J. Theor. Phys.*, 2016, v. 55 (2), 658–668.
9. Czerwinski A. Minimal number of observables for quantum tomography of systems with evolution given by double commutators. *Quantum Stud.: Math. Found.*, 2017, v. 4 (4), 287–294.
10. Gorini V., Kossakowski A., Sudarshan E. C. G. Completely positive dynamical semigroups of n-level systems. *J. Math. Phys.*, 1976, v. 17 (5), 821–825.
11. Lindblad G. On the generators of quantum dynamical semigroups. *Commun. Math. Phys.*, 1976, v. 48 (2), 119–130.
12. Gell-Mann M. Symmetries of Baryons and Mesons. *Phys. Rev.*, 1962, v. 125 (3), 1067–1084.
13. Bartana A., Kosloff R., Tannor D. J. Laser cooling of molecular internal degrees of freedom by a series of shaped pulses. *J. Chem. Phys.*, 1993, v. 99 (1), 196–210.
14. Tannor D. J., Bartana A. On the Interplay of Control Fields and Spontaneous Emission in Laser Cooling. *J. Phys. Chem. A*, 1999, v. 103 (49), 10359–10363.
15. Saffman M., Walker T. G., Molmer K. Quantum information with Rydberg atoms. *Rev. Mod. Phys.*, 2010, v. 82 (3), 2313.
16. Sklarz S. E., Tannor D. J., Khaneja N. Optimal Control of Quantum Dissipative Dynamics: Analytic solution for cooling the three level Λ system. *Phys. Rev. A*, 2004, v. 69 (5), 053408.
17. Henderson H. V., Searle S. R. The vec-permutation matrix, the vec operator and Kronecker products: A review. *Linear and Multilinear A.*, 1981, v. 9 (4), 271–288.
18. Czerwinski A. Optimal evolution models for quantum tomography. *J. Phys. A: Math. Theor.*, 2016, v. 49 (7), 075301.
19. Oren D. *et al.* Quantum state tomography with a single measurement setup. *Optica*, 2017, v. 4 (8), 993–999.

Can the Nuclear Liquid Drop Model Be Improved?

Omar Yépez

E-mail: yepezoj@gmail.com

To be part of a nucleus, the constituent nucleons lose part of the original area they have. This can be measured by subtracting this area from the surface area of the nucleus. This was measured and plotted against the respective nuclear binding energy. A straight linear relationship was found for all elements, light or heavy. For a given element, the nuclear binding energy is inversely proportional to the lost original area. Thus meaning, that more area lost corresponded to a larger binding energy. β^- decay occurred to produce a nucleus with less loss of the nucleons' original area. β^+ decay occurred to produce a nucleus with less Coulomb repulsion. The nucleus stability just follows a trade-off between these two trends.

1 Introduction

Even though there is a very complete understanding of nuclear forces, they are so complicated that this knowledge can not be used to construct a complete theory of the nucleus. In other words, it is not possible to explain all nuclei properties based on the nuclear force acting between protons and neutrons. However, there is a number of models, or rudimentary theories with certain validity, which can explain a limited number of certain properties. In between those theories, the liquid drop model has been used with success and it has not changed for more than sixty years [1]. Theoretically, the nuclear liquid drop model calculates the nuclear binding energy by taking into account a number of interactions [2], i.e.

$$E_b = a_V A - a_S A^{2/3} - a_C \frac{Z(Z-1)}{A^{1/3}} - a_A \frac{(A-2Z)^2}{A} \pm \delta(A,Z) \quad (1)$$

where the coefficients a_V, a_S, a_C, a_A and $\delta(A,Z)$ are determined empirically. The volume of the nucleus is proportional to A, thus the term $a_V A$. Nucleons on the surface of the nucleus have fewer nearest neighbors. This can also be thought of as a surface tension term. If the volume term is proportional to A, the surface term should be proportional to $A^{1/3}$. The Coulomb term is due to the electric repulsion between protons in the nucleus. The asymmetry term a_A is due to the Pauli exclusion principle and the pairing term which capture the effect of spin-coupling. This formula gives the nuclear binding energy with a positive sign for exothermic reactions.

Besides its original success and continuous efforts, this model has not progressed more and still does not perform well with light nuclei [1]. There could be a number of reasons for that. Forcing a correlation between the nuclear binding energy against the number of nucleons, A; or putting several parameters to be fit against powers of A could be some of the reasons.

Nowadays, there is plenty of data about the radiuses of all isotopes for all elements, which are reported in [3]. Thus, a better correlation between the nuclear binding energy and the nucleons' surface term could be achieved. In this paper, a straight linear correlation was found between a geometrical construct that measures how much surface area has been lost by a given isotope's nucleons (Ω) and its nuclear binding energy. Changes between parent and daughter nucleus' Ω and the Coulomb repulsion are sufficient to explain β decay, emission of protons, α particles and neutrons, as well as electron capture. The nucleus stability appears as a consequence of a trade-off between these two trends.

2 Experimental

All isotope radiuses were reported in [3]. The radiuses of the proton and neutron used were: $r_p = 0.8783$ fm [3] and $r_n = 1.21$ fm [4], respectively. Assuming they are all spheres*, the formula created to compute how much of the nucleons spherical surface area has been lost or gained to form the nucleus was

$$\Omega = \frac{4\pi(r_i^2 - Zr_p^2 - Nr_n^2)}{Z+N}\,. \quad (2)$$

Ω is the surface area difference between the isotope and its components per number of nucleons, $A = Z + N$, in fm^2, r_i is the radius of the isotope, Z is the number of protons and N is the number of neutrons. The nuclear binding energy (mass defect) was calculated by the following formula [5]

$$E_b = (Zm_e + Zm_p + Nm_n - m_i)c^2 \quad (3)$$

where m_e, m_p and m_n are the masses of the electron, proton and the neutron respectively and m_i is the mass of the isotope. The masses of the isotopes were reported in [6], the decay mode, energy and yields were reported in [7]. The following figures present the graphs of Ω versus the nuclear binding energy for different elements. In the case of nuclear decays, $\Delta\Omega$ is the difference between daughter and parent nucleus' Ω.

3 Results

Fig. 1 shows that Ω for a given group of isotopes is inversely proportional to its nuclear binding energy. It is also observed that the rate of its change diminished as the number of protons increase. In this way, helium presents the largest changes in

*It is known the nucleus has different shapes. A sphere is one of them.

Ω within smaller changes in nuclear binding energy, whereas radon showed very small changes in Ω corresponding to larger changes in binding energy.

Fig. 2 presents Ω versus nuclear binding energy for He, Li, Be and B isotopes. The isotope with a red circle are the stable ones. It is clearly observed that as the binding energy increases, the nucleons of a given isotope presents a more negative Ω and requires more binding energy to form.

Beginning with two stable isotopes, ^{3}He's Ω is positive because the addition of the area of two protons and one neutron is not larger than the area of the isotope. Whereas ^{4}He's Ω is negative because the addition of the areas of two protons and two neutrons is larger than the area of that isotope. Once ^{6}He formed, the stability is lost. Given that ^{6}Li has a lower mass than ^{6}He, β^- decays occur, liberating 3.51 MeV. This process follows an Ω increase and therefore ΔΩ was 6.48 fm^2 for this reaction.

In the same manner, ^{8}He suffers β^- decay and neutron emission to ^{7}Li, with 16% reaction yield. It liberates 8.63 MeV. This is also accompanied by the emission of one neutron. Again, the daughter nucleus presents a more positive Ω and therefore ΔΩ = 6.41 fm^2 for this reaction.

^{8}He also suffers β^- decay to ^{8}Li, with 83% yield. It liberates 10.66 MeV and ΔΩ = 3.86 fm^2.

^{7}Be suffers 100% β^+ decay into ^{7}Li. Contrary to the previous trend, in this process the daughter presented a more negative Ω than the parent nucleus. But also, β^+ diminished the number of protons in the daughter nucleus, thus diminishing the Coulomb repulsion. Contrary to previous β^- decay, in this case ΔΩ = -3.13 fm^2.

^{9}Li repeats ^{6}He's behavior. ^{11}Li presents neutron emission to ^{10}Be with 86.3% yield and β^- decay to ^{11}Be with 6% yield*. This is very similar to ^{8}He transmutation. Finally, ^{10}Be repeats ^{6}He's behavior. Table 1 summarizes the nuclear processes observed in Fig. 2. It is clearly observed that β^- and neutron emission presents a positive ΔΩ, whereas β^+ decay shows a negative ΔΩ.

Fig. 3 presents Ω versus nuclear binding energy for O, F, Ne, Na and Mg isotopes. A 100% of ^{17}Ne transmutes to ^{16}O after β^+ decay and a proton emission, producing 11.63 MeV. ΔΩ in this case was -1.88 fm^2. A 100% of ^{19}Ne transmutes to ^{19}F after β^+ decay, producing 2.20 MeV and ΔΩ = -0.88 fm^2. ^{20}Na goes to ^{20}Ne with 75% yield, producing 12.87 MeV and ΔΩ = -0.26 fm^2. It also emits an alpha particle and a positron to produce ^{16}O with 25% yield, generating 8.14 MeV and ΔΩ = -0.26 fm^2. Table 2 presents the transitions observed in Fig. 3. It is clearly observed that β^+, proton and alpha particle emissions present a negative ΔΩ, whereas β^- and $2\beta^-$ decays show a positive ΔΩ.

Fig. 4 presents Ω versus nuclear binding energy for Ar, K, Ca, Sc and Ti isotopes. A 100% of ^{38}K transmutes to ^{38}Ar after β^+ decay, producing 4.89 MeV and ΔΩ in this case was -0.28 fm^2.

A 100% of ^{39}Ca transmutes to ^{39}K after β^+ decay, producing 6.52 MeV and ΔΩ = -0.28 fm^2. ^{40}K goes to ^{40}Ca with 89.28% yield, producing 1.31 MeV and ΔΩ = 0.30 fm^2. ^{40}K also suffers electron capture to ^{40}Ar with 10.72% yield, producing 0.48 MeV and ΔΩ = -0.24 fm^2. A 100% of ^{41}Ca transmutes to ^{41}K after β^+ decay, producing 0.42 MeV and ΔΩ = -0.32 fm^2. Also, ^{41}Ar suffers β^- decay to ^{41}Ca producing 2.49 MeV and ΔΩ = 0.21 fm^2. Table 3 depicts the transitions

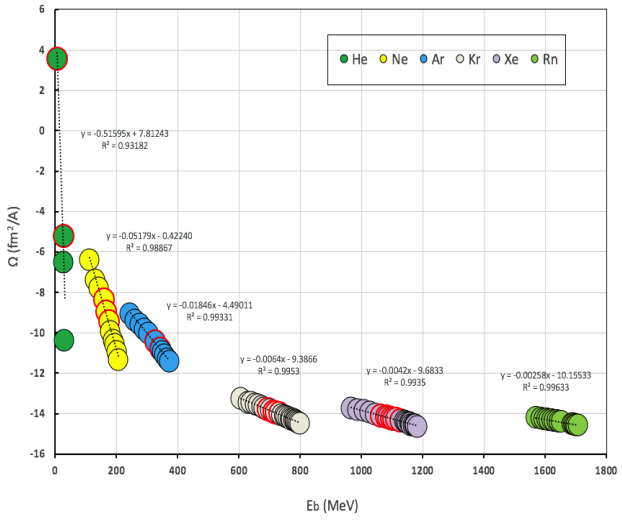

Fig. 1: Ω vs. binding energy for Noble gases. The red circles are the stable isotopes.

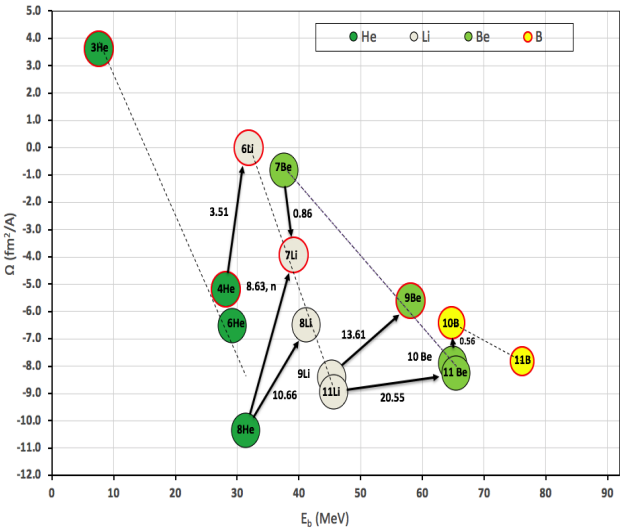

Fig. 2: Ω vs. mass defect for He, Li, Be and B isotopes. The red circles are the stable isotopes. The energy of the transitions (MeV) were reported in [7].

*This nucleus also experiences double and triple neutron emission, α emission and fission in lower yields.

Table 1: Reaction, mass and area (ΔΩ) difference between parent and daughter nuclei, and decay mode for the reactions depicted in Figure 2.

Reaction	Released Energy (MeV) [7]	ΔΩ (fm²)	Decay
$^{4}_{2}\mathrm{He} \rightarrow {}^{6}_{3}\mathrm{Li} + e^{-} + \nu$	3.51	6.48	β⁻
$^{8}_{2}\mathrm{He} \rightarrow {}^{7}_{3}\mathrm{Li} + e^{-} + n + \nu$	8.63	6.41	β⁻ and neutron emission
$^{8}_{2}\mathrm{He} \rightarrow {}^{8}_{3}\mathrm{Li} + e^{-} + \nu$	10.66	3.86	β⁻
$^{7}_{4}\mathrm{Be} \rightarrow {}^{7}_{3}\mathrm{Li} + e^{+} + \nu$	0.86	-3.13	β⁺
$^{9}_{3}\mathrm{Li} \rightarrow {}^{9}_{4}\mathrm{Be} + e^{-} + \nu$	13.61	2.79	β⁻
$^{11}_{3}\mathrm{Li} \rightarrow {}^{10}_{4}\mathrm{Be} + e^{-} + n + \nu$	20.55	0.68	β⁻ and neutron emission
$^{10}_{4}\mathrm{Be} \rightarrow {}^{9}_{5}\mathrm{B} + e^{+} + \nu$	0.56	1.85	β⁻

Table 2: Reaction, mass and area (ΔΩ) difference between parent and daughter nuclei, and decay mode for the reactions depicted in Figure 3.

Reaction	Released Energy (MeV) [7]	ΔΩ (fm²)	Decay
$^{17}_{10}\mathrm{Ne} \rightarrow {}^{16}_{8}\mathrm{O} + e^{+} + p + \nu$	14.55	-1.88	β⁺ and proton emission
$^{19}_{10}\mathrm{Ne} \rightarrow {}^{19}_{9}\mathrm{F} + e^{+} + \nu$	3.24	-0.88	β⁺
$^{20}_{11}\mathrm{Na} \rightarrow {}^{16}_{8}\mathrm{O} + e^{+} + \alpha + \nu$	9.16	-0.26	β⁺ and α emission
$^{20}_{11}\mathrm{Na} \rightarrow {}^{20}_{10}\mathrm{Ne} + e^{+} + \nu$	13.89	-0.30	β⁺
$^{21}_{11}\mathrm{Na} \rightarrow {}^{21}_{10}\mathrm{Ne} + e^{+} + \nu$	3.55	-0.57	β⁺
$^{22}_{11}\mathrm{Na} \rightarrow {}^{22}_{10}\mathrm{Ne} + e^{+} + \nu$	2.84	-0.50	β⁺
$^{23}_{10}\mathrm{Ne} \rightarrow {}^{23}_{11}\mathrm{Na} + e^{-} + \nu$	4.38	0.65	β⁻
$^{24}_{10}\mathrm{Ne} \rightarrow {}^{24}_{12}\mathrm{Mg} + 2e^{-} + 2\nu$	7.99	1.21	2β⁻
$^{25}_{10}\mathrm{Ne} \rightarrow {}^{25}_{12}\mathrm{Mg} + 2e^{-} + 2\nu$	11.15	0.99	2β⁻
$^{26}_{10}\mathrm{Ne} \rightarrow {}^{26}_{12}\mathrm{Mg} + 2e^{-} + 2\nu$	16.70	0.98	2β⁻

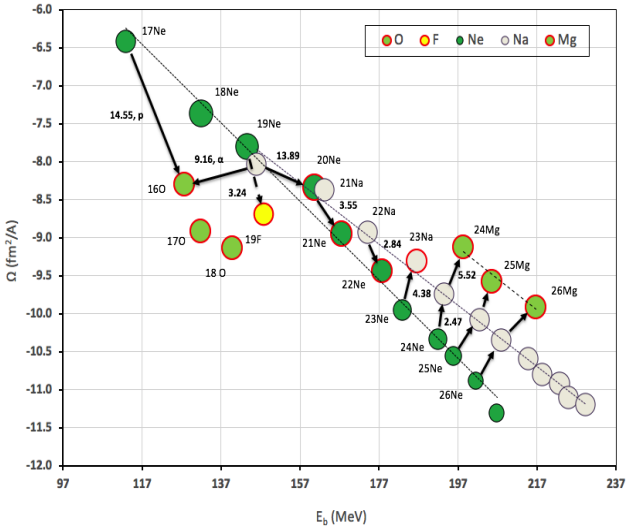

Fig. 3: Ω vs. mass defect for O, F, Ne, Na and Mg isotopes. The red circles are the stable isotopes. The energy of the transitions (MeV) were reported in [7].

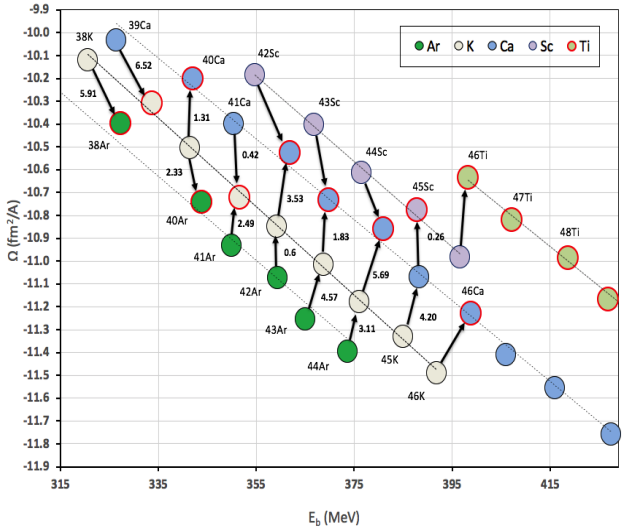

Fig. 4: Ω vs. mass defect for Ar, K, Ca, Sc and Ti isotopes. The red circles are the stable isotopes. The energy of the transitions (MeV) were reported in [7].

observed in Fig. 4. It is clearly observed that electron capture presents a negative ΔΩ.

4 Discussion

4.1 Meaning of Ω and the Nuclear Liquid Drop Model

Ω was computed by using one dimension (the radius) and the three dimensions (the volume). All elements kept a good linear relationship between Ω and the nuclear binding energy. However, in the case of helium, either the linear relationship was lost or the isotopes did not occur proportionally. For example: ^{6}He occurred between ^{3}He and ^{4}He. This relationship is also very sensitive to the neutron radius. Overall, to keep ^{4}He to land between ^{3}He and ^{6}He, r_n needs to be at least 0.05 fm larger than r_p. This may be an indication that the spherical model is only partly applicable to helium. According to the results presented in Fig. 1, it seems that a surface-based Ω is a fundamental property of the isotopes of any element. Given the nature of Ω, it is obvious that larger changes per nucleon would occur in the lowest mass element, helium. This is because the number of nucleons is the lowest. As the number of protons increase, Ω changes less because it is divided by a progressively larger number of nucleons. In a given element, Ω becomes more negative because the addition of the area of the components of the nucleus is progressively larger than its isotope's area. This corresponds to an increasing nuclear binging energy. Which can be interpreted as more energy is

Table 3: Reaction, mass and area (ΔΩ) difference between parent and daughter nuclei, and decay mode for the reactions depicted in Figure 4.

Reaction	Released Energy (MeV) [7]	ΔΩ (fm²)	Decay
$^{38}_{19}\mathrm{K} \rightarrow {}^{38}_{18}\mathrm{Ar} + \mathrm{e}^{+} + \nu$	5.91	-0.28	β⁺
$^{39}_{20}\mathrm{Ca} \rightarrow {}^{39}_{19}\mathrm{K} + \mathrm{e}^{+} + \nu$	6.52	-0.28	β⁺
$^{40}_{19}\mathrm{K} \rightarrow {}^{40}_{18}\mathrm{Ca} + \mathrm{e}^{-} + \nu$	1.31	0.30	β⁻
$^{40}_{19}\mathrm{K} \rightarrow {}^{40}_{18}\mathrm{Ar} + \mathrm{e}^{+} + \nu$	1.50	-0.24	EC
$^{41}_{20}\mathrm{Ca} \rightarrow {}^{41}_{19}\mathrm{K} + \mathrm{e}^{+} + \nu$	0.41	-0.32	β⁺
$^{41}_{18}\mathrm{Ar} \rightarrow {}^{41}_{19}\mathrm{K} + \mathrm{e}^{-} + \nu$	2.49	0.21	β⁻
$^{42}_{18}\mathrm{Ar} \rightarrow {}^{42}_{20}\mathrm{Ca} + 2\mathrm{e}^{-} + 2\nu$	4.10	0.55	2β⁻
$^{43}_{18}\mathrm{Ar} \rightarrow {}^{43}_{20}\mathrm{Ca} + 2\mathrm{e}^{-} + 2\nu$	6.40	0.53	2β⁻
$^{44}_{18}\mathrm{Ar} \rightarrow {}^{44}_{20}\mathrm{Ca} + 2\mathrm{e}^{-} + 2\nu$	9.07	0.54	2β⁻
$^{45}_{19}\mathrm{K} \rightarrow {}^{45}_{21}\mathrm{Sc} + 2\mathrm{e}^{-} + 2\nu$	4.46	0.55	2β⁻

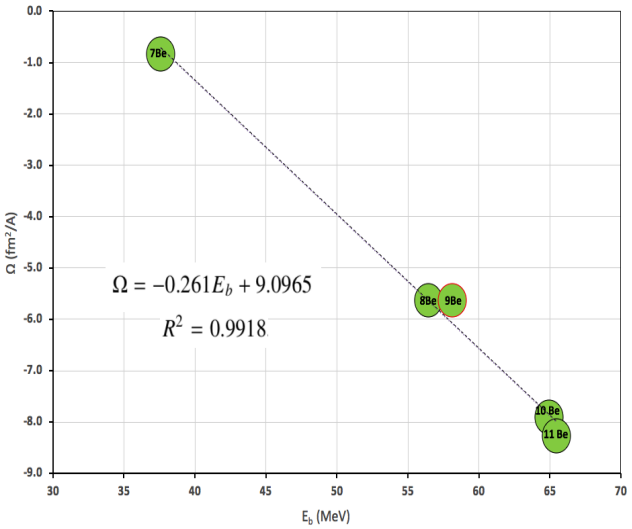

Fig. 5: Ω vs. mass defect for B isotopes. The red circle is the stable isotope.

needed to compress the nucleons' area into the nucleus. This means that all nucleons share the nucleus surface.

This proportionality between the nuclear binding energy and the surface lost to create the nucleus contrasts with the semi-empirical mass formula (1). This is because Fig. 1 presents explicitly that the nuclear binding energy is just proportional to the normalized nucleons' surface area lost to form the isotope. As will be discussed, the other important term is the Coulomb repulsion. This makes (1) to have too many terms to fit. This is because the underlying model for (1) is a sphere-like structure with the neutrons and protons gathered together but still separated as individual spherical particles. The underlying model that Fig. 1 suggests is one where all nucleons share the surface of the nucleus. Which means that protons and neutrons are blended, fused.

4.2 Calculation of ^{8}Be's radius

Not shown in Fig. 2, ^{8}Li transmutes to ^{8}Be and this decays into two ^{4}He. ^{8}Be is not shown in Fig. 2 because its radius was not reported in [3]. An estimation of ^{8}Be's radius can be accomplished by using the inverse proportion between Ω and the other Be isotopes. Fig. 5 shows the result. ^{8}Be nuclear binding energy is 56.50 MeV. Thus, its Ω = -5.65 fm^2 and the calculated ^{8}Be radius was 2.31 fm. This puts ^{8}Be and ^{9}Be at the same Ω as shown in Fig. 5.

4.3 Why a decay occurs

Fig. 2 depicts the helium isotopes in more detail. Given that ^{2}He is unstable, it seems that helium needs at least one neutron for stability, which occurs in ^{3}He. This suggests the neutron is acting as a Coulomb repulsion insulator. This effect continues in ^{4}He. However, ^{5}He and heavier isotopes become unstable again. It seems that there is a limit to how much area can be lost from the nucleons to form the nucleus, after which a decay is needed to resolve the instability. The first beta decay occurs between the more massive parent ^{6}He and the lighter daughter ^{6}Li producing 3.51 MeV. As observed, β^- decay involves: *to go from a heavier and lower Coulomb repulsion, which has more nucleons' surface area lost (NSL), to a lighter and higher Coulomb repulsion, which has less NSL.* Therefore, the driving force for β^- decay is to reduce the NSL. This is why the ΔΩ for this reaction is positive. This is a feature of β^- decay and several examples where ΔΩ is positive are shown in Tables 1, 2 and 3. In a more complicated process with 16% reaction yield , ^{8}He suffered neutron emission and β^- decay to transmute to ^{7}Li. This process, nevertheless, has the same features already described for β^- decay, i.e. in neutron emission ΔΩ is also positive. Another example of a positive Ω is ^{11}Li going to ^{10}Be.

^{7}Be is the first example of β^+ decay to ^{7}Li. As observed, this process involves: *to go from a heavier and higher Coulomb repulsion nucleus, which has less NSL, to a lighter and lower Coulomb repulsion nucleus, which has more NSL.* This is why the ΔΩ for this reaction is negative. Hence, the driving force for β^+ decay is to reduce the Coulomb repulsion. Other examples can be observed in Tables 2 and 3.

Fig. 3 shows that: a) ^{17}Ne transmutes to ^{16}O with 100% yield suffering β^+ decay and proton emission and b) ^{20}Na transforms into ^{16}O by the emission of an α particle and a positron. In both cases, ΔΩ is negative. Therefore, these processes are driven by the reduction of Coulomb repulsion.

Fig. 4 presents ^{40}K suffering β^-decay to ^{40}Ca with 89.28% yield. This overwhelms the β^+ decay to ^{40}Ar with 10.72% yield. This reaction suggests that, in this case, to reduce the nucleons' surface area lost is more favorable than to reduce its Coulomb repulsion.

4.4 Nucleus stability

It seems that there is a trade-off between the NSL and Coulomb repulsion for nucleus stability. In Fig. 2, ^{3}He increases the NSL until it reaches ^{6}He. Then, β decay increases the number of protons to produce ^{6}Li. But also to reduce the original NSL in ^{6}He.

At the same Coulomb repulsion,^{6}Li increases the NSL until it reaches ^{9}Li. Again, β decay diminished the NSL transmuting to ^{9}Be. This element starts again to increase NSL up to ^{10}Be, which again β decayed to ^{10}B to diminish NSL and so on. Hence, every time the surface area per nucleon increases to the unstable limit, β decay occurs to resolve the instability. This produces continuous step decreases all through stable nuclei. The process just described pass through different elements. For example, in Fig. 3 there is an increase in the NSL in the series ^{16}O:^{17}O:^{18}O. Then, there is a small NSL decrease through continuous elements, creating the row ^{18}O:^{19}F:^{20}Ne. This is occurring even though the Coulomb repulsion is increasing. The NSL increases in Ne again, following the series ^{20}Ne:^{21}Ne:^{22}Ne.

Then, another small NSL decrease occurs through elements, forming the row ^{22}Ne:^{23}Na:^{24}Mg with progressive increments in Coulomb repulsion. This is followed by another increase in the NSL in the series ^{24}Mg:^{25}Mg:^{26}Mg. In Fig. 4, the first small decrease in NSL is observed in the row ^{38}Ar:^{39}K:^{40}Ca. If we follow this row, the next element would be ^{41}Sc. This isotope is unstable because it has too much Coulomb repulsion for the small NSL decrease trade-off. As a consequence, the next stable nucleus occurs in an increase of the NSL, producing ^{40}Ar, which also is accompanied by a significant decrease in Coulomb repulsion. From ^{40}Ar a new row of small decrease of the NSL but progressive increase in Coulomb repulsion starts again, ^{40}Ar:^{41}K:^{42}Ca. This will end at ^{43}Sc, which is unstable for the same reasons discussed above.

Once ^{42}Ca is reached, a new trend of increasing NSL started, ^{42}Ca:^{43}Ca:^{44}Ca. This makes a hole in stability for ^{41}Ca. This isotope is not stable because ^{41}K presented a more favorable trade-off between the NSL and Coulomb repulsion. The next row would be ^{44}Ca:^{45}Sc:^{46}Ti. And the next series ^{46}Ti: ^{47}Ti:^{48}Ti and so on.

^{46}Ca however, appeared as an outlier in this trend. It could be argue that it makes a row with ^{46}Sc but it does not decay to it. It looks like it is an island of NSL stability.

The evidence presented calls to build a model where all nucleons share the surface of the nucleus.

5 Conclusions

The nuclear binding energy is directly related to the nucleons' surface area lost (NSL). A trade-off between the NSL and the Coulomb repulsion is related to the nucleus stability. The progressive increase of the mass in an element will produce different isotopes until its NSL reaches an upper limit for its Coulomb repulsion. Then, β^{-} decay or neutron emission occur to diminish the NSL and resolve the instability. If there is not enough neutrons (electric insulation) for a given Coulomb repulsion, β^{+} decay, proton or α emission occur to diminish it.

Received on March 7, 2020

References

1. Pomorski K. and Dudek J. P. Nuclear Liquid Drop Model with the Surface-Curvature Terms: New Perspectives for the Hyperdeformation Studies. arXiv: nucl-th/0205011.
2. Möller P. The limits of the nuclear chart set by fission and alpha decay. *EPJ Web of Conferences*, 2016, v. 131, 03002.
3. Angeli I. and Marinova K. P. Table of experimental nuclear ground state charge radii: An update. *Atomic Data and Nuclear Data Tables*, 2013, v. 99, 69.
4. Abrahamyan S. et al. (PREX Collaboration). Measurement of the Neutron Radius of ^{208}Pb through Parity Violation in Electron Scattering. *Phys. Rev. Lett.*, 2012, v. 108, 112502.
5. Pourshahian S. *J. Am. Soc. for Mass Spec.*, 2017, v. 28, 1836.
6. Wang M., Audi G., Kondev F. G., Huang W. J., Naimi S. and Xu X. The AME2016 atomic mass evaluation (II). Tables, graphs, and references. *Chinese Physics C.*, 2017, v. 41 3, 030003.
7. Audi G., Kondev F. G., Wang M., Huang W. J. and Naimi S. The NUBASE2016 evaluation of nuclear properties. *Chinese Physics C.*, 2017, v. 41 3, 030001.

Properties of Superdeformed Rotational Bands in the Perturbed SU(3) Limit of the sdg Interacting Boson Model

A.M. Khalaf[1], Azza O. El-Shal[2], M.M. Taha[2] and M.A. El-Sayed[2]

[1]Physics Department, Faculty of Science, Al-Azhar University Cairo, Egypt. E-mail: ali_khalaf43@hotmail.com
[2]Mathematics and Theoretical Physics Department, NRC, Atomic Energy Authority Cairo, P. No. 13759, Egypt.
Corresponding Author: E-mail: mathelgohary@yahoo.com (M.A. El-Sayed)

The nuclear superdeformed bands in A∼ 190, A∼ 130 mass regions have been systematically analyzed by using the perturbed SU(3) limit of the interacting boson model. The g-bosons have been taken into consideration and the SU(3) symmetry is perturbed by introducing an interaction holding the SO(5) symmetry. A four parameters simple analytic formula for the eigenvalue equation has been derived. The spin determines of the studied superdeformed (SD) bands are considered from our previous works. The improved model parameters for each nucleus have been determined by operating a computer simulated search program so as to obtain a minimum root mean square divergence of the evaluating gamma ray transition energies and the observed ones. With these adopted model parameters the transition energies E_γ, the rotational frequencies $\hbar\omega$, the kinematic $J^{(1)}$ and dynamic $J^{(2)}$ moments of inertia have calculated and are in accordance with experimental data. The behavior of $J^{(1)}$ and $J^{(2)}$ as a function of $\hbar\omega$ have been studied. The calculated E_γ have been used to investigate the anomalous $\Delta I = 2$ staggering by considering the five point formula of Cederwall staggering parameter which represent the finite deviation calculation to the fourth order derivative of the transition energies at a determined spin.

1 Introduction

It was known that the interacting boson model (IBM) [1] with s and d bosons (sdIBM) is successful in studying the spectroscopic properties of low-lying collective states in heavy and medium nuclei. This simple sdIBM allows the utilization of the algebraic symmetries for approaching different type of nuclear spectra, known as dunamical symmetries U(5), SU(3) and O(6) which geometrically describe vibrational, axially deformed and gamma soft nuclei respectively. These three symmetry limits form a Casten triangle [2], that represent the nuclear phase diagram [3]. Transitions of shape phase between these vertices of Casten triangle were widely calculated along several isotopic chains [4–10]. Extended version of IBM where one includes the g-bosons in addition to s and d bosons to account for hexadecapole deformation of the nucleus is receiving a considerable attension of several research groups [11, 12]. This hexadecapole deformation is the second most important mulitipolarity in the description of nuclear properties in addition to the quadrupole deformation. An interest in this multipolarity is increased by the observation of the $\Delta I = 2$ energy staggering of superdeformed rotational bands (SDRB's) in some nuclei [13, 14], where nuclear spins with rotational sequences splitting by two may divide into two branches. Several theoretical attempts were made for the possible explanation of this $\Delta I = 2$ staggering phenomenon [15–25]. To describe the dynamical symmetries of nuclear states consisting of spdf bosons, it was found [26, 27] that one must begin with a supersymmetric group chain U(15,10) and ending at O(3) due to conservation of angular momentum passing through SU(3) limit of the sdg IBM which is a reasonable starting point to describe SD states in IBM [28]. The sdg IBM is well adopted for study of starting deformed and SD nuclei [15, 16, 26] there is seven different limits of SU(15) [29]. These limits can be splitted into two sets, the first set consists of the three limits which include only partial mixing between the bosons, however the second set consists of four limits which include a mixing of all bosons. If we consider the case of two s, d or g bosons, then the possible angular momenta are $L = 0^3, 2^4, 3, 4^4, 5, 6^2, 8$ where the exponent indicates the multiplicity. The $L = 3, 5$ states are pure dg configurations while the $L = 8$ states is pure g^2. All other states however are mixtures of s, d and g bosons. The difficulty with performing sdg IBM computations for normal deformed and superdeformed nuclei that have boson numbers $N = 12 - 16$ is that the core is too large, and the numerical methods (diagonalization) of the Hamiltonian is not possible. It was proved that the mathematical properties of the $SU(5)_{sdg}$ can be describe the deformed nuclei [30] because by using the intrinsic coherent states [11] the potential energy surface (PES) of the $SU(5)_{sdg}$ limit displays two minima. Since SDRB's are known in the second minimum of the potential well, this property was used [31] to justify an applications of $SU(5)_{sdg}$ limit in SD states. The group SU(3) which relates to the representations $[f_1, f_2, f_3]$ through $\lambda = f_1 - f_2$ and $\mu = f_1 - f_3$ is very important in studying the axial symmetric SDRB's. The one boson state belongs to the $(\lambda, \mu) = (4, 0)$ representation while the two bosons states belongs to (7,0), (4,2), (0,4) rep-

resentation. To appear the $\Delta I = 2$ staggering, the SU(3) must be broken down by adding the $SO(5)_{sdg}$ symmetry as a perturbation. The aim of this work is to use this perturbed SU(3) of sdgIBM to investigate the main properties of superdeformed rotational bands in different nuclei and especially exhibit the $\Delta I = 2$ staggering in their transition energies.

2 Outline of the model

The states of SD bands can be classified in framework of supersymmetric group chain as:

$$\begin{array}{ccccccccccccc} U(m,n) & \supset & U_B(m) & \otimes & U_F(n) & \supset & \ldots & \supset & SO_{B+F}(3) & \otimes & SU_F(\grave{n}) & \supset & O(3) \\ \downarrow & & \downarrow & & \downarrow & & & & \downarrow & & \downarrow & & \downarrow \\ [N] & & [N_B]_m & & [N_F]_n & & & & L & & S & & I \end{array}$$

The notation under those of groups are the corresponding irreducible (irrep) representation. The particles total number $N = N_F + N_B$ with N_F and N_B the fermion and boson numbers respectively. L is the effective core angular momentum and S is the total pseuduspin and I is the total spin of the nucleus. m is determined by the constituent of bosons, while n is determined by the single particle configuration of the fermions and $\grave{n}$ is the total pseudospin. Since the bosons to describe positive parity SD states should be s, d, g bosons [17, 20, 22] and p,f bosons are essential to show negative parity states [27], the space spanned by the single boson states is $\sum_\ell (2\ell + 1) = 1 + 3 + 5 + 7 + 9 = 25$ dimensions. So that, we have the group chain for the boson part

$$\begin{array}{ccccccccccccc} U_{sdgpf}(25) & \supset & U_{sdg}(15) & \otimes & U_{pf}(10) & \supset & SU_{sdg}(3) & \otimes & SU_{pf}(3) & \supset & SU(3) & \supset & O(3) \\ \downarrow & & \downarrow & & \downarrow & & \downarrow & & \downarrow & & \downarrow & & \downarrow \\ [N_B] & & [N_{sdg}] & & [N_{pf}] & & (\lambda,\mu)_{sdg} & & (\lambda,\mu)_{pf} & & (\lambda,\mu) & & I \end{array}$$

The law-lying positive parity states are from the N_{sdg} bosons only, while negative parity states are one pf boson coupled states with $N_{sdg} = N - 1$ sdg bosons. There are also negative parity states formed by coupling odd number of pf bosons with residual sdg bosons and states of positive parity formed by even number of pf bosons with the sdg bosons. Here $N_B = N_{sdg} + N_{pf}$ with $N_{sdg} = 0, 1, 2, ..., N$ physically N is the number of positive parity bosons. All the irres can be determined with the branching rules [14] of the irres reduction. The reduction$SU(3)_{sdg} \otimes SU(3)_{pf} \supset SU(3)$ can be done in standard Young diagram method [10] and the reduction $SU(3) \supset O(3)$ is the Elliott rule [11]. We notice that for the positive parity states the results of the sdgIBM are still valid. The interaction Hamiltonian of the nucleus corresponding to the above chain takes the form

$$H = \epsilon C_1[U(15)] + kC_2[SU(3)] + cC_2[O(3)] \qquad (1)$$

in which $C_k[G]$ is the k-order Casimir operator of the group G. The energy of the states can be formulated as

$$\begin{aligned} E(I) = E_0 + \epsilon N + k[\lambda^2 + \mu^2 + \lambda\mu + 3\lambda + 3\mu] \\ + CI(I+1) \end{aligned} \qquad (2)$$

the $C_2[O(3)]$ operator gives the rotational structure. In varaible moment of inertia model [32], the moment of inertia is spin dependent, such that as I increases, the moment of inertia increase due to the antipairing effect. Therefore, Hamiltonian equation (1) can be written as

$$\begin{aligned} H = \; & \epsilon C_1[U(15)] + kC_2[SU(3)] \\ & + C_0 \frac{C_2[O(3)]}{1 + f_1 C_2[O(3)] + f_2 (C_2[O(3)])^2} \end{aligned} \qquad (3)$$

where the terms with f_1 and f_2 take into account many-body interactions which induce antipairing driving and pairing damping effects on the moment of inertia. The energy of the state I in a band considering only the relative excitation of the states in a rotational band is given by

$$E(I) = C_0 \frac{I(I+1)}{1 + f_1[(I+1)I] + f_2[(I+1)I]^2} \qquad (4)$$

To describe the superdeformed rotational bands, we break SU(3) symmetry by adding the symmetry $SO_{sdg}(5)$ as a perturbation to the Hamiltonian. Therefore, the excited energy of the state of positive parity with spin I in SD band is thus given by

$$\begin{aligned} E(I) = \; & B[\tau_1(\tau_1 + 3) + \tau_2(\tau_2 + 1)] \\ & + \frac{C_0}{1 + f_1[(I+1)I] + f_2[(I+1)I]^2} I(I+1) \end{aligned} \qquad (5)$$

The (τ_1, τ_2) is the irrep of SO(5) group. In practical τ_1, τ_2 being fixed with the branching rules of the irrep reduction as [21–24]

$$\begin{aligned} (\tau_1, \tau_2) &= (\tfrac{I}{2}, 0) \quad \text{if} \quad I = 4k, 4k+1 \quad (k = 0, 1, 2, ...) \\ (\tau_1, \tau_2) &= (\tfrac{I}{2} - 1, 2) \quad \text{if} \quad I = 4k+2, 4k+3 \quad (k = 0, 1, 2, ..) \end{aligned}$$

3 Analysis of ΔI = 2 staggering in transition energies in SD bands

In framework of collective model [33], the rotational frequency $\hbar\omega$, the kinematic moment of inertia ($J^{(1)}$) and the dynamic moment of inertia ($J^{(2)}$) calculated from γ-ray transition energies for SDRB's are given from the following definitions

$$\hbar\omega = \frac{1}{4}\left[E_\gamma(I+2 \to I) + E_\gamma(I \to I-2)\right] \qquad (MeV) \quad (6)$$

$$J^{(2)} = \frac{4}{E_\gamma(I+2 \to I) - E_\gamma(I \to I-2)} \qquad (\hbar^2 MeV^{-1}) \quad (7)$$

$$J^{(1)} = \frac{2I-1}{E_\gamma(I \to I-2)} \qquad (\hbar^2 MeV^{(-1)}) \quad (8)$$

Table 1: The adopted best model parameters C_0, B, f_1, f_2 obtained from the fitting procedure for the studied SD bands. The bandhead spin I_0 and the experimental lowest transition energy $E_\gamma(I_0 + 2 \rightarrow I_0)$ for each SD is also given.

SD band	I_0 ($\hbar$)	C_0 $\hbar^{-2}$ keV	B keV	f_1 $\hbar^{-2}$	f_2 $\hbar^{-4}$	E_γ (keV)
^{194}Tl(SD1)	14	0.503298E+01	0.18912E-02	0.326365E-03	-0.34134E-03	268.00
^{194}Tl(SD3)	12	0.522016E0+1	0.37473E-01	0.401374E-04	-0.39907E-08	240.50
^{194}Tl(SD5)	10	0.492810E+01	0.36833E-01	0.307779E-04	-0.42746E-08	187.90
^{130}Ce(SD2)	24	0.909181E+01	-0.34824E-02	0.171564E-04	-0.50224E-08	841.00
^{132}Ce(SD1)	30	0.647195E+01	-0.13947E-01	-0.299066E-04	0.34647E-10	808.55
^{132}Nd(SD1)	40	0.419310E+01	0.16107E-01	-0.547523E-04	-0.11468E-10	797.00
^{136}Sm(SD1)	30	0.640396E+01	0.51834E-03	-0.111011E-03	0.17709E-07	888.00

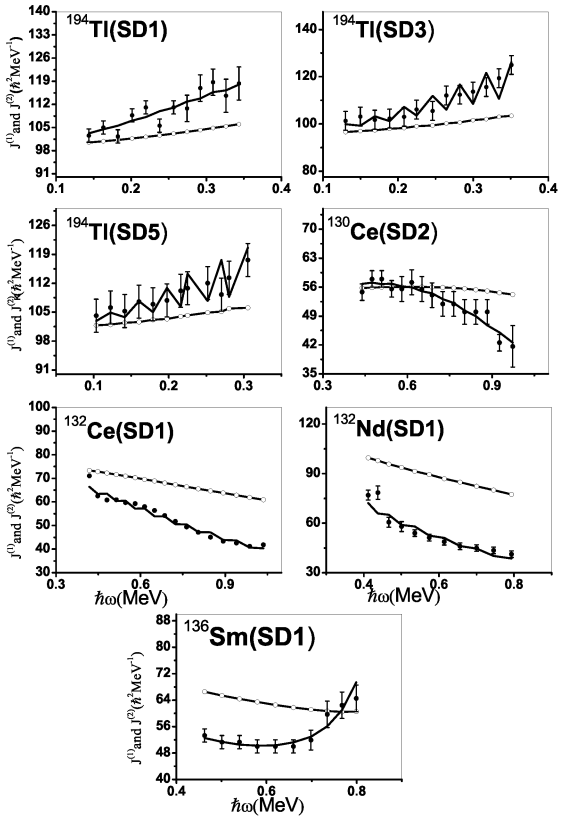

Fig. 1: The calculated results of the kinematic $J^{(1)}$ (open circles) and dynamic $J^{(2)}$ (solid curves) moments of inertia plotted as a function of rotational frequency $\hbar\omega$ for the studied SD bands and the comparison with experimental data for $J^{(2)}$ (closed circles with error bars)

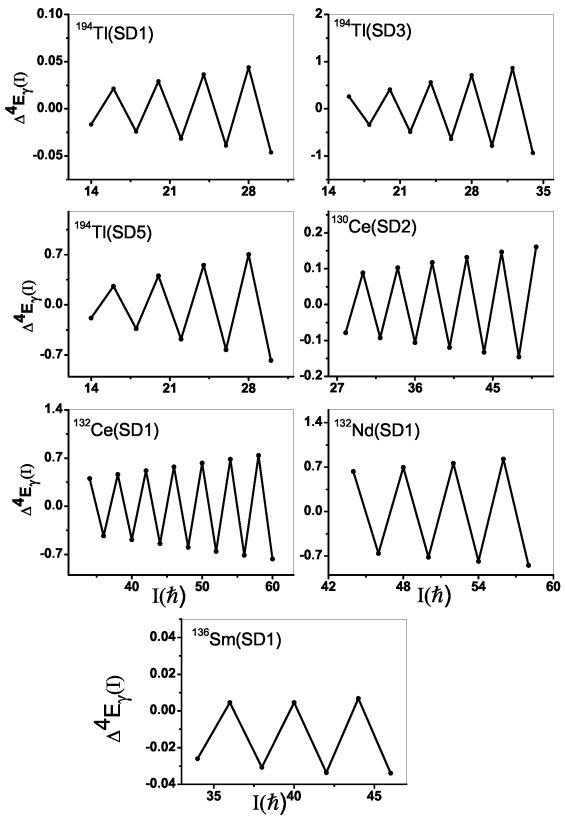

Fig. 2: The calculated $\Delta I = 2$ staggering quantity $\Delta^4 E_\gamma$ obtained by the five point formula as a function of spin for the studied SD bands.

The anomalous $\Delta I = 2$ staggering phenomenon was found in several SD bands [17,18]. Sequences of states which are differing by four units of angular momentum displace relative to each other was shown in superdeformed rotational bands. That is, the SD band can be seen as two sequences of cases with values of spin $I + 4n$ and $I + 4n + 2(n = 1, 2, 3, ...)$, respectively. This is commonly called $\Delta I = 4$ bifurcation, because the bands divide into two branches with levels differing in spin by $4\hbar$. To explore this $\Delta I = 2$ staggering, the deviation of the $\gamma-$ray energies from a smooth reference $\Delta^4 E_\gamma(I)$ was determined by Cederwall [12], by calculating the finite difference approximation of the fourth order derivation of the $\gamma-$ray energies E_γ at a given spin I by

$$\begin{aligned}\Delta^4 E_\gamma^{ref}(I) = \quad & \tfrac{1}{16}\Big[E_\gamma(I-4) - 4E_\gamma(I-2) \\ & +6E_\gamma(I) - 4E_\gamma(I+2) + E_\gamma(I+4)\Big]\end{aligned} \tag{9}$$

with $E_\gamma(I) = E_\gamma(I) - E_\gamma(I-2)$. The formula (9) contains five energies of consecutive transition and is denoted by the five point formula.

4 Numerical calculations and discussion

For each band of our studied SDRB's, the spin of the bandhead I_0 is taken from our previous works [19–25]. The model parameters C_0, B, f_1, f_2 are determined by using a computer simulated search program in order to obtain a minimum root-mean square (rms) deviation of the calculated transition energies $E_\gamma^{cal}(I)$ from the experimental one $E_\gamma^{exp}(I)$, we employed the common definition of χ

$$\chi = \frac{1}{N}\sqrt{\sum_{i=1}^{N}\left|\frac{E_\gamma^{exp}(I_i) - E_\gamma^{cal}(I_i)}{\delta E_\gamma^{exp}(I_i)}\right|^2} \tag{10}$$

where N is the number of the data points entering into the fitting procedure and $\delta E_\gamma^{exp}(I_i)$ are the experimental errors in $\gamma-$ray energies. Table(1) shows the predicted bandhead spins and the best values of the model parameters C_0, B, f_1, f_2 for each band. Also indicated in Table(1) are the lowest $\gamma-$ray transition energies $E_\gamma(I + 2 \to I_0)$. Using the adopted model parameters, the transition energies E_γ, rotational frequencies $\hbar\omega$, the kinematic $J^{(1)}$ and dynamic $J^{(2)}$ moments of inertia of our selected SD bands are obtained. A very good agreement between the calculated and the experimental values is obtained which gives good support to the model. The kinematic $J^{(1)}$ and dynamic $J^{(2)}$ moments of inertia are plotted as a function of rotational frequency $\hbar\omega$ in Figure(1) compared to the experimental ones. In A∼190 mass region, $J^{(1)}$ values are found to be smaller than $J^{(2)}$ and $J^{(2)}$ exhibits a gradual increases with increasing $\hbar\omega$, while in A∼130 the values of $J^{(2)}$ are smaller than that the corresponding values of $J^{(1)}$ for all ranges of frequencies and $J^{(2)}$ mostly decrease with a great deal of variation from nucleus to nucleus. Another result in the present work is the observation of a $\Delta I = 2$ staggering effect in $\gamma-$ray energies $E_\gamma(I + 2 \to I)$ in the studied SDRB's. The the staggering pattern is illustrated in Figure(2) where the staggering parameters $\Delta^4 E_\gamma(I)$ introduced by Cederwall et al [14] defined as the fourth derivative of E_γ are presented as a function of rotational frequency $\hbar\omega$. A significant zigzag has been observed the resulting numerical values for each band are listed in Tables(2 and 3).

5 Conclusion

The SDRB's namely ^{194}Tl(SD1, SD3, SD5), ^{130}Ce(SD1), ^{132}Nd and ^{136}Sm(SD1) are studied in the version of the perturbed SU(3) limit of sdgIBM with supersymmetry scheme including many body interaction. The bandhead spins are taken from our previous works while the model parameters are adjusted by fitting procedure in order to minimize the relative root mean square deviation between experimental transition energies E_γ^{exp} and the calculated ones E_γ^{cal}. Excellent agreement are given which gives good support to the proposed model. Rotational frequencies, kinematic $J^{(1)}$ and dynamic $J^{(2)}$ moments of inertia are calculated and the evolution of $J^{(1)}$ and $J^{(2)}$ with $\hbar\omega$ are studied. The calculated E_γ are used to investigate the occurrence of a $\Delta I = 2$ staggering effect in the studied SDRB's by using the fourth order derivative of the $\gamma-$ray transition energies. A large amplitude staggering pattern is found in all the studied SDRB's.

References

1. Iachello F., Arima A. The Interacting Boson Model. Cambridge University Press, Cambridge (1987).
2. Casten R.F. Nuclear Structure From a Simple Perespective. Oxford University, Oxford (1990).
3. Warner D. A Triple Point in Nuclei. *Nature*, 2002, v. 420, 614.
4. Arias J.M. et al. U(5)-O(6) Transition in the Interacting Boson Model and the E(5) Critical Point Symmetry. *Phys. Rev.*, 2003, v. C68, 041302.
5. Kusnezov D. The U(16) Algebraic Lattice. *J. Phys.*, 1989, v. A22, 4271, and 1990, v. A23, 5673.
6. Sun H.Z., Zhang M. and Han Q.Z. spdf Interacting Boson Model. *Chin. J. Nucl. Phys.*, 1991, v. 13, 121.
7. Lin Y.X., Sun H.Z. and Zhao E.G. Dynamical Symmetries of the spdf Interacting Boson model. *J. Phys. G*, 1994, v. 20, 407.
8. Khalaf A.M. and Abdelfattah Sh. Structural Evolution in Radium Nuclei Using IBM Consistent-Q- Hamiltonian with Coherent State. *Inernational Journal of Advanced Research in Physical Science*, 2015, v. 2, 24–33.
9. Khalaf A.M. et al., Evolution of Ground State Nuclear Shape in Tungsten Nuclei in Terms of Interacting Boson Model, *ProgressinPhysics*, 2016, v. 13(2), 163–168.
10. Long G.L. The Rotational Limit of the Interacting Boson Model3, *Common Theor. Phys.*, 1997, v. 27, 317.
11. Elliot J.P. Collective Motion of the Nuclear Shell Model I, II. *Proc. Roy. Soc.*, 1958, v. A245 (128), 562.
12. Li S.C. and Kuyucak S. Description of Deformed Nuclei in the sdg Boson Model. *Nucl. Phys.*, 1996, v. A604, 305.
13. Flibotti S. et al. $\Delta I = 4$ Bifurcation in a Superdeformed Band : Evidence for a C_4 Symmetry. *Phys. Rev. Lett.* , 1993, v. 71, 4299.
14. Kota V.K. et al. Group Theoretical Aspects of the Extended Interacting Boson Model. *J. Math. Phys.*, 1987, v. 28, 1644.

Table 2: Calculated γ−ray transition energy E_γ(keV) for the studied SD bands and the comparison with experiment and the calculated results of the $\Delta I = 2$ energy staggering parameter $\Delta^4 E_\gamma(I)$ obtained by five point formula.

^{194}Tl(SD1)				^{194}Tl(SD3)			
$I(\hbar)$	$E_\gamma(exp)$	$E_\gamma(cal)$	$\Delta^4 E_\gamma(I)$	$I(\hbar)$	$E_\gamma(exp)$	$E_\gamma(cal)$	$\Delta^4 E_\gamma(I)$
14	268.0	268.6751		12	240.5	238.2344	
16	307.0	307.4222		14	280.0	278.2792	
18	345.1	345.7051	-0.0165531	16	318.8	318.5983	0.262866
20	384.2	383.6179	0.0213944	18	358.1	357.3467	-0.33660
22	421.0	420.9822	-0.0241556	20	39.2	396.8819	0.412796
24	457.0	457.9697	0.0290825	22	425.3	434.1794	-0.486442
26	494.9	494.3612	-0.0316294	24	473.0	472.8180	0.562820
28	530.9	530.4057	0.0365431	26	510.9	508.5947	-0.636306
30	567.0	565.8415	-0.0389094	28	546.6	546.3097	0.712723
32	601.2	600.9968	0.0438844	30	582.2	580.5822	-0.786148
34	634.9	635.5733	-0.0463116	32	617.4	617.4370	0.862580
36	669.8	669.9782		34	652.0	650.3192	-0.935853
38	703.6	703.8759		36	685.5	686.4767	
				38	717.5	718.1790	

^{194}Tl(SD5)				^{130}Ce(SD2)			
$I(\hbar)$	$E_\gamma(exp)$	$E_\gamma(cal)$	$\Delta^4 E_\gamma(I)$	$I(\hbar)$	$E_\gamma(exp)$	$E_\gamma(cal)$	$\Delta^4 E_\gamma(I)$
10	187.9	186.6115		24	841.0	842.347	
12	226.3	225.4885		26	914.0	912.752	
14	264.0	263.6266	-0.183757	28	983.0	982.836	-0.0785506
16	302.0	302.1677	0.258395	30	1052	1053.335	0.0890181
18	339.2	339.3166	-0.330951	32	1124	1123.728	-0.0921319
20	376.6	377.4083	0.405704	34	1196	1194.918	0.10318
22	413.7	413.4865	-0.478076	36	1266	1266.335	-0.105713
24	450.0	451.0842	0.553079	38	1338	1339.059	0.117491
26	486.1	486.0854	-0.625427	40	1412	1412.478	-0.119078
28	521.8	523.2236	0.700607	42	1489	1487.861	0.132018
30	558.4	557.2253	-0.772767	44	1566	1564.571	-0.132682
32	593.7	594.0268		46	1646	1644.083	0.146972
34	627.7	627.2002		48	1726	1725.751	-0.145203
				50	1806	1811.279	0.161256
				52	1900	1900.046	
				54	1996	1994.015	

15. Hamamoto I. and Mottelson B. Superdeformed Rotational Bands in the Presence of Y_{44} Deformation. *Phys. Lett.*, 1994, v. B333, 294.

16. Pavlichenkov I.M. and Flibotte S. C_4 Symmetry and Bifurcation in Superdeformed Bands. *Phys. Rev.*, 1995, v. C51, R460.

17. Kota V.K.B. Interacting Boson Model Basis and Hamiltonian for $\Delta L = 4$ Staggering *Phys. Rev. C*, 1996, v. 53, 2550.

18. Joki H. and Wu L.A. $\Delta I = 4$ Bifurcation in Ground Bands of Even-Even Nuclei and the Interacting Boson Model. *Phys. Rev. Lett.*, 1997, v. 79, 2006.

19. Khalaf A.M., Taha M.M. and Kotb M. Identical Bands and $\Delta I = 2$ Staggering in Superdeformed Nuclei in A∼ 150 Mass Region Using Three Parameters Rotational Model. *Progress in Physics*, 2012, v. 8, 39.

20. Otsuka T. and Honma M. Interacting Boson Model For Superdeformation. *Phys. Lett. B*, 1991, v. 268, 305.

21. Khalaf A.M. and Okasha M.D. Properties of Nuclear Superdeformed Rotational Bands in A∼ 190 Mass Region. *Progress in Physics*, 2014, v. 10, 246.

22. Kuyucak S., Honma M. and Otsuka T. Description of Superdeformation Nuclei in the Interacting Boson Model. *Phys. Rev. C*, 1996, v. 53, 2194.

23. Khalaf A.M., Awaad T.M. and Elgabery M.F. Examination of $\Delta I = 2$ Energy Staggering in the Superdeformed Bands of ^{194}Hg. *International Journal in Pysical and Applied Science*, 2016, v. 3(4), 47.

24. Khalaf A.M., Sirage M.M. and Abdelmageed K.E. Properties of Superdeformed Bands in A∼ 190 Region Within the Framework of Three Parameters Nuclear softness Model. *Chinese Journal of Physics*, 2016, v. 54, 329.

Table 3: Same as Table 2 but for ^{132}Ce(SD1), ^{132}Nd(SD1) and ^{136}Sm(SD1).

^{132}Ce(SD1)				^{132}Nd(SD1)			
$I(\hbar)$	$E_\gamma(exp)$	$E_\gamma(cal)$	$\Delta^4 E_\gamma(I)$	$I(\hbar)$	$E_\gamma(exp)$	$E_\gamma(cal)$	$\Delta^4 E_\gamma(I)$
30	808.55	804.9409		40	797.0	793.4394	
32	864.85	865.2221		42	849.0	848.8271	
34	928.80	928.3618	0.404878	44	900.0	909.5820	0.630371
36	994.63	991.3491	-0.431978	46	966.0	971.1123	-0.658327
38	1060.32	1057.651	0.460603	48	1035.0	1038.912	0.69562
40	1127.27	1123.824	-0.487641	50	1109.0	1107.942	-0.721866
42	1194.72	1193.792	0.516664	52	1187.0	1184.293	0.760989
44	1263.63	1263.680	-0.543336	54	1269.0	1262.507	-0.785341
46	1334.56	1337.876	0.572326	56	1356.0	1349.300	0.826478
48	1408.34	1412.078	-0.599181	58	1445.0	1438.824	-0.847901
50	1452.67	1491.137	0.629027	60	1537.0	1538.453	
52	1566.70	1570.322	-0.655639	62	1634.0	1641.996	
54	1651.49	1654.962	0.685363				
56	1740.29	1739.900	-0.71106				
58	1832.64	1830.941	0.740601				
60	1926.50	1922.515	-0.766111				
62	2023.50	2020.902					
64	2119.00	2120.123					

^{136}Sm(SD1)			
$I(\hbar)$	$E_\gamma(exp)$	$E_\gamma(cal)$	$\Delta^4 E_\gamma(I)$
30	888	887.0356	
32	963	963.2182	
34	1041	1041.0786	-0.0260325
36	1119	1120.2441	0.0045813
38	1199	1199.9257	-0.0306712
40	1279	1279.4072	0.00451688
42	1359	1357.4814	-0.0336294
44	1436	1433.0136	0.00677437
46	1503	1504.3310	-0.0338756
48	1567	1569.8691	
50	1629	1627.5214	

25. Khalaf A.M., Okasha M. and Ragheb E. Anomalous $\Delta I = 2$ Transition Energy Staggering in Nuclear Superdeformed Bands. *Australian Journal of Basic and Applied Science*, 2016, v. 10, 192.
26. Liu Y.X. and Gao D.F. Description of Identical Superdeformed Bands with $\Delta I = 4$ Bifurcation. *Phys. Rev.*, 2001, v. C63, 044317.
27. Liu X.Y., Wang J.J. and Han Z. Description of the Identical Superdeformed Bands and $\Delta I = 4$ Bifurcation in the A$\sim$ 130 Region. *Phys. Rev. C*, 2001, v. 64, 064320.
28. Wu L.A. and Toki H. Anamalous Staggering in the Mass of the Rotational Nuclei in the Actinide Region. *Phys. Lett. B*, 1997, v. 407, 207; $\Delta I = 4$ Bifurcation in Ground Bands of Even-Even Nuclei and the Interacting Boson Model. *Phys. Rev. Lett.*, 1997, v. 79, 2009.
29. Demeyer H. et al. Classification of the Dynamical Symmetries in the Extended Interacting Boson Model. *J. Phys. A: Math. Gen.*, 1986, v. 19, L565.
30. Sun H.Z. et al. SU(3) and SU(5) Dynamical Symmetries in The Extended Interacting Boson Model. *Kinam Rev. Fis.*, 1983, v. 5, 135.
31. Liu Y.X., Sun H.Z. and Zhao E.G. Description of Superdeformed Nuclear States in the Interacting Boson Model. *Commun. Theor. Phys.*, 1997, v. 27, 71.
32. Bonatsos D. and Kelin A. Generalized Phenomenological Models of the Yrast Band. *Phys. Rev. C*, 1984, v. 29, 1879.
33. Bohr A. and Mottelson B. Nuclear Structure. Benjamin, New York, 1975, Vol. II.

A Solution to the Flyby Anomaly Riddle

Eduardo D. Greaves[1], Carlos Bracho[2], and Imre Mikoss[3]

[1]Universidad Simón Bolívar. Apartado 89000, Caracas, Venezuela. E-mail: egreaves20002000@yahoo.com
[2]Facultad de Ingeniería, Universidad Central de Venezuela, Caracas, Venezuela. E-mail: bracho_carlos@hotmail.com
[3]Universidad Simón Bolívar. Apartado 89000, Caracas, Venezuela. E-mail: imikem@gmail.com

The Flyby Anomaly is one of the unsolved problems of current physics in that the Doppler-shift determined speeds are inconsistent with expected values assuming the validity of Newtonian gravity. We postulate that the Flyby Anomaly is a consequence of the assumption that the speed of light is isotropic in all frames, and invariant in the method used to measure the velocity of the space probes by means of the Doppler Effect. The inconsistent anomalous values measured: positive, null or negative are simply explained relaxing this assumption. During space probe energy assistance maneuvers the velocity components of the probe in the direction of the observer V_o are derived from the relative displacement Δf of the radiofrequency f transmitted by the probe, multiplied by the local speed of the light c' by the Doppler effect: $V_o = (\Delta f/f)\, c'$. According to the Céspedes-Curé hypothesis, the movement through variable gravitational energy density fields produces slight variations of the refractive index n' of space and therefore of the speed of light c' which leads to unaccounted corrections of the Doppler data that are based on an invariant c. This leads to incorrect estimates of the speed or energy change in the flyby maneuver in the Earth's frame of reference. The simple theory presented is applied to hyperbolic flyby trajectories of Galileo I and the spacecraft NEAR accurately reproducing the NASA measured values and thereby providing additional experimental evidence for a variable speed of light dependence on the gravitational energy density of space with fundamental consequences in astrophysics and cosmology.

1 Introduction

The Flyby Anomaly is an unexpected energy increase or decrease of spacecraft during flybys maneuvers of Earth and other planets employed as gravitational assist techniques for Solar system exploration. The anomalous measurements have been observed as shifts in the S-band and X-band Doppler and ranging telemetry. It has been observed in a number of spacecraft: NEAR, Galileo I and II, Cassini, Rosetta I, II and III, Messenger, Juno, Hayabusa, and EPOXI I and II [1–3]. The Flyby Anomaly has been included in a list of "unsolved problems in physics". We find very significant a comment of Anderson et al. [2], that the same inconsistency in the Doppler residuals which lead to the velocity anomaly are found in the ranging data, as we believe both can be explained by the theory developed here.

A large number of papers have been advanced in attempts to explain the anomalous, and at times inconsistent, measurement results of the very small, but significant, unaccounted speed and energy change experienced by spacecraft during maneuvers to increase or decrease its relative energy.

A comprehensive review of anomalous phenomena observed in the solar system was published by Lämmerzahl et al. (2006) [4] which includes prominently the Flyby Anomaly. It lists numerous possible causes of the anomaly. It reaches the conclusion, in this respect, that none of them can explain the observed measurements. "New physics" has been attempted by postulating variants of gravitational theories [5–9], or modification of inertia [10], and also the possible influence of halos of dark matter [11].

More conventional causes that have been considered include: The effect of Earth oblateness which is known to produce perturbations of orbiting spacecraft. Hence a possible cause of the Flyby Anomaly might be the non spherical mass distribution of the oblate Earth. An unsuccessful attempt has been made by K. Wilhelm and B.N. Dwivedi (2015) [12] to explain the anomalous Earth flybys of several spacecraft on the basis of asymmetry of the mass distribution of the Earth causing an offset of the effective gravitational centre from the geometric centre.

The possibility of electromagnetic forces acting between a charged probe and the Earth's magnetic fields has been examined [13], also the influence of the Earth high atmosphere [14] or the emission of thermal energy from the spacecraft [15]. However, to this date none of the above adequately explains the cause of the anomaly.

A light speed anisotropy hypothesis is used by R.T. Cahill to argue that the Doppler-shift determined speeds are inconsistent with expected speeds, and hence affect the measurement of the probe during flyby [16]. Cahill revisits the Michelson-Morley experiment controversy citing numerous new interferometer results which take into account the effect if the medium that light transverses in these experiments (e. g. gas, coaxial cable or optical fiber). He points out that speed anomalies are not real and are actually the result of using an incorrect isotropic light speed relationship between the observed Doppler shift and the speed of the spacecraft.

An empirical formula that adequately predicts the flybys measured up to 2005 was published by Anderson et al. [1, 2] using all likely variables in the problem. The empirical formula developed by Anderson et al. did not fit later anomalous flybys. However, a modification by Jouannic et al. (2015) [3] was able to predict the new data. From the conclusions of this work we read that "This could signify that it (*the anomaly*) is caused by a force related either to mass, altitude, or both". In this paper we show that indeed, planet mass and distance from the planet, which are some of the important variables in determining the gravitational energy density of space and hence of the local index of refraction of quasi-empty space [17, 18] produces minute variations in the local speed of light c' due to the Céspedes-Curé hypothesis [19], explained below. These unaccounted variations of the local index of refraction lead to small erroneous measurements of spacecraft velocity and derived energy, based on a constant c, and is shown here to be the cause of the Flyby Anomaly. Hence we coincide with Cahill in that speed anomalies are not real but rather an artifact of how the speeds are measured with the Doppler effect. In this paper the fundamentals of the proposed Flyby Anomaly explanation are presented with analytical relations showing how the anomalous behavior can be accurately predicted. Numerical calculations are presented for the Galileo I (December, 1990) Earth flyby and NEAR (January, 1998) Earth flyby. We also show how the anomaly can be simply predicted for any other spacecraft provided detailed information of the measurement of entry and exit points are available. Additionally we briefly discuss some of the fundamental consequences of the Céspedes-Curé hypothesis for astrophysics and cosmology.

2 Speed and energy measurement of spacecraft and the Doppler effect

All remote velocity estimations of astronomical bodies use the first order Doppler effect of light [20]. In spacecraft the procedure employs a locally produced radio or light frequency f of accurately known value, or it could be a retransmitted signal such as the case of Pioneer spacecraft [21]. The speed component in the direction of the observer V_{o} is deduced from the shift Δf of the radio or light frequency f, times the local speed of light c' by means of $V_{\mathrm{o}} = (\Delta f/f)\, c'$. At the present time (year 2020) it is conventionally assumed that the local speed of light c' at any point in the universe is isotropic and identical to the speed of light $c = 299792458\,\mathrm{ms}^{-1}$ measured in vacuum to high accuracy on the surface of the Earth. Clearly, if there are small variations of c' as a result of changing locations with differing gravitational energy density ρ, as occurs during flyby maneuvers, the measured speed component in the direction of the observer V_{o}, calculated with the Doppler effect, assuming a constant c, will lead to erroneous estimations of the spacecraft speed and resulting energy change during the maneuver. Presently the speed of light c is considered a fundamental constant being the base of the definition of the meter, the length unit in the SI system of units. However, a variable speed of light has been considered by a number of authors, notably including A. Einstein in 1907 [22] and in 1911 [23] and also by R. Dicke in 1957 [24]. In Einstein's early work the speed of light was influenced by the gravitational potential and a constant speed could not be conceived in a gravitational field with variable strength. In Dicke's work he assumes a refractive index n of empty space, different from 1, given by an expression where the value increases with the gravitational field:

$$n = 1 + \frac{GM}{r\,c^2}\,.$$

This proposal provides an alternative to the lensing phenomenon predicted by General Relativity Theory (GRT). There are other more modern variable speed of light theories as reviewed by Magueijo J. in 2003 [25]. The Céspedes-Curé hypothesis [19] is reminiscent of the early proposals of Einstein and Dicke. It predicts that the speed of light is a function of the local total energy density of space ρ according to (1), so that if this hypothesis is correct, it could explain the spacecraft anomalous behavior derived by the Doppler effect.

$$c = \frac{k}{\sqrt{\rho}}\,, \tag{1}$$

where k is a proportionality constant and ρ is the sum of all the sources of energy density including gravitational, ρ_G, electric, ρ_E, magnetic, ρ_M, and any other that may be acting at the site. Calculations [26] show that gravitational energy density is much larger than electric or magnetic. And that the most important source of energy density by several orders of magnitude is the "Cosmic energy density" due to the far away stars and galaxies which has a value of $\rho^* = 1.094291 \times 10^{15}\,\mathrm{Jm}^{-3}$ deduced by Céspedes-Curé [19], see Appendix A, and by Greaves E.D. [18, 26, 27], see Appendix B. Compared to ρ^*, the Sun's ρ_S, the planet about which the flyby maneuver is being done, ρ_p, and all other massive bodies in the vicinity contribute in a very minor amount to the variable total energy density at points along the trajectory of the spacecraft. Hence, this is the cause of the minute amount found for the anomalous values of velocity and energy of spacecraft performing the flyby maneuver. The gravitational energy density ρ due to a mass M at a distance r from its center is given by [19, see page 163],

$$\rho = \frac{1}{2}\,\frac{GM^2}{4\pi r^4} = \frac{GM^2}{8\pi r^4}\,, \tag{2}$$

where G is the universal constant of gravitation. Using this relation the gravitational energy density of any astronomical mass can be calculated at any point in space located a distance r from the mass center. The energy density of space ρ_B and ρ_E associated with the presence of static magnetic B and electric

E fields are given by [28]:

$$\rho_B = \frac{1}{2\mu_0} B^2 , \tag{2a}$$

and

$$\rho_E = \frac{1}{2}\varepsilon_0 E^2 , \tag{2b}$$

where μ_0 is the magnetic permeability and ε_0 is the electric permittivity of free space. With the usual definition of the index of refraction at a point in space, n', as the ratio of the speed of light of vacuum c on the surface of Earth to the speed of light c' at the point considered (conventionally inside a transparent material) $n' = c/c'$ it is possible with the use of (1) to obtain a relation for n' which is only dependent on values of the energy density of space at the point in question and at the surface of the Earth:

$$n' = \frac{c}{c'} = \frac{\sqrt{\rho'}}{\sqrt{\rho}} = \frac{\sqrt{\rho'}}{\sqrt{\rho^* + \rho_S + \rho_E}}. \tag{3}$$

Here $\rho^* + \rho_S + \rho_E$ is the gravitational energy density at the surface of the Earth. The terms in the sum are: the energy density due to the far away stars and galaxies ρ^*, the Sun, ρ_S and Earth, ρ_E. The values shown in Table 1 and Fig. 1 indicate that the contributions to the local gravitational energy density due to nearby planets is small and negligible compared to the all-pervading energy density ρ^* due to the far away stars and galaxies. Hence for a spacecraft in a flyby maneuver the local value of the index of refraction n' and the local value of the speed of light c' is very nearly equal to the values on the surface of Earth. This leads to the fact that the observed anomalous variations of the speed of spacecraft deduced by the Doppler effect are very small indeed. It also shows that the anomalies are dependent on the mass of the planet and on the distance to the planet as mentioned in the conclusions of the work of Jouannic et al. in [3].

3 Calculation of the anomaly

In order to predict quantitatively the measured energy change that shows an anomalous value it is necessary to have very detailed information of the particular flyby event considered. The information required is data that refers to the spacecraft such as the radio frequencies used for transmission which are used for determining the relative radial velocity via the Doppler effect. The information related to the planet, about which the maneuver takes place, is information that defines the orbit of the spacecraft: the hyperbolic orbit parameters of the flyby: a (semi-mayor axis) and e (eccentricity) and the entry and exit velocity of the probe: V_∞^- and V_∞^+, the measured anomalous velocity V_{anom} and, most important, the points of entry and exit where the velocities were measured. NASA determines the Flyby Anomaly with the Orbit Determination Program (ODP) of the Jet Propulsion Laboratory

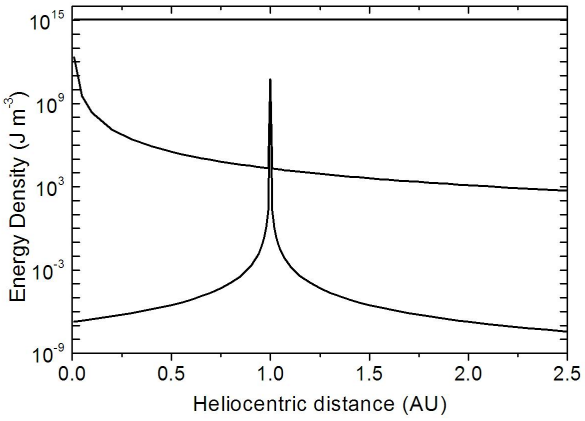

Fig. 1: Gravitational energy density (Jm^{-3}) as a function of distance from the center of the Sun in AU (0 to 2.5 AU) due to the far away stars and galaxies (top line $\rho^* = 1.094291\times10^{15}$ Jm^{-3}), ρ_S due to the Sun (middle line) and ρ_E due to Earth (Line centered at 1 AU) [26].

(JPL) as well as other software at the Goddard Space Flight Center and at the University of Texas [2]. These programs incorporate all the physics mentioned above and the information gathered by the Deep Space Network (DSN) during the flyby. According to the hypothesis presented in this paper the anomaly is due to errors committed due to sub-estimation or over-estimation of the velocity calculated by the use of the Doppler effect formula as explained previously. Below we show how the anomaly can be calculated in reference to Earth flybys. The same considerations apply to flybys about other planets. From (3) we derive

$$c' = c\,\frac{\sqrt{\rho}}{\sqrt{\rho'}} . \tag{4}$$

The radial velocity of the spacecraft during the flyby is obtained by the use of $V_r = \Delta f/f\; c'$ which with (4) gives

$$V_r = c'\,\frac{\Delta f}{f} = c\,\frac{\Delta f}{f}\,\frac{\sqrt{\rho}}{\sqrt{\rho'}} , \tag{5}$$

where the gravitational energy density ρ' is a function of the position of the spacecraft in its orbit and ρ is the gravitational energy density on the surface of the Earth whose value is $\rho = \rho^* + \rho_S + \rho_E$ with ρ_S and ρ_E calculated on the surface of Earth. As the spacecraft nears the planet it moves into varying values of ρ' which according to (5) results in a sub-estimation or over-estimation of the velocity. Likewise, as the spacecraft leaves the vicinity of Earth and gets further away, it travels into different values of the gravitational energy density ρ' which according to (5) results in differing values of the velocity. Important factors determining the value of ρ' are the radial distance to the center of the planet producing the energy

Table 1: Values of the energy density of space at the surface of Earth produced by: the far away stars and galaxies, the mass of the Sun, Earth, the Moon and other planets.

Source of energy density	Symbol	Energy density due to source at	Magnitude (Joules/m^3)‡	Reference
Far away Stars and Galaxies	ρ^*	Earth	1.094291×10^{15}	Céspedes-Curé [19, p. 279]
Sun	ρ_S	Earth 1 AU	2.097×10^4	Greaves [17, 18]
Sun	$\rho_{S\,@AU-}$	1 AU$-E_{\rm SI}{}^\dagger$	2.150250×10^4	This work
Sun	$\rho_{S\,@AU+}$	1 AU$+E_{\rm SI}{}^\dagger$	2.046034×10^4	This work
Earth	ρ_E	Earth surface	5.726×10^{10}	Greaves [18]
Moon	$\rho_{\rm Moon}$	Earth	6.57×10^{-1}	Greaves [18]
Jupiter	$\rho_{\rm Jup}$	Earth	1.91×10^{-2}	Greaves [18]
Venus	$\rho_{\rm Ven}$	Earth	2.14×10^{-5}	Greaves [18]
Mars	$\rho_{\rm Mar}$	Earth	2.91×10^{-8}	Greaves [18]

† $E_{\rm SI}$ is the radius of Earth's Gravitational Sphere of Influence: (929000 km) [29, 30].
‡ These values are deceptive due to the $1/r^4$ dependence of the gravitational energy density (2). The energy density of the Earth at its surface is 6 orders of magnitude greater than the Sun's. However, it decreases abruptly so that at a distance greater than 41 earth radii the energy density due to the Sun is higher.

assistance and the radial distance to the Sun. Hence, in order to calculate exactly the anomalous energy change reported, it is necessary to know the exact position of the spacecraft at the point or points where its velocity was calculated in order to establish the initial spacecraft energy and the point or points where the velocity was finally calculated to establish the final spacecraft energy. Also needed are the methods used for the speed measurements such as the frequency used by the spacecraft in its transmission to the Earth tracking stations, and whether it is a spacecraft transmission or an Earth sent-signal retransmitted by the spacecraft. Such detailed information is ordinarily not included in papers publicly available.

Examination of (5) shows that the anomaly is caused by the square root term (SQR)

$$\mathrm{SQR} = \sqrt{\frac{\rho}{\rho'}} = \sqrt{\frac{\rho}{\rho^* + \rho_S + \rho_E}}\,. \tag{6}$$

Here ρ and ρ^* are constants while ρ_S and ρ_E are functions of position, ρ_S is dependent on the radial distance to the center of the Sun and ρ_E is dependent on the radial distance to the center of Earth.

Let us consider ρ_S first, which is given by

$$\rho_S = \frac{GM_S^2}{8\pi r_S^4}\,. \tag{7}$$

Here M_S is the mass of the Sun and r_S the radial distance from the center of the Sun. In order to estimate the influence of this term we calculate the value of ρ_S over the Earth's gravitational Sphere of Influence, $E_{\rm SI}$, that is at a distance of one AU from the Sun in the range of 1 AU $\pm E_{\rm SI}$ (plus or minus the radius of the Earth's Sphere of Influence). The values obtained range from $\rho_S = 2.150250{\times}10^4$ to $2.046034{\times}10^4$ Jm^{-3} as shown in Table 1. The variation over the Earth's sphere of influence is of the order of 5%. However, the values of the variation of the gravitational energy density due to the Sun are 5 orders of magnitude less than the energy density due to Earth at its surface. But, as shown by calculations, they become more important than the Earth's energy density due to the $1/r^4$ term in (2) as discussed below.

In (6), the value of ρ_E is given by

$$\rho_E = \frac{GM_E^2}{8\pi r_E^4} \tag{8}$$

with M_E the mass of the Earth and r_E the radial distance from the center of Earth.

Taking these considerations into account in (5) we can write an expression for the corrected speed of the spacecraft which takes into account the change of the index of refraction of space due to the variation of the space gravitational energy density along the spacecraft trajectory:

$$\begin{aligned} V_r &= c\,\frac{\Delta f}{f}\,\sqrt{\frac{\rho}{\rho^* + \rho_S + \rho_E}} \\ &= c\,\frac{\Delta f}{f}\,\sqrt{\frac{\rho}{\rho^* + \frac{GM_S^2}{8\pi r_S^4} + \frac{GM_E^2}{8\pi r_E^4}}}\,. \end{aligned} \tag{9}$$

Numerical calculations show that the influence of the third

term of the denominator, namely the variation of the Earth's gravitational energy density is important only at small distances above the surface of the Earth and it becomes very small at distances where a spacecraft is beginning its approach to the surface of the planet during a flyby.

4 Calculation of the Flyby Anomaly in three cases

To calculate the anomaly, we suppose that the speed of the spacecraft is measured at two points: a point of entry into the Earth's sphere of influence where the speed is V_∞^- and a point of exit from the Earth's sphere of influence where the speed is V_∞^+. If we ignore the change of c, the measured velocities are given by:

$$V_\infty^+ = c\,\frac{\Delta f^+}{f} \quad \text{and} \quad V_\infty^- = c\,\frac{\Delta f^-}{f}.$$

Hence the anomaly measured by NASA is given by

$$\mathrm{An} = V_\infty^+ - V_\infty^- = \frac{c}{f}\left(\Delta f^+ - \Delta f^-\right). \tag{10}$$

At each of these points a correct measurement, one that takes into account the change of the index of refraction, as we propose in this paper, must be done with (9), with V_∞^- the observed Doppler shift at the point of entry, and with V_∞^+ the observed Doppler shift at the point of exit as shown below:

$$V_\infty^+ = c\,\frac{\Delta f^+}{f}\sqrt{\frac{\rho}{\rho^* + \frac{GM_S^2}{8\pi\left(r_S^+\right)^4} + \frac{GM_E^2}{8\pi\left(r_E^+\right)^4}}} \tag{11a}$$

$$V_\infty^- = c\,\frac{\Delta f^-}{f}\sqrt{\frac{\rho}{\rho^* + \frac{GM_S^2}{8\pi\left(r_S^-\right)^4} + \frac{GM_E^2}{8\pi\left(r_E^-\right)^4}}} \tag{11b}$$

In the Earth's coordinate system, energy is conserved, so that if the correct equations (11a) and (11b) are used, then measurements *should* give: $V_\infty^+ - V_\infty^- = 0$ that is:

$$0 = c\,\frac{\Delta f^+}{f}\sqrt{\frac{\rho}{\rho^* + \frac{GM_S^2}{8\pi\left(r_S^+\right)^4} + \frac{GM_E^2}{8\pi\left(r_E^+\right)^4}}} - c\,\frac{\Delta f^-}{f}\sqrt{\frac{\rho}{\rho^* + \frac{GM_S^2}{8\pi\left(r_S^-\right)^4} + \frac{GM_E^2}{8\pi\left(r_E^-\right)^4}}}. \tag{12}$$

However, if the SQR terms are different, for (12) to be true it requires that $\Delta f^+ \neq \Delta f^-$, and hence measurements done by NASA with (10) will show an anomaly. The anomaly is contained in the difference of the SQR terms in (12). Since

$$V_\infty^+ = c\,\frac{\Delta f^+}{f} \quad \text{and} \quad V_\infty^- = c\,\frac{\Delta f^-}{f}$$

are almost the same, both of the order of km/s differing by an amount 6 orders of magnitude smaller, of the order of mm/s, we can write the following relation to calculate the measured anomaly:

$$V_{\mathrm{anom}} = V_\infty\sqrt{\frac{\rho}{\rho^* + \frac{GM_S^2}{8\pi\left(r_S^+\right)^4} + \frac{GM_E^2}{8\pi\left(r_E^+\right)^4}}} - V_\infty\sqrt{\frac{\rho}{\rho^* + \frac{GM_S^2}{8\pi\left(r_S^-\right)^4} + \frac{GM_E^2}{8\pi\left(r_E^-\right)^4}}}. \tag{13}$$

Numerical analysis of (13) shows it is possible to identify three cases.

4.1 First case

The distances from the point of entry and the point of exit to the Sun and to Earth are the same. ($r_S^+ = r_S^-$ and $r_E^+ = r_E^-$). In this case the two terms in the parenthesis of (13) are the same and no anomaly will be detected (incoming and outgoing points are symmetric with respect to the Sun and Earth).

4.2 Second case

In this second case entry point and the exit point are at different distances from the Sun but at the same distance from Earth. It means that $r_S^+ \neq r_S^-$, hence:

$$\frac{GM_S^2}{8\pi(r_S^+)^4} \neq \frac{GM_S^2}{8\pi(r_S^-)^4},$$

so that the SQR terms in (12) are different. For this relation to be correct it requires that $\Delta f^+ \neq \Delta f^-$. Hence if the speeds are being measured with relations

$$V_\infty^+ = c\,\frac{\Delta f^+}{f} \quad \text{and} \quad V_\infty^- = c\,\frac{\Delta f^-}{f}$$

as in (10) the flyby will certainly show an anomaly: $V_\infty^+ \neq V_\infty^-$. However, numerical calculations show that the anomalous values in this case are very small and non measurable.

4.3 Third case

In this third case entry point and the exit point are at different distances from the Sun and at different distance from Earth. It means that, $r_S^+ \neq r_S^-$ and $r_E^+ \neq r_E^-$. In this case the two terms in the parenthesis of (13) are different. Hence if the speeds are being measured with relations

$$V_\infty^+ = c\,\frac{\Delta f^+}{f} \quad \text{and} \quad V_\infty^- = c\,\frac{\Delta f^-}{f}$$

as in (10) the flyby will certainly show an anomaly: $V_\infty^+ \neq V_\infty^-$. Numerical calculations show that an anomaly will be measured in the range of values reported, negative or positive, with a value and sign that depends on the entry and exit points used for measurement. We conclude that the anomaly is due to neglect of the SQR terms in the calculation of the entry and exit velocities derived from the Doppler flyby data.

Table 2: Distances to the Sun and to Earth with calculated entry and exit points that predict, with (13), the measured Flyby Anomaly of the Galileo 1 (December 1990) flyby and the NEAR (January 1998) flyby.

	Galileo 1		NEAR	
	Entry point	Exit point	Entry point	Exit point
Distance from Sun (m)	1.502803×10^{11}	1.502831×10^{11}	1.495630×10^{11}	1.495950×10^{11}
Distance from Earth (m)	1.7651×10^{7}	1.4864×10^{7}	7.2000×10^{7}	1.2200×10^{7}
Spacecraft Velocity (m/s)	8949		6851	
Measured Flyby Anomaly (mm/s)	3.930		13.46	
Calculated Flyby Anomaly (mm/s)	3.944		13.38	
Difference (%)	+0.40		−0.57	

5 Results

In order to apply the theory described above to predict the anomaly measured for any given spacecraft flyby it is necessary to introduce into (13) the values of the parameters of the spacecraft maneuver, namely the spacecraft speed at the entry point and the distances to the Sun and to Earth of the incoming and outgoing points. The spacecraft speed is available, however, the required information of entry and exit points has not been possible to obtain. Only the right ascension and declination of these vector directions are given by Anderson et al. [2]. With these angular parameters we have defined vectors, from the Earth, for incoming and outgoing directions as well as from the Earth to the Sun's direction along its right ascension and declination on the day of the Flyby. Then with calculated tables of numerical values of the SQR terms of (13) for varying entry and exit points along the incoming and outgoing vectors (i.e. values of r_S^+, r_S^- and of r_E^+, r_E^-) excluding the immediate distances (1h 40min before and after the closest approach location) we have arrived at likely entry and exit points that closely predict the observed NEAR (January 23, 1998) flyby. For Galileo I (December 8, 1990) flyby the incoming and outgoing points were calculated along likely in and out points not specifically along the actual incoming and outgoing vectors. Results of these calculations are shown in Table 2.

6 Possible measurement of ρ^* with the Flyby Anomaly

Based on the Flyby Anomaly explanation given above, it is possible to use the experimental results of measured flyby anomalies in spacecraft to calculate, in an independent way, the gravitational energy density values that lead to the measured anomalies. Since the gravitational energy density is composed of the contribution due to the planets and the Sun, which can be accurately calculated with (8), the contribution due to the far away stars and galaxies, ρ^*, could be solved as a single adjustable parameter, and calculated. This could be done by programming the theory presented here in the Orbit Determination Program of the JPL, or by an accurate knowledge of the points of entry and exit in the hyperbolic trajectory where the measurements were made that produced a Flyby Anomaly. This measurement of ρ^*, the gravitational energy density of the far away stars and galaxies, would provide an additional estimation of its value besides that given by Jorge Céspedes-Curé [19, page 279], $\rho^* = 1.094291 \times 10^{15}\,\mathrm{Jm}^{-3}$, obtained using starlight deflection measurements during total sun eclipses, see Appendix A, or that given by Greaves [26]: $\rho^* = 1.0838 \times 10^{15}\,\mathrm{Jm}^{-3}$, obtained using NASA accurate measurement of the Pioneer Anomaly when Pioneer 10 was at 20 AU, see Appendix B.

7 Discussion

Eq. (2) assumes a spherical mass distribution for the mass of the Earth or Sun in the calculation of the gravitational energy density. It does not consider the possible influence of the Earth's oblate shape, which is known to affect orbiting spacecraft and could affect hyperbolic orbits.

Estimation has been done of the magnitude of the mass of Earth that deviates from spherical shape in order to calculate to what extent this can affect the gravitational energy density along the Flyby Anomaly trajectory. The calculation gives that the non spherical mass is of the order of less than 0.337% of the Earth mass. This amount influences the third term of the denominator in (9) and quantities derived from it. However, the subtraction or addition of this mass to the mass of Earth on the SQR term of (9) affects this term in less than the tenth significant figure. This estimate implies that the mass of Earth causing the gravitational quadrupole does not affect the calculations based on the Céspedes-Curé hypothesis.

The hypothesis also predicts that ranging measurements based on a constant value of c will be affected in the same manner as the anomalous speed measurements based on the Doppler data. Anomalous ranging is briefly mentioned by Anderson et al. [2]. However, no numerical data of this anomaly has been provided. Perhaps due to the small signal-to-noise ratio on the incoming ranging signal and a long integration time (typically minutes) that must be used for correlation purposes [21, page 7].

We calculate the speed of light at the International Space

Station to be

$$c' = 299798845.6\,\mathrm{ms}^{-1},$$

that is $6387.6\,\mathrm{ms}^{-1}$ higher than c on the Earth's surface, about 0.002% [31]. Ranging measurements based on a constant c that is lower than is predicted by this theory will be in slight error. And the error will be in the same manner as the anomalous speed measurements. The Cépedes-Curé hypothesis predicts the anomalous measurements of the Pioneer spacecraft without any adjustable parameter [27]. There are reports that that the Pioneer Anomaly was resolved as a thermal effect on papers by Rievers and Lammerzahl [15], Turyshev et al. [32] and Francisco et al. [33]. These reports do complex parameterized models of the thermal recoil to explain the anomaly.

We have reasons to doubt this explanation:

First. A detailed paper about the Pioneer Anomaly (55 pages in Phys. Rev. by Anderson et al. 2002) [21] clearly argues (see sections VIII. B, C and D, pages 32–35) that thermal recoil cannot account for the anomaly,

Second. Rievers and Lämmerzahl [15] do a very complex computational model of the spacecraft constructing all parts of the spacecraft internal and external in finite elements; assigning thermal, and radiative properties for each component, (absorption, reflection and emittance coefficients) in order to arrive at their resulting thermal radiation pressure.

Turyshev et al. [32] do a complex parameterized model for the thermal recoil force of the Pioneer spacecraft with several adjustable parameters. In particular the two adjustable parameters of Eq. (1) on page 2 predict the anomaly. However, any other parameters would negate the thermal origin of the anomaly.

Francisco et al. [33] use different modeling scenarios resulting in different acceleration values and choosing the 4^{th} one with which a Monte Carlo modeling procedure is used to arrive at a value of the reported acceleration of the Pioneer 10 at an instant 26 years after launch.

All of these reports imply models with numerous adjustable parameters which could disprove the thermal origin of the anomaly.

Third. If the anomalous acceleration towards the sun depended on the thermal emission of heat from the RTG, Plutonium ^{238}Pu power sources, with a half life time of 87.74 years, the anomalous acceleration should decrease in time at the same rate, however, this is contrary to the almost flat long term behavior observed [21].

Forth. An anomaly similar to the Pioneer spacecraft was detected in Galileo spacecraft (see Section V. C, page 21) with a value of (acceleration) of $(8 \pm 3) \times 10^{-8}\,\mathrm{cm/s}^2$, a value similar to that from Pioneer 10, with additional evidence based on ranging data, and in the Ulysses spacecraft (see Section V. D, page 21) Ulysses was subjected to an unmodelled acceleration towards the Sun of $(12 \pm 3) \times 10^{-8}\,\mathrm{cm/s}^2$, in Anderson et al. [21]. Both spacecraft have completely different geometries and the thermal recoil theory is not applicable to them.

There are some unexplored fundamental aspects to the Céspedes-Curé hypothesis. The elementary relation (4) that is deduced for the relative speed of light c' measured on a space site relative to c on Earth, coupled to Einstein's relation for the rest mass $E = mc^2$ leads to an analytical relation that predicts Mach's principle, i.e. that mass and inertia depend on the far away stars and galaxies. Likewise, the Céspedes-Curé Hypothesis coupled to the electromagnetic expression for the speed of light, $c = 1/\sqrt{\varepsilon_0 \mu_0}$ leads to a direct relationship between the electromagnetic and gravitational forces.

8 Conclusions

The values shown in Table 2 indicate that the Flyby Anomaly can be accurately predicted by the theory presented in this work. This theory is capable of explaining qualitatively and quantitatively the anomaly, both, the measured positive, null and negative values. To calculate exact values of the anomaly of a spacecraft it is necessary to know the incoming and outgoing points where the spacecraft velocity was measured. The precise calculation of the Flyby Anomaly provides additional confirmation of the Céspedes-Curé hypothesis, that c the speed of light depends on the gravitational energy density of space as defined by (1) namely:

$$c' = \frac{k}{\sqrt{\rho'}}\,.$$

The evidence presented in this work for the Céspedes-Curé hypothesis has profound consequences in the current cosmology theories since it implies a revision of all astronomical measurements of velocity based on the Doppler, blue and red shifts, of stars and galaxies. These have importance in determination of matters such as the Hubble constant, the expansion of the universe, the flat rotation curve of galaxies (which gave birth to the theory of dark matter) and the extreme values of the redshifts of very far away galaxies (so called inflation) which gave birth to the theory of dark energy. These redshifts do not follow the linear relation proposed by Hubble but rather seem to imply an accelerated rate of expansion. The theories that follows from this hypothesis, the evidence and attempts to gather evidence for it and some of its consequences on current physics are explored in [18] and in the unpublished work mentioned above in [31].

Appendix A. Supporting data (Céspedes-Curé)

See Table 3: Data of starlight deflection measurements, reported by P. Merat [34] (δ in seconds of arc) at different distances from the Sun during total eclipses, used by J. Céspedes-Curé [19, see page 279], to calculate $\rho^* = 1.094291 \times 10^{15}\,\mathrm{Jm}^{-3}$, the energy density of space due to far-away stars and galaxies.

Appendix B. Supporting data (Greaves)

Data used by E. D. Greaves in [26] for the arithmetic to calculate $\rho^* = 1.0838 \times 10^{15}\,\mathrm{Jm}^{-3}$, the energy density of space

Table 3: Data of starlight deflection measurements, reported by P. Merat [34] (δ in seconds of arc) at different distances from the Sun during total eclipses, used by J. Céspedes-Curé [19, see page 279], to calculate $\rho^* = 1.094291 \times 10^{15}\,\mathrm{Jm}^{-3}$, the energy density of space due to far-away stars and galaxies.

Row	r (R_o Units)	$\delta \pm \Delta\delta$ (Merat)
1	2.09	1.02 ± 0.11
2	3.12	0.67 ± 0.08
3	4.02	0.58 ± 0.04
4	5.10	0.40 ± 0.07
5	6.06	0.41 ± 0.04
6	7.11	0.31 ± 0.04
7	7.84	0.24 ± 0.04
8	9.51	0.20 ± 0.06
9	11.60	0.16 ± 0.03

due to far-away stars and galaxies.

The calculation uses the following equations from [26]:

$$\text{Eq. (8)} \quad \rho^* = \frac{\rho_{\mathrm{Sfar}} + \rho_{\mathrm{Efar}} - n'^2(\rho_{S\,1AU} + \rho_E)}{n'^2 - 1}, \text{ and}$$

$$\text{Eq. (19)} \quad n' = 1 - \frac{E_D\, c}{2 f_e\, G\left(\frac{M_S}{r_S^2} + \frac{M_E}{r_E^2}\right)},$$

where: (numerical values in SI units)

n', index of refraction of space at 20 AU (comes out to 0.999973567943846),

ρ^*, energy density of space due to far-away stars and galaxies,

E_D, a steady frequency drift of 5.99×10^{-9} Hz/s from the Pioneer 10 spacecraft [21, page 20],

$f_e = 2295$ MHz, the frequency used in the transmission to the pioneer spacecraft [21, page 15],

$c = 299792458.0$ m/s. Speed of light on Earth at surface,

$G = 6.67300 \times 10^{-11}\,\mathrm{m^3 kg^{-1} s^{-2}}$, Newton's universal constant of gravitation,

$M_S = 1.98892 \times 10^{30}$ kg, mass of the Sun,

$M_E = 5.976 \times 10^{24}$ kg, mass of the Earth,

1 Astronomical Unit (AU) = 149 598 000 000 m.

The distances r_S and r_E are the distances from the spacecraft at 20 AU (20 AU from the Sun, 19 from Earth) to the center of the Sun and Earth respectively. To calculate Eq. (8) of [26] use is made of the energy density ρ_i given by Eq. (4) also of [26]:

$$\rho_i = \frac{G M_i^2}{8\pi r^4},$$

where r is the distance from the centre of the Sun or Earth to the point where the energy density is being calculated as follows:

For the Earth's surface: $r_E = 63781.40$ m, radius of Earth,

For the Sun at 1 AU: $r_S = 149598000000$ m,

For the Sun at 20 AU: Twenty times the previous value used to calculate ρ_{Sfar},

For the Earth at 20 AU: radius of earth + 19 times 149 598 000 000 m used to calculate ρ_{Efar}.

All values were calculated with Microsoft Office Excel 2003 which uses 15 significant digits of precision.

Acknowledgements

We would like to thank Simón E. Greaves for help in independent verification of the Flyby Anomaly and Pioneer Anomaly calculations and thank Andres Sajo-Castelli for valuable suggestions to improve the manuscript. Also acknowledge help in the literature search to Laszlo Sajo-Bohus, Universidad Simón Bolívar, Caracas, Venezuela, Jorge A. Lopez, Physics Department, University of Texas at El Paso, USA, and Ricardo Alarcon, Arizona State University, USA.

Received on March 22, 2020

References

1. Anderson J. D., Campbell J. K. and Nieto M. M. The energy transfer process in planetary flybys. *New Astronomy*, 2007, v. 12 (5), 383–397. arXiv: astro-ph/0608087. DOI: 10.1016/j.newast.2006.11.004.
2. Anderson J. D., Campbell J. K., Ekelund J. E., Jordan E. and Jordan J. F. Anomalous Orbital-Energy Changes Observed during Spacecraft Flybys of Earth. *Phys. Rev. Letters*, 2008, v. 100, 091102, 1–4.
3. Jouannic B., Noomen R. and van den Ijssel J. A. A. The Flyby Anomaly: An Investigation into Potential Causes. Proceedings of the 25th International Symposium on Space Flight Dynamics ISSFD, Munich, Germany, 19–23 October 2015.
4. Lämmerzahl C., Preuss O., and Dittus H. Is the physics within the Solar system really understood. arXiv: gr-qc/0604052.
5. Acedo L. The Flyby Anomaly in an Extended Whitehead's Theory. *Galaxies*, 2015, v. 3 (3), 113–128. DOI: 10.3390/galaxies3030113.
6. Iorio L. A flyby anomaly for Juno? Not from standard physics. *Advances in Space Research*, 2014, v. 54 (11), 2441–2445.
7. Acedo L. The flyby anomaly: A case for strong gravitomagnetism? *Advances in Space Research*, 2014, v. 54 (4), 788–796.
8. Varieschi G. U. Kerr metric, geodesic motion, and flyby anomaly in fourth-order conformal gravity. *Gen. Relativ. Gravit.*, 2014, v. 46, 1741. DOI: 10.1007/s10714-014-1741-z
9. Acedo L. Kinematics effects of atmospheric friction in spacecraft flybys. arXiv: space-ph/1701.06939v1.
10. McCulloch M. E. Modeling the flyby anomalies using a modification of inertia. *Monthly Notices of the Royal Astronomical Society: Letters*, 2008, v. 389 (1), L57–L60.
11. Adler S. L. Can the flyby anomaly be attributed to earth-bound dark matter? arXiv: astro-ph/0805.2895v4.
12. Wilhelm K. and Dwived B. N. Anomalous Earth flybys of spacecraft. *Astrophys Space Sci.*, 2015, v. 358, 18. DOI: 10.1007/s10509-017-3205-x
13. Atchison J. A. and Peck M. A. Lorentz accelerations in the Earth flyby anomaly. *J. Guid. Control Dyn.*, 2010, v. 33, 1115–1122.
14. Acedo L. Anomalous accelerations in spacecraft flybys of the Earth. arXiv: astro-ph/1711.02875v2.

15. Rievers B. and Lämmerzahl C. High precision thermal modeling of complex systems with application to the Flyby and Pioneer Anomaly. *Annalen der Physik*, 2011, v. 523 (6), 439–449.
16. Cahill R. T. Resolving Spacecraft Earth-Flyby Anomalies with Measured Light Speed Anisotropy. *Progress in Physics*, 2008, v. 4 (3), 9–15. arXiv: gen-ph/0804.0039.
17. Greaves E. D. La hipótesis de Céspedes-Curé y el índice de refracción del espacio en un campo magnético. (The Céspedes-Curé hypothesis and the index of refraction in a magnetic field). *Acta Científica Venezolana*, 2015, v. 66 (4), 226–229.
18. Greaves E. D. Propiedades del espacio vacío. (Properties of empty space). Memorias del II Congreso de ABAE. September 18–22. 2017. http://2cvte.abae.gob.ve/ejes.php?idiomas=es. Retrieved 10 January 2019.
19. Céspedes-Curé J. Einstein on Trial or Metaphysical Principles of Natural Philosophy. 1st ed. Ramsey Laboratory, Inc, 2002. ISBN: 978-0971387300. http://www.nuclear.fis.usb.ve/Cespedes-Cure-2002-Einstein-on-Trial-J.pdf. Retrieved 10 January 2019.
20. Struve O. Elementary Astronomy. 1st ed. New York, Oxford University Press. 1959.
21. Anderson J. D., Laing Ph. A., Lau E. L., Liu A. S., Nieto M. M. and Turyshev S. G. Study of the anomalous acceleration of Pioneer 10 and 11. *Phys. Rev. D*, 2002, v. 65, 082004.
22. Einstein A. Über das Relativitätsprinzip und die aus demselben gezogenen Folgerungen. (About the principle of relativity and the consequences derived from it). *Jahrbuch für Radioaktivität und Elektronik*, 1907, v. 4, 411–462.
23. Einstein A. Über den Einfluß der Schwerkraft auf die Ausbreitung des Lichtes. (About the influence of gravity on the propagation of light). *Annalen der Physik*, 1911, v. 35 (10), 898–906. DOI: 10.1002/andp.19113401005.
24. Dicke R. Gravitation without a Principle of Equivalence. *Reviews of Modern Physics*, 1957, v. 29 (3), 363–376. DOI: 10.1103/RevModPhys.29.363.
25. Magueijo J. New varying speed of light theories. *Reports on Progress in Physics*, 2003, v. 66 (11), 2025–2068. DOI: 10.1088/0034-4885/66/11/R04.
26. Greaves E. D. NASA's astonishing evidence that *c* is not constant: The Pioneer Anomaly. arXiv: gen-ph/0701130.
27. Greaves E. D. A Neo-Newtonian Explanation of the Pioneer Anomaly. *Rev. Mex. AA (Serie de Conferencias)*, 2009, v. 35, 23–24.
28. Halliday D. and Resnick R. Physics for Students of Science and Engineering, Part II. John Wiley & Sons, Inc, New York and London, 1960.
29. Bate R., Mueller D. and White J. Fundamentals of Astrodynamics. 1st ed. Dover Publications Inc, New York, 1971.
30. Kaplan M. Modern Spacecraft Dynamics and Control. 1st ed. John Wiley & Son Inc, New York, 1976, 287–289.
31. Greaves E. D. The index of refraction of quasi-empty space. Universidad Simón Bolívar, Caracas Venezuela. 2015. Unpublished. http://www.nuclear.fis.usb.ve/fn/wp-content/uploads/2015/07/GREAVES-ED-Index-of-refraction-of-quasi-empty-space-V11.pdf, Retrieved 19 April 2019.
32. Turyshev S. G., Toth V. T., Kinsella G., Lee S. C., Lok S. M. and Ellis J. Support for the Thermal Origin of the Pioneer Anomaly. *Phys. Rev. Letters*, 2012, v. 108 (24), 241101. arXiv: gr-qc/1204.2507. Bibcode: 2012PhRvL.108x1101T. DOI: 10.1103/PhysRevLett.108.241101.
33. Francisco F., Bertolami O., Gil P. J. S. and Páramos J. Modelling the reflective thermal contribution to the acceleration of the Pioneer spacecraft. arXiv: space-ph/1103.5222v2.
34. Merat P. Analysis of the optical data on the deflection of light in the vicinity of the solar limb. *GRG*, 1974, v. 5 (3), 757–764.

Gravity in the Microworld

Anatoly V. Belyakov
E-mail: belyakov.lih@gmail.com

A brief review article gives examples of using the physical model based on the mechanistic interpretation of J. Wheeler's geometrodynamics. The examples show the need to consider gravity in the microworld. The latter is based on the balance of magnetic and gravitational forces.The gravitational constant was used in calculating the masses of quarks, neutrinos, proton size, coupling constants, etc. A new deviation of 28 GeV in the physical experiments of CMS Collaboration was confirmed by calculations. The unusual value of s- quark and b- quark masses is explained.

1 Introduction

In the Standard Model of Fundamental Interactions (SM), gravitational forces are not taken into account. However, the model based on the geometrodynamics of John Wheeler (Wheeler John Archibald) has proved the need for introducing gravitational forces into the microworld.

In the mechanistic interpretation of J. A. Weheler's geometrodynamic, charged microparticles are singular points on a non-simply connected two-dimensional surface of our world, connected by a "wormhole" or a drain-source current line in an additional dimension, forming a closed contour. But "wormholes", by necessity and by virtue of physical analogy in their mechanistic interpretation, can only be vortex current tubes, where the charge is in the "coulombless" form proportional to the medium momentum along the vortex current tube, spin, respectively, to the angular momentum relative to the longitudinal contour axis, and the magnetic interaction between the conductors is similar to the forces acting between the current tubes [1].

In this model, the electron size with mass m_e and radius r_e is taken as a medium unit element, and then the contour mass becomes proportional to its length. It is this hidden mass and its motion that is responsible for gravity, charge, spin, and magnetic interaction in the microworld. The introduction of gravity into the microworld allows one to explain various micro-phenomena and in some cases to calculate some important parameters quite accurately, using only fundamental constants and an elementary mathematical apparatus.

2 On the structure of microparticles

Thus, microparticles are not point objects, but are likened to vortex formations in an ideal fluid, which can reside in two extreme forms — the vortex *on the surface* of radius r_x along the X-axis (let it be the analog of a fermion of the mass m_x) and the vortex thread *under the surface in depth* of radius r, of the angular velocity v, and of the length l_y, filling the current tube of the radius r_e along the Y-axis (let it be the analogue of a boson of the mass m_y).

In a real medium these structures oscillate, passing into each other (oscillation of oscillators), where fermions retain part of the bosonic mass, introducing a half spin. Note that bosonic masses cannot in principle be stable, like their physical counterparts — vortex formations in a continuous medium (if they do not lean on a phase boundary). The parameters of the vortex thread m_y, v, r, l_y for an arbitrary p^+-e^--contour were determined in dimensionless units of the electron mass m_e, its classical radius r_e, and the speed of light c [2]:

$$m_y = l_y = (an)^2, \tag{1}$$

$$v = \frac{c_0^{1/3}}{(an)^2}, \tag{2}$$

$$r = \frac{c_0^{2/3}}{(an)^4}, \tag{3}$$

where n is the main quantum number, a is the inverse fine structure constant, while c_0 is the dimensionless light velocity c/[m/sec].

It is further shown particles themselves to be similar to the contour and have their own quantum numbers n_i, which determine, as it were, the zone of influence of these microparticles with the size $l_i = (an_i)^2$. For the proton and electron n_i are 0.3338 and 0.5777, respectively. A vortex tube of radius r_e is filled spirally with a vortex thread; therefore, with extreme "compression" and full filling, its length along the Y-axis is shortened proportional to $1/r$. In this case its compressed length $L_p = l_y r$ coincides numerically with the boson contour mass energy of units $m_e c^2$, and then it is true:

$$L_p = l_y r = m_y r = m_y v^2 = \frac{c_0^{2/3}}{(an)^2}. \tag{4}$$

It is obvious that an arbitrary boson mass in the mass-energy units will match of its own numerical value m_y only when the vortex tube ultimate excitation's case, wherein we have $r \to r_e$, $v \to c$, and $n_i \to 0.189$ (in experiments at high energie, for example). According to [2], the standard contour bosonic mass m_y is $c_0^{2/3} = 4.48 \times 10^5$ (in units of m_e), which approximately corresponds to the summary mass of W, Z-bosons. Therefore, it can be argued the vortex current tube to be form by three vortex threads rotating around

m_x	6.10×10^6	2090	1	$(4.4 \pm 0.1) \times 10^{-7}$
n_i	0.189	0.334	0.577	1.643
r_x	669	2090	6270	5.07×10^4
$m_k = L_p$	1.02	1.80	3.10	8.83
n	4.88	3.64	2.77	1.643
$l_y = m_y$	4.48×10^5	2.49×10^5	1.44×10^5	5.07×10^4

a common longitudinal axis. These threads are finite structures. They possess, by necessity, the right and left rotation; the last thread (it is evidently double one) possesses summary null rotation. They can be associated with the vector bosons W^+, W^-, Z^0.

This model assumes that a closed contour is created between charged particles in a region X (a p^+-e^--contour, for example); and only a temporary contour appears in a region Y, when a case of the weak interaction occurs (when a proton absorbs an electron, for example). The temporary contour then loses its charge (longitudinal momentum) and becomes a one-dimensional neutrino vortex tube, retaining spin. Since current tubes (i.e. field lines of some field) are treated as material objects, there are gravitational and magnetic interactions between them.

For a counter-currents closed contour the characteristic contour size l_k, which is the geometric mean of two linear quantities, is derived. This size is based on the balance of gravitational and magnetic forces written in the "Coulomb-less" form [2]. Applied to the X-axis l_k is:

$$l_k = (l_x r_x)^{1/2} = \left(\frac{z_{g_1} z_{g_2}}{z_{e_1} z_{e_2}}\right)^{1/2} (2\pi\gamma\rho_e)^{1/2} \times [\mathrm{sec}], \qquad (5)$$

where z_{g_1}, z_{g_2}, z_{e_1}, z_{e_2}, r_x, l_x are gravitational masses and charges expressed through the mass and charge of the electron, the distance between the current tubes (charges) and theirs length, γ is the gravitational constant, while ρ_e is the electron density $m_e/r_e^3 = 4.07 \times 10^{13}$ kg/m^3.

A vortex tube having a momentum equivalent to the electron charge was shown in [3] really to contain three single vortex threads (the calculated value is 2.973). These unidirectional vortex threads rotate about a longitudinal axis. Their peripheral speed v_0 is derived from the balance of magnetic and inertial (centrifugal) forces. In the case of unit charges, it is equal to:

$$v_0 = \frac{r_e}{(2\pi)^{1/2} \times [\mathrm{sec}]} = 1.12 \times 10^{-15} \text{ m/sec}, \qquad (6)$$

and does not depend on the length of the vortex threads and the distance between them.

3 On the weak interaction

The proton has a complex structure, and quarks are in this model an active part of its mass, a kind of ring currents inside the proton, where in three local sections the medium velocity reaches critical parameters [2]. In the p^+-e^--contour, proton quarks are involved in the circulation, and their mass as z_{g_1} is included in equation (5) and depends on the contour size. For the weak interaction, the contour is limited only by its influence zone $l_i = (an_i)^2$. Setting $r_x = l_i$ and taking into account formulas (1–5), for the mass of quarks at unit charges, we obtained:

$$m_k = z_g = \frac{an_i c_0^{1/3}}{2\pi\gamma\rho_e \times [\mathrm{sec}^2]}. \qquad (7)$$

It should be noted that the quarks charges are integer ones inside the proton, and in the form of fractional quantities they are only projected onto the outer surface of the proton.

In the case of the weak interaction (electron absorption by the proton) the quark mass-energy is assumed to compar with the compressed bosonic contour mass-energy L_p in the Y-region, which, having lost a longitudinal momentum (charge), becomes the bosonic neutrino vortex tube [4]. This process is something similar to the charge and spin separation — a phenomenon registered in ultrathin conductors [5], which can be likened to a one-dimensional vortex current tube. Under this condition $m_k = L_p$, the quantum number n of Y-contour is calculated from formula (4), and the mass m_y (relative length) according to formula (1).

Table 1 that above shows the calculated parameters under various conditions of the weak interaction, i.e. for various distances between the proton and the electron, namely: the characteristic masses of fermions m_x, their own quantum numbers n_i, distances between charges r_x, quark masses m_k, boson tube quantum numbers and masses n and m_y.

The relationship between the fermion and bosonic masses was established in [2]. The most probable fermionic mass of neutrinos was determined in [4] under the additional condition of symmetry, when $r_x = l_y$ and $n = n_i$ (see Table 1); moreover, there are three more independent formulas containing the gravitational constant and giving actually that the result, equal to 4.4×10^{-7} (0.225 eV). It is not known whether neutrinos appear as a fermion at higher n; in these cases, their masses would be negligible, because they are inversely proportional to n^{14}. As for the structure of the neutrino, then, having no charge, it should have a closed shape. Apparently, the bosonic vortex tube, consisting a total of four vortex threads, is as a result organized into a pair of closed vortex

threads with left-right rotation and, conversely, with right-left rotation (with respect to the motion axis direction).

The minimum quark mass, as follows from the table, matches to the electron mass, and the most probable one (when neutrino is released) matches to the d-quark mass of 8.83 (4.8 MeV). The bosonic masses m_y are close to the masses of three, two (Higgs mass), one and one third of the W, Z particles masses. Although the last boson with a mass of 5.07×10^4 (26 GeV) has not yet been detected, events with close energies of about 28 GeV have already been recorded in the CMS Collaboration experiments [6].

These bosons are considered, on the one hand, to be truly fundamental particles, and on the other, to be pointlike virtual particles, moreover having enormous mass-energy. This fact is in no way compatible with the particles or atoms internal energy. They exist only about 10^{-25} seconds, although the duration of the weak interaction is $t > 10^{-12}$ seconds. The latter in this model is understandable, because t determines the time of a medium runing with speed v around the entire "extended" contour length. That is, given (1–4), we have:

$$t = \frac{a^8 n^8}{c_0} \frac{r_e}{c}, \tag{8}$$

that in the indicated range n gives $10^{-9} \ldots 10^{-13}$ seconds, there is an interval corresponding to possible times of the weak interaction.

Given the inconsistencies in the W and Z bosons properties and based on the calculated masses m_y, these bosons (including the Higgs boson) are probably not fundamental particles, but rather the excited boson forms of neutrinos, which during high energy experiments acquired (or did not have time to lose) for a short time a longitudinal momentum (charge).

4 On the coupling constants

It was found [7] that the formula for the number of threads in a vortex tube, cubed, is the ratio of the inertia forces arising from the acceleration of the bosonic standard contour mass and acting towards the periphery, to the gravitational forces acting between fermionic masses of m_e at a distance r_e. The numerator is a constant, so this dependence is only determined by gravity, i.e. interacting masses and the distance between them

$$n_i^3 = \frac{m_e c_0^{2/3} r_e / ((2\pi)^{1/2} \times [\sec^2])}{(2\pi)^{1/2} \gamma m_e^2 / r_e^2} = 26.25. \tag{9}$$

This formula indicates the strength of bonds between the structural elements of microparticles (quarks) and, as it turns out, can serve as the equivalent of the coupling constant a_s for weak and strong interactions. Suppose that quarks are located in the corners of a regular triangle at a distance r_e. Then, taking into account the geometry of their interaction and after calculating the constants, the formula (9) can for the general case be represented in a dimensionless form:

$$a_s = 15.15\,(r/m)^2. \tag{10}$$

At low energies of interacting particles, affecting only the external structure of nucleons (small "depth" along Y), the peripheral inertia forces exceed the attractive forces, therefore quarks are weakly coupled to each other within a vortex tube of radius r_e, and they interact with quarks of nearby nucleons. At high energies (about 100 GeV, a great "depth" along Y) they reach within the proton itself vortex thread the minimum distance of $r \sin 60^\circ$ (here r is calculated from (3)); in this case the mutual attraction forces keep the quarks in a bound state within the nucleon size. Then, with the quark minimum mass, $m_k = 1$, substituting $r = 1$ and $r = 0.0887$ in (10), we obtain: $a_s = 15.15$ and $a_s = 0.119$. These values coincide with the actual ones.

The validity of the above is also convincingly confirmed by the determination of the proton radius r_p provided that $a_s = 1$ and $m_k = 1$. Obviously, it is the vortex tube circumferential size and it is equal to $r/\sin 60^\circ$. Revealing the constant in (10) and using the above formulas, we finally get:

$$r_p = \left(\frac{8\pi\gamma\rho_e}{3^{1/2} c_0^{2/3}} \right)^{1/2} \times [\sec] = 0.297 \text{ or } 0.836 \text{ Fm}, \tag{11}$$

which *exactly coincides* with the value obtained in recent experiments (0.833 femtometers, with an uncertainty of ±0.010 femtometers) [8].

In the weak interactions, bosonic vortex tubes take part in, but since their mass is high, the coupling constant for the weak interaction is very low (about 10^{-5}). With increasing interaction energy, vortex tubes are excited and their radius increases, and then this constant increases significantly. Thus, the coupling constant determines neither the nature of nuclear forces, nor the strength of interaction, but only indicates the strength of bonds within the complex structure of nucleons.

5 On the masses of s- and b- quarks

In [2] the total masses of the second and third generation quarks were approximately determined. But the masses of negative s- and b- quarks was in experiments found to be much smaller than the masses of their positive partners, and it can not be explained in SM. In this model the mass order of these quarks is at least reliably determined when using formula (5), derived from the balance of magnetic and gravitational forces. It was shown in [2] that any contour connecting charged particles can consider similar to a particle that is part of a larger contour, where the smaller contour mass is assumed to be a hypothetical fermion mass (a proton analog) for the larger one. Thus three generations of elementary particles are formed.

For the second generation (μ-contour), the proton analog is the mass of the standard contour $c_0^{2/3}$, for the third (τ-contour) one is the mass of the μ-contour, determined from the limiting conditions at $n_i = 0.189$ and equal to 6.10×10^6. Thus, for contours of subsequent orders it can be assumed of linear scale unit's increasing in proportion to the ratios of the μ-contour and τ-contour masses to the proton mass m_p. Since quarks masses is directly proportional to $l_x r_x$, i.e. to a linear parameter square, and inversely proportional to leptons masses, then, bearing in mind (5), we can write the relation:

$$\text{s- quark mass} \quad m_{k\,s} = \frac{m_k(c_0^{2/3}/m_p)^2}{m_\mu} = 222\, m_k\,,$$

$$\text{b- quark mass} \quad m_{k\,b} = \frac{m_k(6.10 \times 10^6/m_p)^2}{m_\tau} = 2450\, m_k\,,$$

where m_μ and m_τ are the μ- and τ- particles masses.

Consequently, the s- and b- quarks masses order is determined correctly: for the s- quark it is several hundred masses of the first generation quark, for b- quarks it is several thousand masses of the first generation quark.

6 Conclusion

Thus, the above examples show that gravity has a significant effect in the microworld, and the gravity constant should inevitably be included in the more accurate theories describing the microworld. Perhaps it is just this factor that may contribute to the further creation of the "theory of everything".

Submitted on April 15, 2020

References

1. Belyakov A.V. Charge of the electron, and the constants of radiation according to J. A. Wheeler's geometrodynamic model. *Progress in Physics*, 2010, v.4, 90–94.
2. Belyakov A.V. Macro-analogies and gravitation in the micro-world: further elaboration of Wheeler's model of geometrodynamics. *Progress in Physics*, 2012, v.2, 47–57.
3. Belyakov A.V. On Materiality and Dimensionality of the Space. Is There Some Unit of the Field? *Progress in Physics*, 2014, v.10, 203–206.
4. Belyakov A.V. Determination of the Neutrino Mass. *Progress in Physics*, 2016, v.12, 34–38.
5. Jompol Y., Ford C.J.B., Griffiths J.P., Farrer I., Jones G.A.C., Anderson D., Ritchie D.A., Silk T.W., and Schfield A.J. Probing Spin-Charge Separation in a Tomonaga-Luttinger Liquid. *Science*, 31 July 2009, v.325, no.5940, 597–601.
6. arXiv: 1808.01890 [hep-ex]. High Energy Physics — Experiment (hep-ex). CMS-HIG-16-017, CERN-EP-2018-204.
7. Belyakov A.V. Nuclear Power and the Structure of a Nucleus According to J. Wheeler's Geometrodynamic Concept. *Progress in Physics*, 2015, v.11, 89–98.
8. Bezginov N., Valdez T., Horbatsch M., Marsman A., Vutha A.C., Hessels E.A. A measurement of the atomic hydrogen Lamb shift and the proton charge radius. *Science*, 06 Sep. 2019, v.365, issue 6457, 1007–1012.

Application of the Theory of Hyperrandom Phenomena in the Search for Signs of the External Influence on Radioactive Decay and the Possibility of Quantitative Estimates

S. V. Adamenko[1], A. S. Kapshuk[1], V. E. Novikov[1], A. D. Skorbun[2*], S. N. Shpyl'ka[1], V. A. Yatsyshyn[1]

[1]Laboratory "Proton 23", 48-A, Chornovil Str., Vyshneve, Kyiv-Svyatoshyno district, Kyiv region, 08132, Ukraine.
[2]Institute for Safety Problems of Nuclear Power Plants of the NAS of Ukraine, 36a, Kirov Str., Chornobyl' 07270, Ukraine.
*Corresponding author E-mail: anskorbun@gmail.com

We have developed the relevant setup and studied a possibility of the influence on the radioactive decay by an external impulsive electromagnetic field. It is shown that such action can result not only in a change in the rate of decay (rate of counting of gamma-quanta), but also in a clear variation of the statistical properties of the series of successive measurements of the counting rate such as the appearance of periodicities and hyperrandom properties. It is found that the excitation of a system of radioactive nuclei induced by the external influence disappears approximately in 4–6 days.

1 Introduction

We will describe our attempt to find a possibility to affect parameters of the radioactive decay with the help of an impulsive electromagnetic field. As is known, at the radioactive decay, the number of decays per unit time is a random variable which is described by the Poisson distribution [1]. Hence, from the viewpoint of the statistical analysis, the problem of search for the signs of changes after some treatment of a radioactive specimen can be reformulated as a problem of changes in the statistical properties of samples which are the records of the results of measurements before and after the treatment.

It should be emphasized that we intend to seek the weak changes which can be only precursors of the changes seen by naked eye (hence, of those possessing a practical significance). From the viewpoint of the dominant theory, the rate of radioactive decay cannot be affected at all (see [2]). While experimentally determining the influence of some factor, the researchers try to find, as a rule, the changes in the counting rate at least on the level of the statistical effects. We pose the problem in a more general form: to seek the differences between samples which can or cannot be reduced to a change in the mean counting rate.

The sought signs can be the periodic variations in a counting rate or the appearance of irregular "splashes" of the intensity or other irregularities leading to that the series of measurements of the counting rate cease to be random in the sense of mathematical statistics. In this case, a change in the form of a distribution function (loss of the Poisson property) can be only one of the possible sought signs.

The radioactive decay can be considered as an example of the process (if the radioactive half-life is much more than the time of measurements), for which the long series of measurements of its parameters is considered to be stationary in the sense of mathematical statistics, i.e. its statistical parameters do not vary with time. For comparison, we can indicate examples of other natural processes without the property of stationarity such as the noise of the ocean, where ships move from time to time near a detector of noises. The problem of the analysis of such data was considered, for example, in [3, 4].

In the present work, we will analyze changes in the decay statistics for signals of the rate of counting of gamma-quanta from radioactive specimens after the action of an impulsive electromagnetic field onto them.

2 Data and methods of their analysis

We will examine a possibility to influence the process of radioactive decay by external impulsive electromagnetic field. The setup generating the electromagnetic impulses that act on a radioactive specimen will be called a driver for simplicity. In order to use the statistical methods of analysis, we need the long series of regular measurements of the rate of decay. Such series were recorded with the use of a dosimeter-radiometer "Pul's" aimed at the remote radiation control. The device was produced at the small joint-stock enterprise "Opyt", includes a detector on the basis of NaI(Tl), and allowed us to execute every-second measurements with the record of results into a memory unit.

We analyzed the results of measurements of a specimen treated with a driver during February–May in 2018 in the city of Chornobyl'. As a specimen, we took monazite sand, i.e. we measured and analyzed the summary signal (gamma-radiation) from decay products of ^{232}Th. First, before the treatment of the specimen with a driver, we carried out the measurements of the counting rate for several days. Later on, we compared those data with the results obtained after the action of a driver onto the specimen.

In the analysis of the statistical properties of the measured signals, we used the statistical theory of hyperrandom phenomena [5]. This theory is based on the hypothesis that the results of measurements of natural processes are not independent and identically distributed. Hence, they do not obey the

basic preconditions for the application of well-known methods of mathematical statistics. In other words, the basic assertion of the theory of hyperrandomness consists in that the process under study can undergo the action of external influences, which induces, respectively, changes in the statistics of a signal. This is manifested in the loss of the statistical stability by data, i.e. the results of measurements become dependent on the time. However, it can turn out that very long series of measurements should be made for such changes to be revealed.

The main distinction of the hyperrandom data from the standard random numbers which are independent and identically distributed consists in that the variance of the former does not decrease, as the number of measurements increases (increase in the size of a sample). On the contrary, starting from some number of measurements, the variance of hyperrandom data increases [3, 4]. Such effect can be a consequence of the tendency to a change in the mean, the autocorrelated function, *etc* during the measurement. (We emphasize once more that the similar changes in a sample can have the statistical character and can be invisible for naked eye.)

The formulas for the analysis of hyperrandom data can be found in [5, 6]. We now indicate only the principle of such analysis. Let us have the sample of the results of measurements X with size N: $X = (x_1, x_2, \dots x_N)$ is a regular temporal series of the results of measurements. We accentuate that the series is ordered in the meaning that the elements of the series should not be permuted. We are interested in the dependence of its parameters on the size of a sample, i.e. on the time. For this purpose, we calculate the accumulated means, i.e. the means for the first two, three, *etc* elements of the input series. As a result, we get a new first-order series of data in the form of accumulated means $Y^{(1)} = (Y_1, Y_2, \dots Y_N)$, where $Y_n = \frac{1}{n}\sum_{i=1}^{n} x_i (n = \overline{1, N})$, with its mean $\overline{m}_{Y_N} = \frac{1}{N}\sum_{n=1}^{N} Y_n$. Then we can repeat the procedure and form the series of higher orders $Y^{(2)}$, $Y^{(3)}$, *etc*.

The object of our analysis is the function, being the unbiased variance of fluctuations from the accumulated mean, $\overline{D}_{Y_N} = \frac{1}{N-1}\sum_{n=1}^{N} (Y_n - \overline{m}_{Y_N})^2$.

As the quantitative measure of one of the hyperrandom properties, specifically, the statistical instability of a series of data, we take the coefficient γ_N characterizing the absolute level of statistical instability: $\gamma_N = \frac{M[\overline{D}_{Y_N}]}{N D_{Y_N}}$, where $M[*]$ is the operator of mathematical expectation.

To have a possibility to compare different samples with one another, the units of statistical instability are introduced in the theory. For the coefficient γ_N, the role of a unit of statistical instability of measurements is played by the quantity γ_{0N} which corresponds to the noncorrelated series of readings with constant variance $D_{x_n} = D_x$ and zero mathematical expectation at a fixed value of N. The coefficient γ_{0N} is given by the formula

$$\gamma_{0N} = \frac{N+1}{(N-1)N} C_N - \frac{2}{N-1}, \text{ where } C_N = \sum_{n=1}^{N} \frac{1}{n}.$$

Using the unit of measurements γ_{0N}, we introduce the ratio $h_N = \frac{\gamma_N}{\gamma_{0N}}$, i.e. the coefficient characterizing the absolute level of statistical instability in units of γ_{0N}. These coefficients are dimensionless. The degree of hyperrandomness h_N of the analyzed data will be considered in what follows.

We note that though the hyperrandom properties of our data are manifested undoubtedly (see below), the derivation of the quantitative estimates of the degree of hyperrandomness is not a simple matter. We clarify this point by the example. Let us deal with a really random stationary process, so that its signal has no signs of the hyperrandomness. At some time moment, let a quite short external influence arise (the duration of the external action is assumed to be much less than the time of observations). It causes an increase in the mean and, respectively, to the appearance of the hyperrandomness. After some time period, the signal again becomes random and stationary.

Hence, the sample as a temporal signal can be partitioned into three parts. The midsection is hyperrandom, and the beginning and the end are normal stationary signals. In this situation, the sample has, on the whole, hyperrandom properties. But the results of calculations for each of the three parts separately will give different results.

In real situations, the information about the very fact of the external influence (treatment by a driver) can be unknown. Hence, we should consider the problem of determination of changes in the statistics of a series, the problem of analysis of the dynamics of those changes in time, and the problem of searching for the time, when the driver acts. If, for example, the aftereffect is present and varies in time, we can say nothing about the time moment of the transition of the sample into the third part, even if we are based on the analysis of the whole series. Moreover, the very fact of such transitions should be studied. We reformulate this problem as follows: Are there some regularities of changes in the hyperrandomness indicating the action of a driver and can we determine, for example, the characteristic time of relaxation of the "hyperrandomness state" arisen due to the action of a driver?

In view of the above discussion, we need to analyze the separate parts of samples with the purpose to find the distinctions between them and to establish the optimum size of such subsamples. To make it, we chose a "window" of a definite size, i.e. we set the size of a subsample. With such window, we scan the whole series of measurements. For each "window", we calculated the necessary parameters.

3 Results and discussion

As was indicated, the hyperrandomness by its nature arises at a change in time of some parameters of the process such

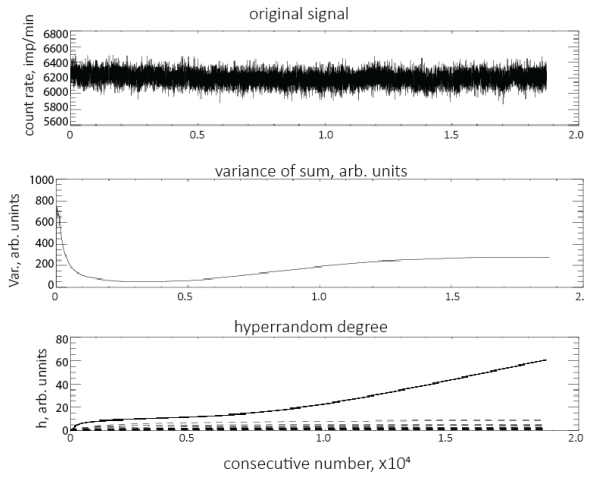

Fig. 1: Analysis for hyperrandomness of a series of measurements during 13 days from 14.02.2018 to 26.02.2018 (prior to the treatment). There is the sign of the hyperrandomness, which is revealed as an increase in h_N after approximately 5000–8000 min of measurements.

as, in particular, the solitary short-time splashes. The statistical characteristics of a series calculated before the splash can be changed after it. If the duration of the action of a driver is from several minutes up to several hours, it can be considered a short-time influence against the background of measurements during several days.

One of the tasks of the present work is the search for the time of relaxation of a signal after the action of a driver, which is reduced to the analysis of short segments of the entire series. In Fig. 1, we present the results of a test for the hyperrandomness. We took a sufficiently long-time (13 days) series of measurements before the action of a driver in order to estimate the order of long-time changes.

In each of the figures below, the upper plot is the input series of data; the middle plot presents a variation in time of the accumulated variance; and the lower plot shows the parameter h_N which characterizes the degree of hyperrandomness. The results of calculation of the hyperrandomness parameter are accompanied by the analysis of whether such result can be formed accidentally. It is a reasonable question, because we analyze the series of random numbers. For this purpose, we generated a computer-created sample of random numbers with the same parameters (mean and variance), as those of the experimental series. For such model sample with the same programs, we made analysis for hyperrandomness. This procedure was repeated several times for the sake of reliability, and the results were drawn on one figure. In the presence of a noticeable hyperrandomness, the experimental curve must be outside the zone, where the curves for model samples are placed. This zone for the model series of random numbers is shown in the lower plot by dotted lines.

As is seen in Fig. 1, the series manifests some hyperrandomness during 13 days before the treatment. It starts to reveal itself after approximately 5–6 days of measurements.

Then, on 27.02.2018, we executed the treatment of the specimen with a driver (impulsive electromagnetic field).

In Fig. 2, we present the results of analysis for the hyperrandomness of a series of measurements before and after the action of a driver. We recall that our purposes are to register the time of a manifestation of the action of a driver and to determine the temporal changes of the signs of such action. We analyzed the subsamples 4 days in duration. In other words, we analyzed a part of the series 4 days in duration, then the "window" was shifted by one day, and so on. Hence, the subsamples were overlapped during 3 days in order to more or less reliably notice the times of changes in the degree of hyperrandomness.

In view of Fig. 2, we can formulate the following main results:

1. After the action of a driver, the rate of counting of gamma-quanta somewhat increased.
2. In the analyzed series, the hyperrandomness was not observed practically for 4 days (accepted size of a scanning "window") before the treatment: the variance decreased, as the size of a sample increased.
3. After the action of a driver on 27.02.2018, we observe a sharp increase in the hyperrandomness. The variance starts to grow already approximately in 1200 min (20 h).
4. This effect of hyperrandomness practically disappeared on 04.03.2018 (in 4–5 days) to the level of noises.

4 Conclusions

1. We have revealed that, under the action of electromagnetic impulses, the statistics of the radioactive decay is changed.
2. It is found that, after the action of a driver, the process of decay became hyperrandom. This means that its characteristic such as the accumulated variance increases in time, rather than decreases. In turn, this means that the process of decay stops to be stationary.
3. This forced nonstationarity was observed during approximately 5 days. Then the process of decay returns to the stationary mode (experimental curve in Fig. 2f is located in the zone of random values).
4. Such time of existence of the aftereffect (tens of hours), which is much more than the characteristic time of the evolution of a separate nucleus, is, most probably, the experimental confirmation of the theories (see [7–10]) that assert that the radioactive decay is a collective process in the system of correlated nuclei. From this position, we may assert that the quantitative estimates of the process of relaxation of a system of nuclei are made

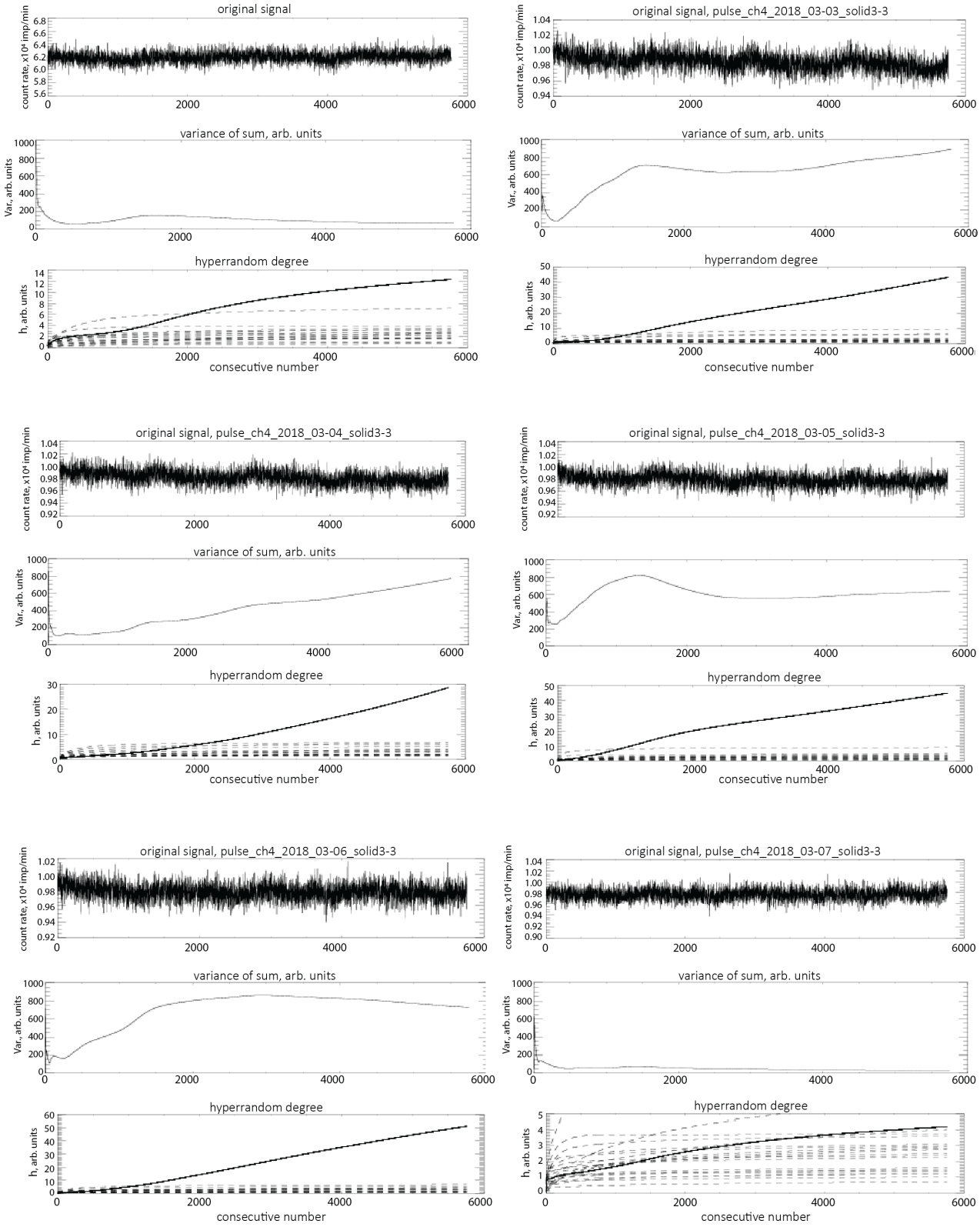

Fig. 2: Analysis for hyperrandomness: the series of successive overlapping subsamples from 28.02.2018 to 03.03.2018. The measurement at once after the treatment which occurred 27.02.2018. After the action of a driver, the hyperrandomness appeared: an increase in the variance and in h is clearly seen. On the fifth day, the hyperrandomness drops to the level of random noises.

for the first time. The determined time of the relaxation has the order of hours.

Received on May 4, 2020

References

1. Gol'danskii V. I., Kutsenko A. V., Podgoretskii M. I. Statistics of Readings at the Registration of Nuclear Particles. GIFML (State Publishing House of Physical and Mathematical Literature), Moscow, 1959, p. 411.
2. Gareev F. A., Zhidkova I. E., Ratis Yu. L. Influence of the excitation and ionization of atoms in the rate of nuclear processes at low energies. Preprint R4-2004-68, JINR, Dubna, 2004, p, 54.
3. Gorban' I. I., Yaroshchuk I. O. Study of the statistical stability of oscillations of the temperature and the sound velocity in the ocean. Proceedings of the Acoustic Symposium "Consonance-2011", Institute of Hydromechanics of the NAS of Ukraine, Kiev, 2011, pp. 99–104.
4. El'yasberg P. E. Measurement Information: How Much Is It Needed? How Is It Processed? Nauka, Moscow, 1983, p, 208.
5. Gorban' I. I. Theory of Hyperrandom Phenomena. Institute of Problems of Mathematical Machines and Systems of the NAS of Ukraine, Kiev, 2007, p. 184. http://ifsc.ualr.edu/jdberleant/intprob/.
6. Gorban' I. I. Statistical instability of physical processes. *Radioelectronics*, 2011, v. 54 (9), 40–52.
7. Torchigin V. P., Torchigin A. V. Features of ball lightning stability. *Eur Phys J. D*, 2005, v. 32, 383—389. Torchigin V. P., Torchigin A. V. Ball Lightning (from the Improbable to the Obvious). MTsNMO, Moscow, 2009, p. 148.
8. Adamenko S. V., Selleri F., van der Merwe A. Controlled Nucleosynthesis. Breakthroughs in Experiment and Theory. Springer, Berlin, 2007.
9. Adamenko S. V., Vysotskii V. I. Correlated states of interacting particles and the problem of transparency of a Coulomb barrier at a low energy in nonstationary systems. *Zh. Tekh. Fiz.*, 2010, v. 80 (5), 23–31.
10. Adamenko S. V., Vysotskii V. I. Peculiarities of the formation and application of correlated states in nonstationary systems at a low energy of interacting particles. *ZhETF*, 2012, v. 141 (2), 276–287.

Periodic Phenomena in the Rate of Radioactive Decay Under the Action of an Electromagnetic Field

S. V. Adamenko[1], A. S. Kapshuk[1], V. E. Novikov[1], A. D. Skorbun[2], S. N. Shpyl'ka[1], V. A. Yatsyshyn[1]

[1]Laboratory "Proton 23", 48-A, Chornovil Str., Vyshneve, Kyiv-Svyatoshyno district, Kyiv region, 08132, Ukraine.
[2]Institute for Safety Problems of Nuclear Power Plants of the NAS of Ukraine, 36a, Kirov Str., Chornobyl' 07270, Ukraine.
*Corresponding author E-mail: anskorbun@gmail.com

We have determined a mode of treatment of a radioactive material (^{232}Th and daughter products in a colloid solution of monazite sand) with a sequence of short impulses of an electromagnetic field which results in a change in the intensity (counting rate) of gamma-radiation. The value of changes in the intensity as a general trend is approximately 1.8 % for a period of about 1 month. In addition to the changes in the intensity, we observed changes in the statistics of the radioactive decay. In the long-term signal of every-second regular measurements of the counting rate for daughter products of the decay of ^{232}Th obtained after the treatment of the specimen with an impulsive electromagnetic field, we have found the periodic components among which the periods of 0.5, 1, and 6.6 days are distinguished most clearly.

1 Statement of the problem

The regular periodic changes in the intensity of signals of the radioactive decay, as well as the sporadic splashes of the counting rate, were observed many times (see [1]). They include the seasonal changes with periods of 1 year, 1 month, and 1 day which can be obviously related to astronomical phenomena. While analyzing the periodicity of the 1-day radioactive decay, it is necessary to separate the studies of the changes in the intensity of signals from radon and beryllium in the near-Earth layer of the atmosphere, which are caused mainly by geophysical or meteorological factors and are omitted in the present work, from the studies of the radioactive decay under controlled conditions (see [2–4] and references therein), where the manifestations of the variability of a signal are assigned to changes namely in the rate of radioactive decay. The presence of changes in the rate of decay can be related, in our opinion, to such fundamental causes as cosmophysical factors. Separately, we mention the works by S. E. Shnoll [5], where the regular changes in the statistics of separate parts of the series of measured data on the rate of radioactive decay, namely, the changes in a form of the distribution function, were observed. It is worth to note the fundamental cycle of works executed by opponents of this idea [6–8], where the special studies of this question revealed no existence of seasonal changes in the half-life period.

But earlier, the existence of that or other regularities of the radioactive decay was discussed without any experimental interference at laboratories. Moreover, the possibility of the influence of external physical factors, being outside the nuclear scale of energies, on the rate of radioactive decay was considered impossible since Rutherford's times [1, 9, 10]. Hence, the studies in this direction have a fundamental meaning, because they would prejudice the basic assertions of the theory that, first, all events of a radioactive decay are mutually independent, and, second, the internal processes in a nucleus which define the processes of decay can be affected only by the fluxes of particles and quanta with energies of the order of those of nuclear transitions from kiloelectronvolts to megaelectronvolts. However, we mention a well-known exclusion, isotope ^{229}Th, whose excitation energy is about 1 eV.

In this work, we present the results of laboratory studies of the influence of an external electromagnetic field with sufficiently low intensity on the rate of counting of gamma-quanta from a radioactive specimen and will show that such influence is possible.

Especially, we note that, though the revealed changes in the intensity of a signal after the action of an external factor for the period of observations up to 40 days are rather small, the changes in the statistical properties of the obtained regular series of measurements are obvious and objective.

2 Materials and methods

The setup realizing the action on a specimen (for simplicity, we call it a driver) is a system of coils with special structure aimed at the creation of an impulsive electromagnetic field. The duration of impulses is 1–10 nsec. The treatment was carried on for 10–30 min. The power of the setup is about 25 W. The energy of impulses is at most 2.5 J.

The scheme of the experiment is as follows. First, we carried on the control measurements for some time. After the action of a driver, the specimen was returned to a counter, and we measured the radiation from the specimen for several days. Such procedure can be repeated several times. In this case, we studied the intensity of the summary gamma-radiation from a specimen of natural monazite sand (mineral with ^{232}Th) for the period from 20.12.2017 to 15.01.2018. The results are obtained in a laboratory, i.e. under controlled conditions. During the indicated period of measurements, the driver did not act on the specimen, i.e. the presented results

are a manifestation of the aftereffect.

To gauge the counting rate, we used a counter of gamma-quanta such as a dosimeter "Pul's" for the remote radiation control. It was produced at the small joint-stock enterprise "Opyt" and includes a detector on the basis of NaI(Tl). The construction of the counter itself contains no lead-based protection. The counter can operate in the automatic mode and can write the result of measurements in the memory every second. During the measurements, the counter with a specimen have no special protection or can be placed inside a lead cylinder. The latter was open from one end, was about 30 cm in length, and has walls 10 cm in thickness. The measurements were carried out on different specimens, in different modes of action of a driver, many times, under the lead protection, and without it. On the whole, the results were invariable, i.e. the below-described effects did not disappear. The described conditions of measurements are given for the concreteness. The measurements were performed in heated premises. The changes on the temperature were in the interval 17–22 °C, but they were not regular with daily period.

In the room, where the measurements were performed, the background was much lower than the level of signals. For the indicated period, we have got a series of every-second measurements of the intensity of gamma-radiation with interruptions for the time, when the treatment of a specimen was executed.

Since the purpose of the present work is the search for the periodicity of a signal, we applied the wavelet-analysis using Gauss–Morlet wavelets [11, 12].

In Fig. 1, we show the signal from the untreated specimen in the form of a noisy path and its wavelet-expansion as a two-dimensional pattern of disordered spots. If some periodic regularities of the type of modulation by a sinusoid are present in the signal, the pattern of coefficients of the Gauss wavelet-expansion will contain the series of spots regularly arranged along the horizontal. The distance between such regular spots along the horizontal is equal to the half-period in units of the horizontal axis.

In view of the low rate of counting, while seeking the periodicities with a period of 1 h and more, we transformed the input series of data into a series of measurements for each 10 minutes (sum of sequential values for each 600 sec without the overlapping of intervals, where the number of counts is calculated).

3 Results

The analyzed signal itself after the action of a driver and the result of its wavelet-expansion are given in Fig. 2. The upper plot is the series of data which should be analyzed. Below, the two-dimensional pattern is the representation of coefficients of the wavelet-expansion (result of a wavelet-transformation of some series of data is the two-dimensional matrix of coefficients of the expansion). On the horizontal axis of the pattern, we indicate the number of a measurement which is proportional to the time from the start of measurements.

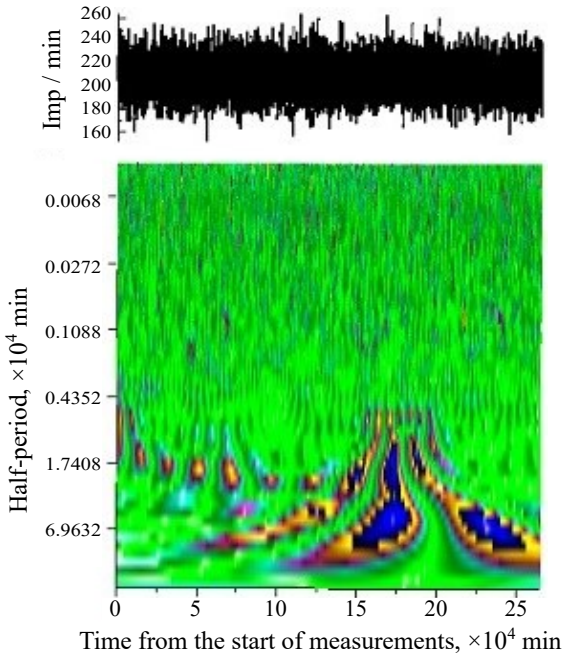

Fig. 1: Wavelet-expansion of a signal of the intensity of gamma-radiation from a specimen of monazite sand without the treatment with a driver. The upper plot is a signal; below, the two-dimensional pattern is the representation of the matrix of coefficients of the wavelet-expansion of this signal.

We note that the measurements are regular, and, in this case, each measurement corresponds to a time interval of 10 min. Therefore, for example, the number 1000 on the horizontal axis corresponds to a time moment of 10 000 min from the start of measurements. Along the vertical axis of the two-dimensional pattern, we give the half-period of a signal in units of the horizontal axis. We see clearly several horizontal rows of "spots," the distances between which are equal to the half-period (by assuming the modulation by a sinusoid).

In the table near the wavelet-expansion pattern, we show, as an example, several distances between spots for the rows indicated by arrows directly from the two-dimensional pattern in Fig. 2. This allows us to draw conclusion about the uncertainty of those estimates.

In addition to the appearance of a periodic daily modulation on the wavelet-expansion patterns, we observe that the signal itself looks as a uniform noisy path. We see also a tooth ripple of the daily variation and a small asymptotic decline.

4 Discussion of results and conclusions

The obtained array of results about the dynamics of the rate of counting of gamma-quanta after the treatment of a specimen with a driver testifies indisputably to the presence of the

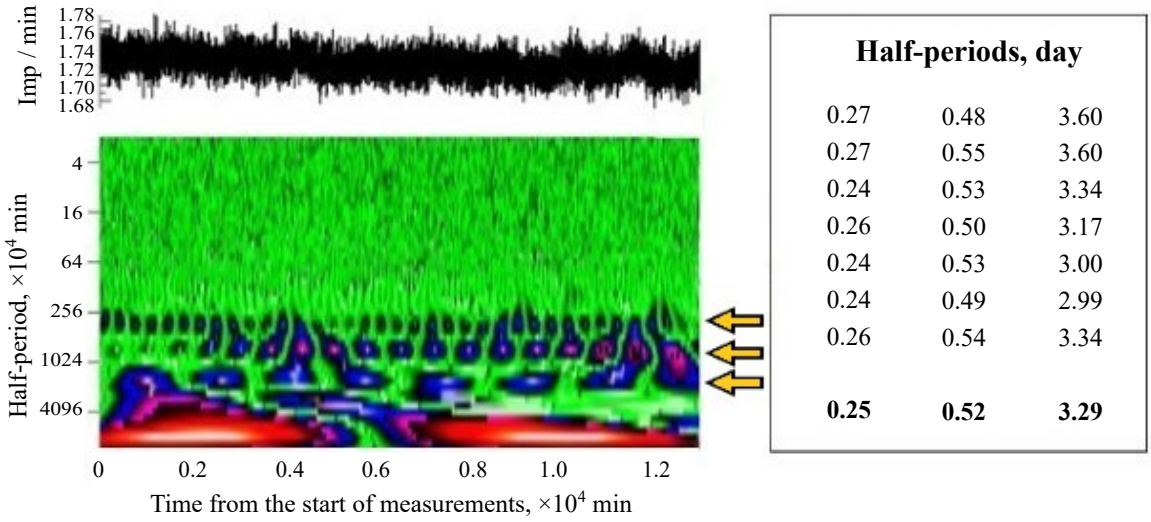

Fig. 2: Wavelet-expansion of a signal of the intensity of gamma-radiation of a specimen with Th after the treatment with a driver. The upper plot is the signal; below, the two-dimensional pattern is the representation of the matrix of coefficients of the wavelet-expansion of this signal. Arrows indicate the periodic series. The signal is the number of impulses for 1 min. The table on the right shows some examples of the estimates of distances between spots. The lower row gives the mean values.

external influence on the process of radioactive decay. This fact cannot be a result of erroneous measurements or, especially, improper analysis: the effect is not observed prior to the treatment and is seen after it.

Because the described result, i.e. the appearance of a periodicity in the noisy signal, is reliably established experimentally, we may ask: why was no effect observed earlier? The possible causes are as follows:

1. The effect is reliably registered only in definite operational modes of a driver. To observe it, one needs to perform special long-term experiments, since the effect can reveal itself in several tens of days after the action of a driver.
2. In the whole array of experimental data, the effect of a variation of the trend of the rate of counting is not strong (several percents) and is variable in time. Therefore, without regular long-term measurements, the effect can be considered as a noise or the uncertainty of a procedure of measurements.

Thus, we showed experimentally the presence of many periodicities with noninteger ratios in measured sequences of the rates of counting. The logical consequence of these results and of the up-to-date model representations about the fractal dynamics of intranuclear clusters [13–15] and about the nuclear structure [13–18] is the conclusion that sufficiently weak electromagnetic signals can excite the dynamics of intranuclear clusters, and, hence, it is possible to observe a manifestation of this changed dynamics in the probabilities of nuclear processes.

Received on May 4, 2020

References

1. Parkhomov A. G. Deviations from Beta Radioactivity Exponential Drop. *Journal of Modern Physics*, 2011, v. 2, 1310–1317.
2. Sturrock P. A., Steinitz G., Fischbach E. Analysis of Radon-Chain Decay Measurements: Evidence of Solar Influences and Inferences Concerning Solar Internal Structure and the Role of Neutrinos. arXiv: astro-ph/1705.03010.
3. Steinitz G., Kotlarsky P., and Piatibratova O. Observations of the relationship between directionality and decay rate of radon in a confined experiment. *Eur. Phys. J. Special Topics*, 2015, v. 224, 731–740.
4. Jenkins J. H., Fischbach E., Buncher J. B., Gruenwald J. T., Krause D. E., Mattes J. J. Evidence for Correlations Between Nuclear Decay Rates and Earth-Sun Distance. arXiv: astro-ph/0808.3283v1.
5. Shnoll S. E. Cosmophysical Factors in Stochastic Processes. American Research Press, Rehoboth, NM, USA, 2012, p, 430.
6. Pomme S. *et al*. On decay constants and orbital distance to the sun – part II: beta minus decay. *Metrologia*, 2017, v. 54, 19–35.
7. Pomme S. *et al*. On decay constants and orbital distance to the Sun – part I: alpha decay. *Metrologia*, 2017, v. 54, 1–18.
8. Pomme S. *et al*. On decay constants and orbital distance to the Sun – part III: beta plus and electron capture decay. *Metrologia*, 2017, v. 54, 36–50.
9. Glasstone S. Sourcebook on Atomic Energy, Krieger, Malabar, FL, 1979.
10. Gareev F. A., Zhidkova I. E., Ratis Yu. L. Influence of the excitation and ionization of atoms in the rate of nuclear processes at low energies. Preprint R4-2004-68, JINR, Dubna, 2004, p. 54.
11. Astaf'eva N. M. Wavelet-analysis: foundations of the theory and applications. *Uspekhi Fiz. Nauk.*, 1996, v. 166 (11), 1145–1170.

12. Torrence C. A practical guide to wavelet analysis. *Bulletin of the American meteorological society*, 1998, v. 79 (1), 61–78.

13. Adamenko S. V., Selleri F., van der Merwe A. Controlled Nucleosynthesis. Breakthroughs in Experiment and Theory. Springer, Berlin, 2007.

14. Adamenko S., Bolotov V., Novikov V., Yatsyshin V. Control of multiscale systems with constraints 4. Control of the evolution of nuclear systems on the basis of the principle of dynamical harmonization. *Interdisciplinary Studies of Complex Systems*, 2013, No. 3, 35–95.

15. Greiner W. Exotic nuclei: from super-heavies to hyper and antimatter. *Yadern. Fiz.*, 2001, v. 64 (6), 1191–1197.

16. Maruyama T., Niita K., Oyamatsu K., Chiba S., and Iwamoto A. Quantum molecular dynamics approach to the nuclear matter below the saturation density. *Phys. Rev. C*, 1998, v. 57 (2), 655.

17. Dechargeé J., Berger J.-F., Girod M., Dietrich K. Bubble and semibubbles as a new kind of superheavy nuclei. *Nuclear Physics A*, 2003, v. 716, 55–86.

18. Berezovoj V. P., Bolotin Yu. L., Yanovsky V. V. *et al*. Stochastic Rezonance in nuclear fission. *Problems of Atomic Science and Technology*, 2001, No. 6, 226–229.

Progress in Physics is an American scientific journal on advanced studies in physics, registered with the Library of Congress (DC, USA): ISSN 1555-5534 (print version) and ISSN 1555-5615 (online version). The journal is peer reviewed and listed in the abstracting and indexing coverage of: Mathematical Reviews of the AMS (USA), DOAJ of Lund University (Sweden), Scientific Commons of the University of St.Gallen (Switzerland), Open-J-Gate (India), Referential Journal of VINITI (Russia), etc. Progress in Physics is an open-access journal published and distributed in accordance with the Budapest Open Initiative: this means that the electronic copies of both full-size version of the journal and the individual papers published therein will always be accessed for reading, download, and copying for any user free of charge.
The journal is issued quarterly (four volumes per year).

Electronic version of this journal: http://www.ptep-online.com

Postal address:
Department of Mathematics and Science, University of New Mexico,
705 Gurley Avenue, Gallup, NM 87301, USA